Order Number 1342681

Fabrication of a micro-Fresnel lens on a spherical substrate

Trusty, Robert Mason, M.S.

The University of Arizona, 1990

U·M·I
300 N. Zeeb Rd.
Ann Arbor, MI 48106

FABRICATION OF A MICRO-FRESNEL LENS ON A SPHERICAL SUBSTRATE

by

Robert Mason Trusty

A Thesis submitted to the Faculty of the

COMMITTEE ON OPTICAL SCIENCES (Graduate)

In Partial Fulfillment of the Requirements
For the Degree of

MASTER OF SCIENCE

In the Graduate College

THE UNIVERSITY OF ARIZONA

1990

STATEMENT BY THE AUTHOR

This thesis has been submitted in partial fulfillment of the requirements for an advanced degree at the University of Arizona and is deposited in the University Library to be made available to borrowers under rules of the Library.

Brief quotations from this thesis are allowable without special permission provided that accurate acknowledgement of the source is made. Requests for permission for extended quotation from or reproduction of this manuscript in whole or in part may be granted by the head of the major department or the Dean of the Graduate College when in his or her judgement the proposed use of the material is in the interests of scholarship. In all other instances, however, permission must be obtained from the author.

Signed: _____

APPROVAL BY THESIS DIRECTOR

This thesis has been approved on the date shown below:

_____ _____

T.D. Milster — Date

Assistant Professor of Optical Sciences

ACKNOWLEDGMENTS

I would first and foremost like to thank my wife Sue for all of her support and encouragement during our year-long adventure.

I would also like to thank my major professor, Dr. Thomas D. Milster, for providing guidance and direction during the past year. I would also like to thank Dr. James Burke and Dr. Raymond Kostuk for being on my committee.

I wish to acknowledge Lawrence Livermore National Laboratory for providing funding and equipment loans for this work, especially Dave Dye, Don Davis, Anne Freudendahl, and Steve Root. Thanks also to LLNL employees Ricke Behymer for providing the microspheres and expert advice on handling them, Milton D. Bell for providing precision equipment, technical advice and encouragement during the past year, and Hector Medecki for sharing his experimental philosophy.

I wish also to acknowledge OSC engineer, Kevin Erwin, for his innovative ideas and experimental guidance throughout the lens fabrication process. Without him, there may have been no experimental results.

I wish also to acknowledge Mark Shi-Wang for his tolerance analysis and modeling work which I summarized in Chapter IV.

I would also like to thank Chien-Wei Han for my introduction to the fabrication of holographic optical elements.

Finally, I would like to acknowledge Photon Incorporated of Los Gatos, CA. for providing a spot scanner for use in the experimental work.

TABLE OF CONTENTS

TABLE OF CONTENTS (Continued)

LIST OF ILLUSTRATIONS

LIST OF ILLUSTRATIONS (Continued)

LIST OF ILLUSTRATIONS (Continued)

LIST OF ILLUSTRATIONS (Continued)

ABSTRACT

A decrease in the size and weight of the objective lens in an optical data storage system (ODS) would improve performance. Limits on reducing the lens size were investigated. Size reduction is limited by aberrations introduced by the disk cover plate that protects the recording medium from dust and scratches. Size reduction is also limited by off-axis aberrations introduced by beam tilt required to maintain a field of view similar to conventional ODS objectives.

It was shown that a Fresnel microlens on a thin spherical shell is acomatic for all field angles. A technique used to fabricate such a lens was demonstrated. The resulting lens was presented.

Chapter I

Introduction

Optical data storage (ODS) methods include techniques that optically store and recover digital information on a medium. Current systems include the popular compact disk (CD) music players, CD read only memory (CD-ROM) data bases, write-once-read-many (WORM) drives, and read, write and erase storage systems that are beginning to compete with magnetic disk drives. Optical systems offer the promise of very high storage densities, high media ruggedness, and removability.

Each type of ODS system is composed of a laser source, collimating and circularizing optics, beam splitter, turning mirror, objective lens, storage medium, and data detection, tracking and focus servo optics, detectors, and actuators. Such a system is shown schematically in Figure 1.1. The laser source (usually a laser diode operating around 830 nm) is collimated and circularized. The collimated beam is passed through a beam splitter and is turned 90º by the turning mirror, and is focused onto the medium by the objective lens. The objective lens is mounted on a focus actuator, and its location relative to the medium surface is controlled by the focus servo. The objective is corrected for spherical aberration introduced by the cover plate. The reflected light is re-collimated by the objective lens and turned back to the beam splitter where it is split away from the incoming beam. The light is passed to data detectors and focus and tracking servo optics and

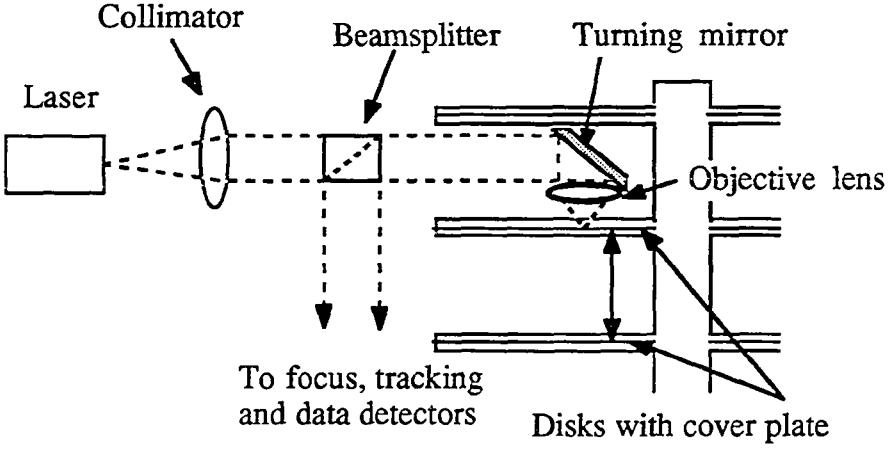

Figure 1.1. Sketch showing a stacked optical disk system, turning mirror and objective lens.

detectors. Many different techniques, such as knife edge, astigmatic, wax-wane and differential wax-wane, can be used for the focus servo [1]. Disks are usually grooved, with one groove per data track. Diffraction from grooves can provide an error signal to a push-pull tracking servo that keeps the focused spot on the proper data track. The push-pull tracking servo involves interfering the 0^{th} and the $\pm 1^{st}$ diffraction orders in an aperture and imaging the interference pattern on a split detector. If the beam is properly centered on a track, the interference pattern is uniform on each detector. If slightly off track, one detector is illuminated more than the other, and the difference between the detectors is the tracking error signal [2]. Focus and tracking servos and sensors are very interesting topics and worthy of lengthy treatment, but this thesis will deal exclusively with objective lens issues.

Data are written as streams of bits along a circular track embedded in a spinning disk. Tracks are concentric circles or spiral grooves in recording media. Track separation is on the order of 1.7 μm [3]. Volumetric storage density (bits/ mm^3) is the amount of data stored in a disk system per unit volume and is a product of the areal density (bits/ mm^2) and the number of disks stacked per mm of stack height. The areal density is a product of the linear bit density (the number of bits per mm along a particular track) and the track spacing. These definitions are summarized by Equations 1.1-1.3. A typical areal density for disk systems is 10^6 bits/mm^2 (6×10^8 bits/in^2) [2]. If a microlens is used as the objective lens for an ODS system, the

same number of disks can fit in a smaller stack height and, therefore, volumetric storage density will increase.

$$\text{Volumetric density} \equiv \text{Areal density} \times \frac{\text{no. of disks stacked}}{\text{stack height}} \qquad \text{Equation 1.1}$$

$$\text{Areal denstiy} \equiv \text{Linear bit density} \times \frac{\text{no. of tracks}}{\text{track spacing}} \qquad \text{Equation 1.2}$$

$$\text{Linear bit density} \equiv \frac{\text{no. of bits per track}}{\text{track length}} \qquad \text{Equation 1.3}$$

A mechanical actuator is used to move the objective lens and turning mirror as required to maintain tracking and focus. The actuator response is limited by the amount of mass it must move. Replacing a conventional objective lens with a microlens will allow reduction of the collimated beam diameter, so the turning mirror can also be smaller. When the optical hardware size is reduced there is a corresponding size reduction of the hardware used to mount and move the optics. If all of the hardware dimensions scale linearly with the optics size, a reduction in lens size by some factor will allow a reduction in moving mass by that factor to the third power, since mass scales with volume. The access time of a disk system is the time required to move the optical beam to a desired track of data. Significantly improved access time can be realized due to the reduced mass. Typical ODS systems have access times on the order of 200 ms [2].

However, the extent of the miniaturization possible is limited by; (i) the required working distance between the objective lens and the disk cover plate, (ii) the disk cover plate thickness, and (iii) the required objective lens field of view. This thesis explores these fundamental size limits, searches the literature for candidate microoptics that will meet these requirements, and selects a lens type that promises best performance. Fabrication of a prototype lens is described and test results are given. Some general background information about ODS systems follows.

Background

Erasable ODS systems are of two varieties: phase change and magneto-optical (M-O). An erasable phase change disk is made of multi-component alloys. It has a stable crystalline phase and a metastable amorphous phase with different optical properties, eg. reflectance. The material is prepared as a crystalline film. Recording is accomplished by locally melting the material with a focused laser beam and then cooling it quickly enough to quench it in the amorphous phase. A lower power laser beam is used to erase data by heating the track to a temperature just below the melting point long enough to re-crystallize and erase any amorphous marks. The reflectivity is detected using a low power, CW laser beam scanning the disk [4]. A phase-change medium must have moderate thermal conductivity, low melting point, high annealing rate and a high activation energy for annealing to facilitate erasure and marking from the modulated laser output [2].

In an M-O system, the medium is heated above its Curie temperature in the presence of a bias magnetic field oriented either into or out of the disk plane. Heat is provided by the focused spot of the laser beam. When the laser beam is turned off, the spot freezes with its magnetic moment aligned with the bias field. The data pattern is determined by the orientation of the magnetic moment. For example, if a data "1" is indicated by the moment out of the disk plane, a data "0" is indicated by the moment into the disk plane. The medium must be erased before data are written. One erase scenario is to set the bias coil for a data "0" and scan the focused spot over a track. To write data, the bias field is set to a data "1", and the laser beam is modulated while scanning the track. Moment reversal occurs over small regions on the order of the focus spot size. To read the data, a lower laser power level is used. The written data will rotate the polarization of the incident beam on reflection, usually much less than 1º. This is known as the Kerr effect. A data "1" will rotate the polarization in one direction, while a data "0" will rotate it in the other direction. Data are detected by sensing the direction of rotation. [2]

A "mark" is a data "1" or "0" written into a disk medium. Its size is limited by the laser spot that is focused on the disk during the writing process. The smallest possible mark can be written only by a diffraction-limited laser spot. The approximate full-width at half maximum intensity (FWHM) diffraction-limited spot size is given by Equation 1.4. This limit is only achieved by high quality lenses and careful alignment. The

theoretical spot size is decreased as the lens numerical aperture (NA) is increased, so high NA objective lenses are always used in optical data storage systems. An NA of ≥ 0.5 is typical [5].

$$FWHM \approx \frac{0.6\,\lambda}{NA} \qquad \text{Equation 1.4}$$

Today's state-of-the-art systems use a single molded glass or plastic aspheric objective lens, that has a 4.5 mm clear aperture and is 3 mm thick and weighs approximately 0.25 g. The objective lens is designed to correct for spherical aberration introduced by a flat cover plate that is used to protect the storage medium. The cover plate is typically about 1.2 mm thick. However, a cover-plate concept that utilizes a thin (as small as 50 - 125 μm) glass or plastic cover plate with an air gap between it and the medium has been described [2]. A properly designed objective lens will be diffraction limited when used in conjunction with the cover plate on the disk. Typical systems have 15-25 mm high optical heads and 50-100 g of moving mass [5].

In addition to on-axis spherical aberration, off-axis aberrations, such as field curvature, astigmatism and coma, can be introduced if the focused beam is passed through the medium cover plate at an angle. These aberrations can become large enough to increase the spot size above the diffraction limit, thus increasing the required track separation, decreasing linear density, and reducing volumetric storage density.

In a stacked disk system, the vertical spacing between each disk must accommodate the optical head. A smaller optical head would allow smaller spacing, and more disks could fit in a given volume, providing a higher volumetric storage density. The optical head includes the objective lens , turning mirror, lens servo and mounting fixtures. The height of the head is set by the collimated beam size and the NA of the objective. An industry rule of thumb is that the minimum platter spacing is two to three times the objective lens diameter. So, smaller lenses will decrease platter separation and translate into increased volumetric storage density.

Storage systems can have either removable or non-removable (fixed) media. The removable system is more likely to collect dust on the medium than the fixed system, which can be designed to be environmentally sealed. Because of the loading mechanics and wear incurred, removable systems can be more susceptible to disk wobble, misalignment and tilt between the disk and lens.

Limits on Size Reduction

One factor to consider in determining what the smallest usable microlens might be is the obscuration of the laser beam by dust particles residing on the cover-plate surface. As the beam is focused onto the medium, it has some diameter, D, at the cover-plate surface. The area at the cover-plate surface is $\pi D^2 / 4$. As the lens shrinks, this diameter may remain the same if the working distance is allowed to decrease, as shown in Figure 1.2. As

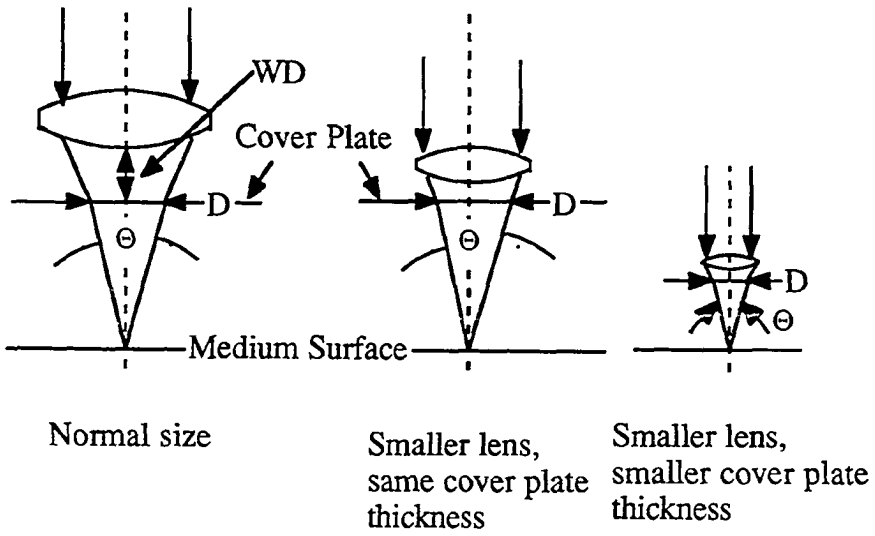

Figure 1.2. As a lens of a given NA shrinks in size, it's working distance and the cover-plate thickness must also decrease to maintain the same focal point.

the lens shrinks even further, the working distance is reduced to unrealistic amounts, so the cover-plate thickness must be reduced. This will also cause the beam diameter at the cover-plate surface to be reduced. For this case, a given dust particle will obscure more of the beam than for the case where the cover plate is thicker. A dust-induced beam obscuration will cause a higher bit error rate (BER) than if there were no obscuration [2].

In a non-removable, sealed system it is possible to design and build a flying head, as shown in Figure 1.3, which is similar to those designed for magnetic systems [6]. This type of design places the objective lens and turning mirror on a small sled that floats on a micron-size cushion of air generated by the moving disk surface. Since the system is sealed, no cover plate is required to protect the optical medium, so the objective lens can be much closer to the medium. A sealed system is required to eliminate large (>1μm) dust particles that would hit the flying head and cause a crash. Since a removable system must have a cover plate to protect the medium, a lens of a given NA must be larger for the removable system. A sealed system would, therefore, allow significantly smaller optics than the removable system.

One final constraint on changing the lens size is not technical in nature, but is practical and important. To minimize the lens size, it is desirable to reduce the cover-plate thickness. In doing so, non-standard discs must be manufactured, and a change in the industry standard must be considered if

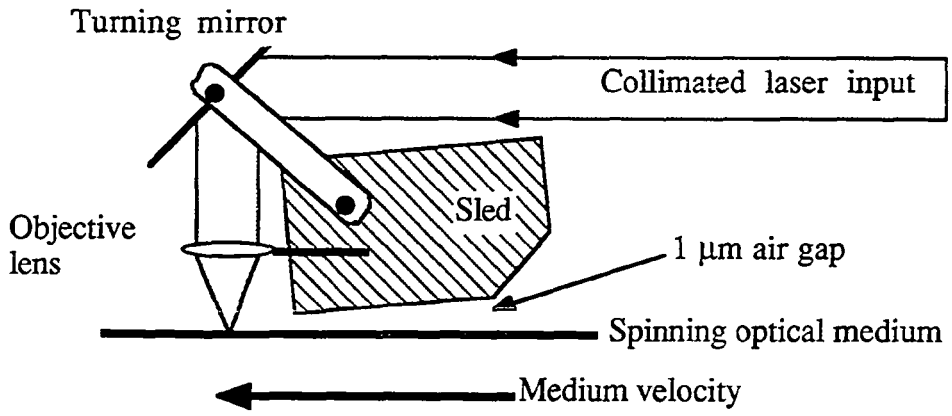

Figure 1.3. Sketch of a flying head similar to those used in the magnetic storage industry, but adapted to an optical system.

small lenses become widely used. This would cause incompatibilities between the systems already in production and any new type of system.

It is clear that it is desirable to reduce the size of the objective optics in an ODS system. This thesis will explore the limitations on size reduction and will offer a new type of microlens as a candidate for improving volumetric storage density and access time.

Chapter II of this thesis describes a model that yields dust-related lower size limits for fixed and removable systems. An optimum cover-plate thickness and the effect of tilt between lens and disk is examined. A practical objective lens lower size limit and an appropriate cover-plate thickness is proposed. Chapter III examines the literature for various types of microoptics available and analyzes their applicability to the optical data storage problem. Chapter IV introduces the proposed solution, which is a Fresnel zone lens formed on a hemispherical shell substrate approximately 0.8 mm diameter. A tolerance analysis is performed to guide fabrication methods. Chapter V describes the fabrication technique of the lenslet. Chapter VI presents a prototype lenslet, shows an evaluation of its performance and summarizes the conclusions of this thesis.

CHAPTER II

OBJECTIVE LENS LOWER SIZE LIMITS

To improve the performance of an optical data storage (ODS) system, one may decrease the size of the objective lens. This chapter will describe limits on size reduction of the objective lens. The first limit described is due to the cover-plate thickness required to keep dust and scratches out of the focus of the objective lens. The second limit described is due to field of view considerations for microlenses.

Dust-related Lens Size Limitations

The bit error rate (BER) of an optical disk system is defined as the ratio of bits recovered in error divided by the total number recovered [2]. For reliable system operation, the BER should be as low as possible. The signal to noise ratio (SNR) is defined as the ratio of the average signal power divided by the total noise power in the data channel [2]. In general, the BER will be large for systems with low SNR. Therefore, it is desirable to keep the signal level as high as possible. Dust particles in the beam can reduce the optical power incident on the disk and the signal detector, causing a lower signal power output from the detector.

The purpose of a disk cover plate is to keep surface defects, scratches and dust out of focus of the objective lens. The effect of scratches and dust on the cover-plate surface on a disk system is a minor modulation of the

amplitude of the data signal. Different geometries for protecting the optical medium have been described in the literature [2]. Figure 2.1 is a cross section of a Kodak 14" optical disk with thin (~0.1 mm) cover sheets stretched across spacers and an air gap between the cover and the optical medium. Figure 2.2(a) is a two-sided disk with thick (1.2 mm) cover plates on which the optical medium has been deposited. Figure 2.2(b) is a disk with a solid material between the two cover plates instead of an air gap.

For a fixed laser power, the power density (W/mm^2) at the cover-plate surface increases as the beam diameter at the surface decreases. Dust particles on the cover-plate surface will obscure a higher percentage of the focusing beam for higher power densities, as shown in Figure 2.3. When enough dust accumulates on the cover layer or the upper surface of the layer is too close to the medium, the BER of the system can increase. This is the point when the dust-related lower lens size limit of the lens has been surpassed. Therefore, the minimum acceptable size of the objective lens is dependent on the thickness, d, of the cover plate.

The working distance (WD) is the distance between the objective lens/mounting hardware package and the disk cover-plate surface. WD is needed to avoid head crashes, that is, the physical contact of the optical head with the disk. As WD is increased, the lens is moved away from the medium and must increase in size to remain focused on the medium for a given numerical aperture (NA). As shown earlier in Figure 1.2, when a

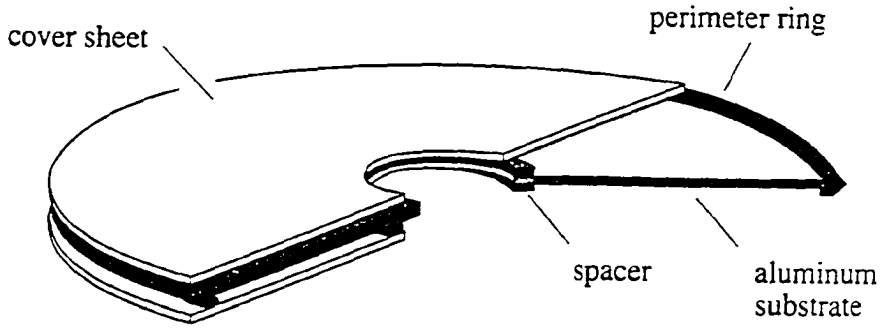

Figure 2.1 This disk geometry uses thin flexible cover sheets with an air separation to protect the optical medium that is coated onto an aluminum substrate. (After [2])

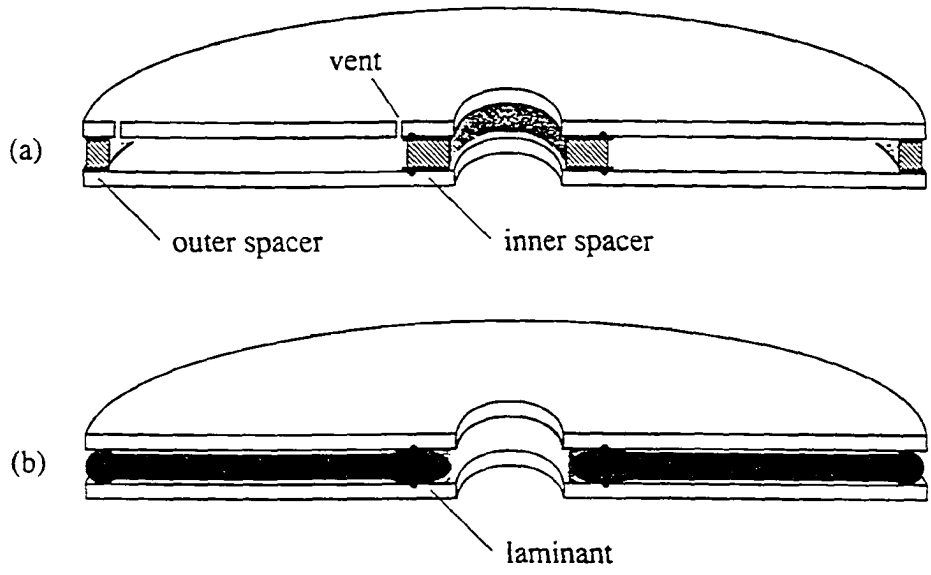

Figure 2.2 These disk geometries use thick cover plates with the optical medium coated directly on the inner surface of each cover plate. (After [2])

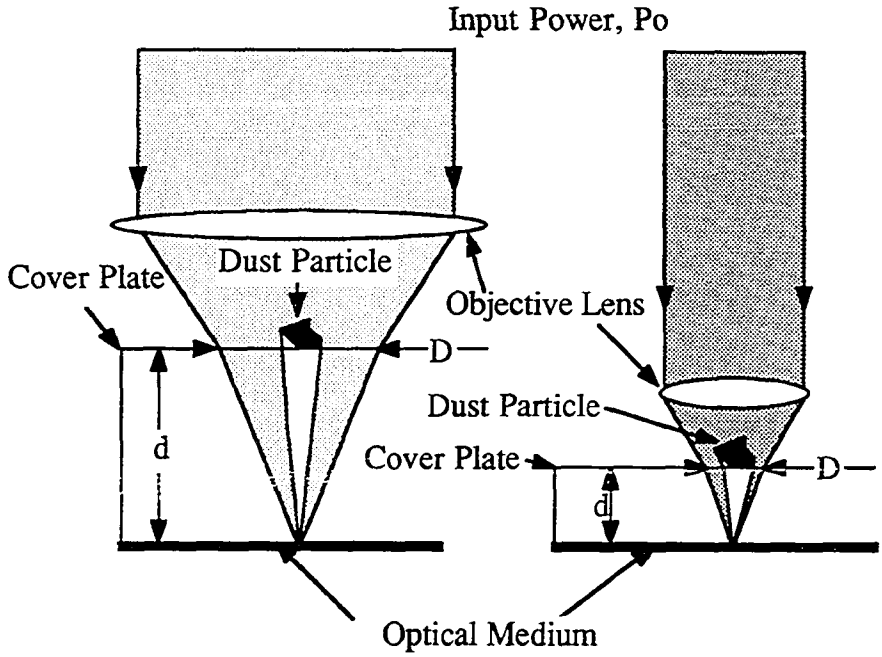

Figure 2.3. Dust particles on a disk surface will obscure a higher percentage of a focused beam for smaller lenses than larger ones, assuming both lenses are of the same NA.

lens of a given NA is significantly reduced in size, the beam diameter, D, at the cover-plate surface is reduced as the lens moves closer to the medium. D can be calculated exactly using Equation 2.1, while equation 2.2 is a good approximation since the NA of a typical ODS system is 0.5.

$$D = \frac{2\,d\,NA}{n\sqrt{1-\left(\frac{NA}{n}\right)^2}}$$

Equation 2.1

$$D \cong \frac{d}{n}$$

Equation 2.2

The beam diameter at the disk cover-plate surface must be large compared to the fractional coverage of dust and defects [2]. Most dust particles that will remain airborne long enough to enter a disk system are < 30 μm diameter. Typical scratches are < 20 μm wide and can be many millimeters long. A model was developed by Marchant [7] that showed that if the beam is more than 5% obscured, significant digital read and write errors are introduced. Equation 2.3 calculates the theoretical disk cover thickness required to minimize the obscuration below 5%, where ρ is the radius of the largest particle on the disk surface, n is the refractive index, and NA is the numerical aperture of the focusing beam.

$$d > 7\,\frac{\rho\,n}{NA}$$

Equation 2.3

Marchant performed an experiment to verify this calculation. Figure 2.4 is a plot showing the results of this experiment. A disk similar to that shown in Figure 2.1 was modified to include variable thickness spacers. The effective cover thickness is the optical thickness, nd. The air-gap cover plate used in the experiment had an effective thickness of 1.2 d because the cover sheet/air composite had an equivalent index of 1.2. Bit error rates were measured for a clean disk at various cover-plate thicknesses, then it was covered with carbon toner particles to simulate a dusty environment (7-30 μm, 1% coverage). The BER was again measured as a function of the cover-plate thickness. It was found that, if the cover thickness was greater than 0.3 mm, the BER approached baseline BER from the clean plate measurements. For the parameters of this experiment, $n_{effective}$ =1.2, ρ≈15 μm, and NA=0.6, Equation 2.3 predicted a minimum thickness of 0.21 mm to introduce no dust related increase in BER, which was in very good agreement with experiment. It was also found that, if the effective layer thickness was smaller than 0.1 mm, the BER approached the fractional coverage by dust and defects. It was concluded that, to remain free of dust and scratch induced BER increase, a cover plate in contact with the medium surface should be at least 0.35 mm thick for an NA of 0.6 [7]. A 0.5 NA lens with 0.075 mm WD focusing through a 0.45 mm cover plate (d_{min}=0.315 mm from Equation 2.3) must be 0.43 mm diameter to focus on the medium surface. This is the smallest lens size for designing defect-limited BER performance in a moderately dusty environment.

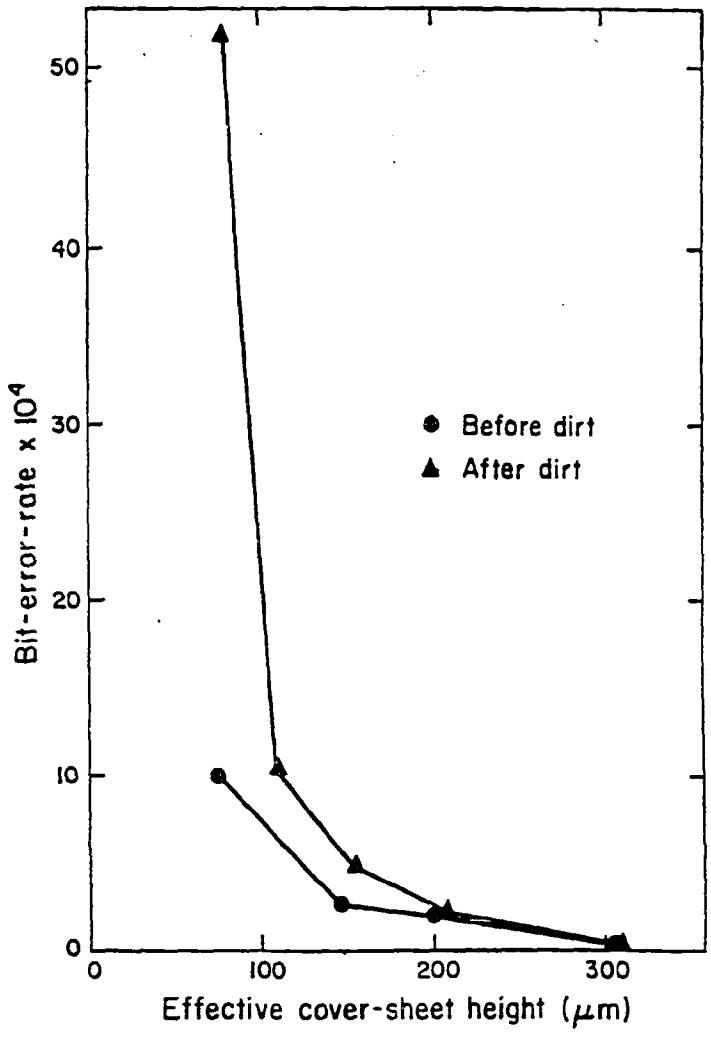

Figure 2.4 If the protective layer is too thin, dust and surface defects will increase the system bit error rate. (After [7])

A sealed system will provide a cleaner environment as well as improved scratch protection than will a removable system. This type of environment will be more accepting of thinner disk cover layers and the associated smaller optics. Since removability is an area in which ODS offers an advantage over magnetic storage technology, size limitations for a removable system are of great interest.

Effect of Cover-plate Induced Aberrations on Lens Size

An optical head focuses light onto the medium surface through a flat protective cover layer. One must account for aberrations introduced by the flat plate must be accounted for when designing an objective lens to produce diffraction-limited performance. When the system is in perfect alignment with the optical axis normal to the cover plate, only spherical aberration is introduced. The spherical aberration worsens with increased cover thickness or index of refraction, but is independent of angle of incidence (except for the increased optical path length in the cover due to non-normal incidence, that may be neglected for small incidence angles normally found in ODS systems). The spherical aberration for small NA lenses is given by Equation 2.4 for a cover of thickness, d, index, n, and a beam convergence angle of U. The correct amount of spherical aberration may be designed into the lens to offset that introduced by the cover, but the lens must only be used with the cover material and thickness for which it was designed. It is interesting to note that the disk design mentioned earlier, which used an air gap and thin cover sheet, would introduce

significantly less spherical aberration than the thick plate design for the same effective thickness.

$$\text{Longitudinal spherical aberration} = \frac{d\,U^4(n^2 - 1)}{8\,n^3} \qquad \text{Equation 2.4}$$

When the angle of incidence becomes non-zero, off-axis aberrations such as coma and astigmatism are introduced. Some ODS systems purposefully introduce a small angle of incidence in order to improve access time. This technique is described below.

ODS systems have both fine and course servo mechanisms. Figure 2.5 is a schematic of one type of an ODS system and shows the servo functions and optical head layout. The objective lens and turning mirror is mounted on a course actuator that is used to locate the focused beam to the desired track on the disk based on the expected radius of the track. Disk stamping imperfections, spindle vibration and worn disk mounting hardware can combine to cause a track to rotate off-center as it spins, causing the track to move laterally relative to the optical head. Typical track runout tolerance is ± 50 μm [2], and tilt is usually less than 0.5º [3]. When the focused beam interrogates the information on the track, a servo system detects the lateral track motion and controls a fine actuator that precisely tilts the turning mirror to keep the beam precisely located on the track as the disk spins. To shorten access time, the fine tracking actuator is also used to quickly move the focused beam to other desired tracks in the

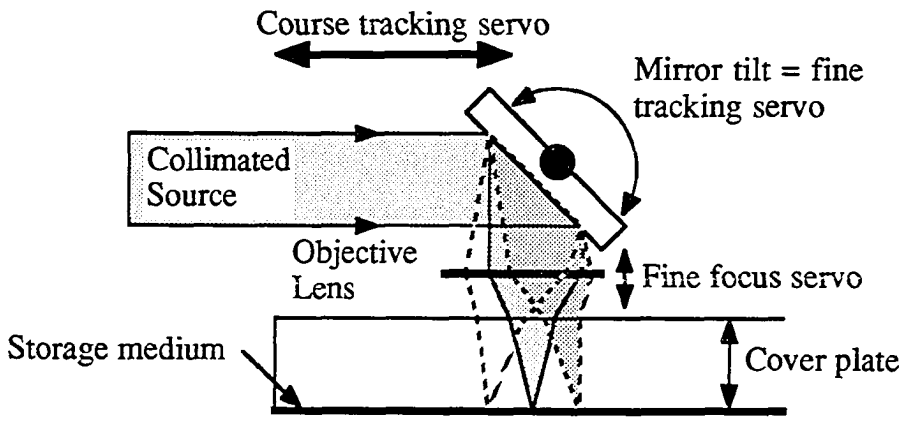

Figure 2.5. An ODS design that allows fine tracking adjustment through the use of a tilting mirror.

near vicinity of the track already being interrogated. It is desirable to be able to access ± 30 tracks, or ± 50 μm using the fine actuator. The objective lens is also located on a fine actuator, that moves the lens normal to the plane of the disk for focus control. A servo system is used to optimize focus and control the actuator.

The optical head must be designed to provide diffraction-limited performance over the expected operation range of the servo mechanisms. This includes tilt introduced by the fine tracking actuator. For a typical objective lens (0.5 NA, 4.5 mm diameter) [5], the ± 30 track field of view corresponds to an objective field of 0.74º. However, for a smaller lens, to maintain the same ± 30 track field of view, the optical head must remain diffraction limited over a much larger field angle. For a 1 mm diameter, 0.5 NA lens, the field increases to 3.3º.

An increased field angle introduces increased off-axis aberrations as the beam is focused through the flat cover plate. Equations 2.5 and 2.6 give the small angle approximations of off-axis wave aberrations for a beam focused through a plate of thickness, d, index, n, convergence angle, U, and incidence angle, u [8]. Figure 2.6 illustrates a focusing beam passing through a tilted plate. For a 1 mm diameter lens and ± 30 data track requirement, the angle of incidence of the beam on the cover plate is increased by a factor of 4.5 (= 3.3 / 0.74). The coma is increased by 4.5 and the astigmatism is increased by 20. These aberrations serve to decrease the focused spot quality by enlarging the spot. This, in turn, causes

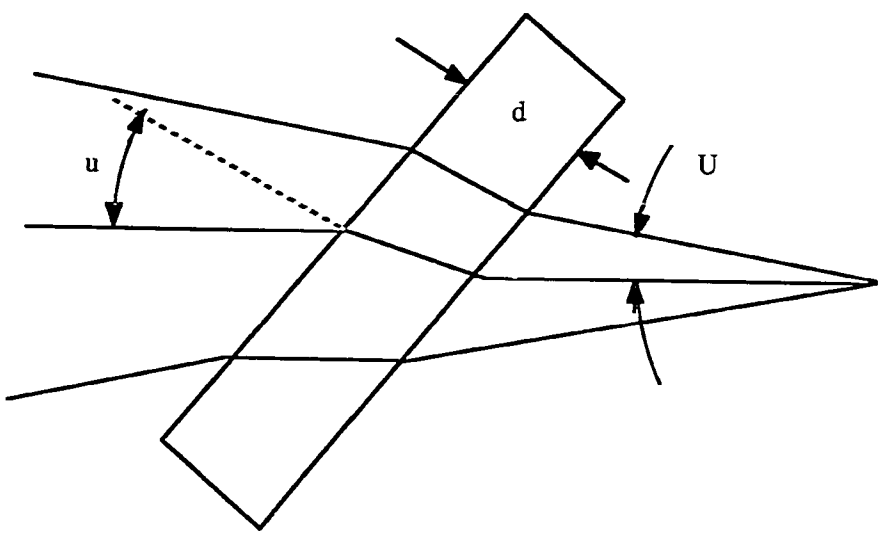

Figure 2.6. Spherical wavefront passing through tilted plane parallel plate.

enlargement of the data mark written on the medium and could reduce the areal data density. Therefore, the design of a miniature objective lens must also consider cover-plate aberrations for the system to be diffraction limited over much larger field angles than conventionally sized lenses.

$$\text{Sagittal coma} = \frac{d\,U^3 u\,(n^2 - 1)}{2n^3} \qquad \text{Equation 2.5}$$

$$\text{Longitudinal astigmatism} = \frac{d\,u^2\,U^2\,(n^2 - 1)}{2\,n^3} \qquad \text{Equation 2.6}$$

Equations 2.5 and 2.6 are approximations for small incidence angles. Also, these equations assume that the beam passes completely through the cover plate before coming to a focus in air outside of the plate. For the thick plate disk design, the focus is on the medium surface and never exits the plate into air. As will be shown in Chapter 4, the most severely limiting aberration of the type of microlens that was designed and fabricated for this thesis is coma. Because of the high NA lenses used in ODS, the small angle approximations were not accurate enough. For more precise results, and to properly model the case when the beam is focused inside of the cover plate, an exact solution was found to model coma for focusing both in and out of the cover plate. The results of the exact aberration model are compared to results from Equation 2.5 and are also compared to results obtained from a computer ray trace.

The model calculates the ray aberration for both zero and non-zero incidence angles as shown in Figure 2.7. For zero incidence angle, the Z value for Gaussian focus was found, Z_G. For the thick cover-plate geometry, this involved only a single refraction through the plate front surface. For the thin cover-plate geometry, the focus was outside of the cover, and a second refraction occurred (See Figure 2.7 I & II (a)). The plate was then tilted relative to the objective lens, and two diametrically opposed edge rays were traced from the objective lens outer edge and refracted through one or both surfaces of the flat plate as needed. The deviation of each ray from the optical axis at Z_G was calculated, and the average of the two deviations was taken to be the sagital transverse ray aberration, ε_y (See Figure 2.7 I & II (b)). The tangential ray aberration is a factor of 3 larger than the sagital ray aberration. The ray aberrations were converted to wave aberrations using Equation 2.7. Figure 2.8 illustrates this conversion.

$$\Delta W = \frac{r}{R} \varepsilon_y \qquad \text{Equation 2.7}$$

The model was verified by comparison with the results of a PC-based ray-trace program, OPTEC 11/87, written by Sciopt Enterprises. An ideal lens was not available as an option in OPTEC, so three user-defined rays were set up that traced the path of the two diametrically opposed rays and an axial ray. The first case verified was the thick plate design, with focus outside of the plate. A plate of 1.2 mm thickness and n=1.5 was set up perpendicular to the optical axis, and the focal plane, Z_G, was found. The

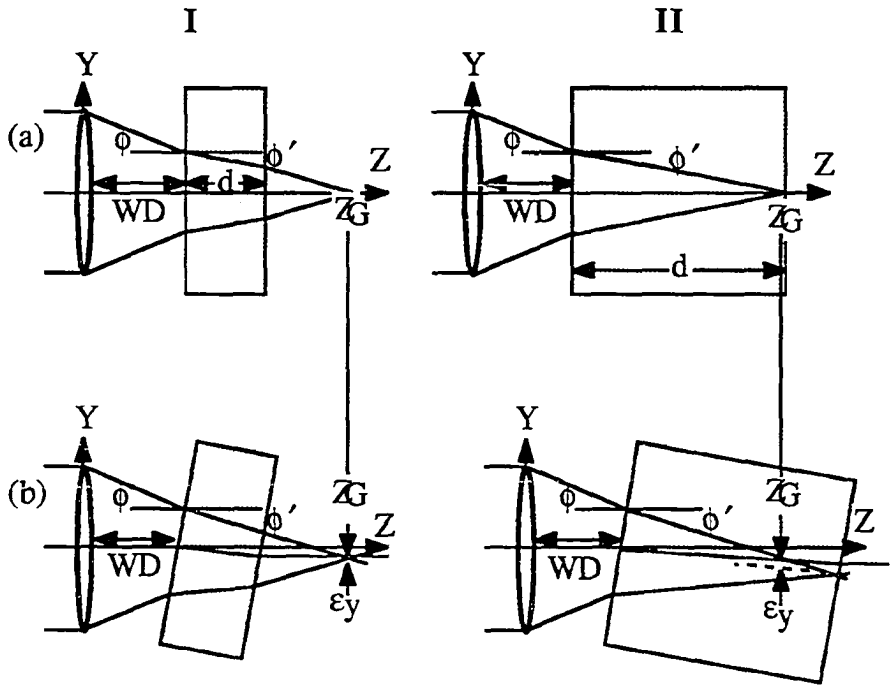

Figure 2.7 A ray model was used to calculate the transverse ray aberration due to a plate tilted in the presence of a converging beam.

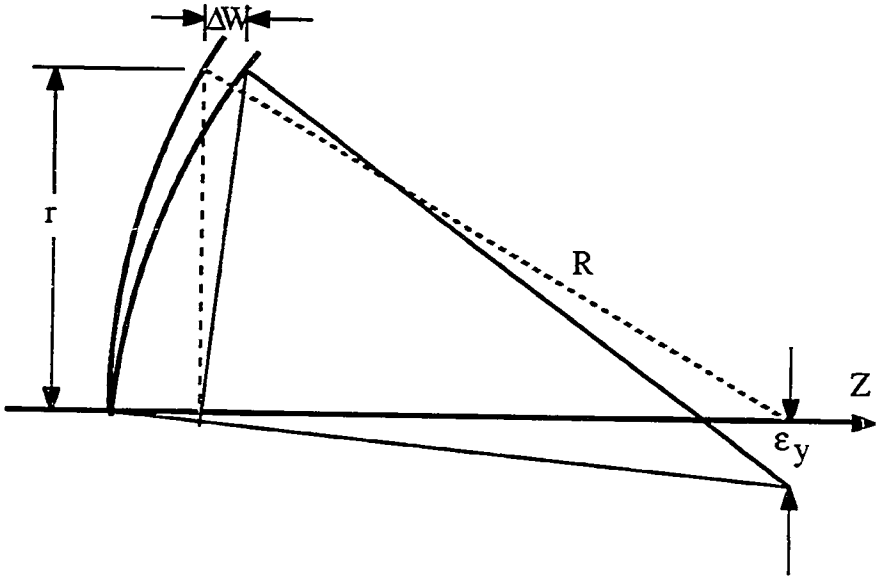

Figure 2.8 The wave aberration can be calculated knowing the transverse ray aberration.

plate was then tilted, and coordinates of the three rays were found in the Z_G plane. The difference between the axial ray and the average of the edge ray coordinates was calculated. The results of the spread sheet model and the ray trace program were identical. Figure 2.9 shows the graphical and tabular output of OPTEC for the focus-through-the-plate case.

A second case was run to verify the spreadsheet for the model where the focus was internal to the cover plate. The plate was increased in thickness until the no-tilt focus was inside of the glass, and the axial value was noted. The plate was tilted and the ray coordinates yielded the same value of the ray aberration as the spreadsheet model. Figure 2.10 is the OPTEC graphical and tabular output for this case.

A comparison of the exact solution and the small angle approximation of the wave aberration was made to determine if the high NA of an ODS system requires an exact solution for accurate modeling results. Figure 2.11 shows the exact and the small angle approximation model's calculated value of the wave aberration vs tilt for focusing through glass of various thicknesses using 0.65 and 0.55 NA objective lenses. The exact model calculates a wave aberration that is approximately 30% higher than the small angle approximation given by Equation 2.5. This factor is different than the factor accountable by the small angle approximation of the sine function ($\{\sin(U)/U\}^3 \approx 0.775$ for NA = 0.65 objective lens). This implies that, for determining the maximum acceptable tilt for an ODS system, it is important to use exact calculations if the results needed are to

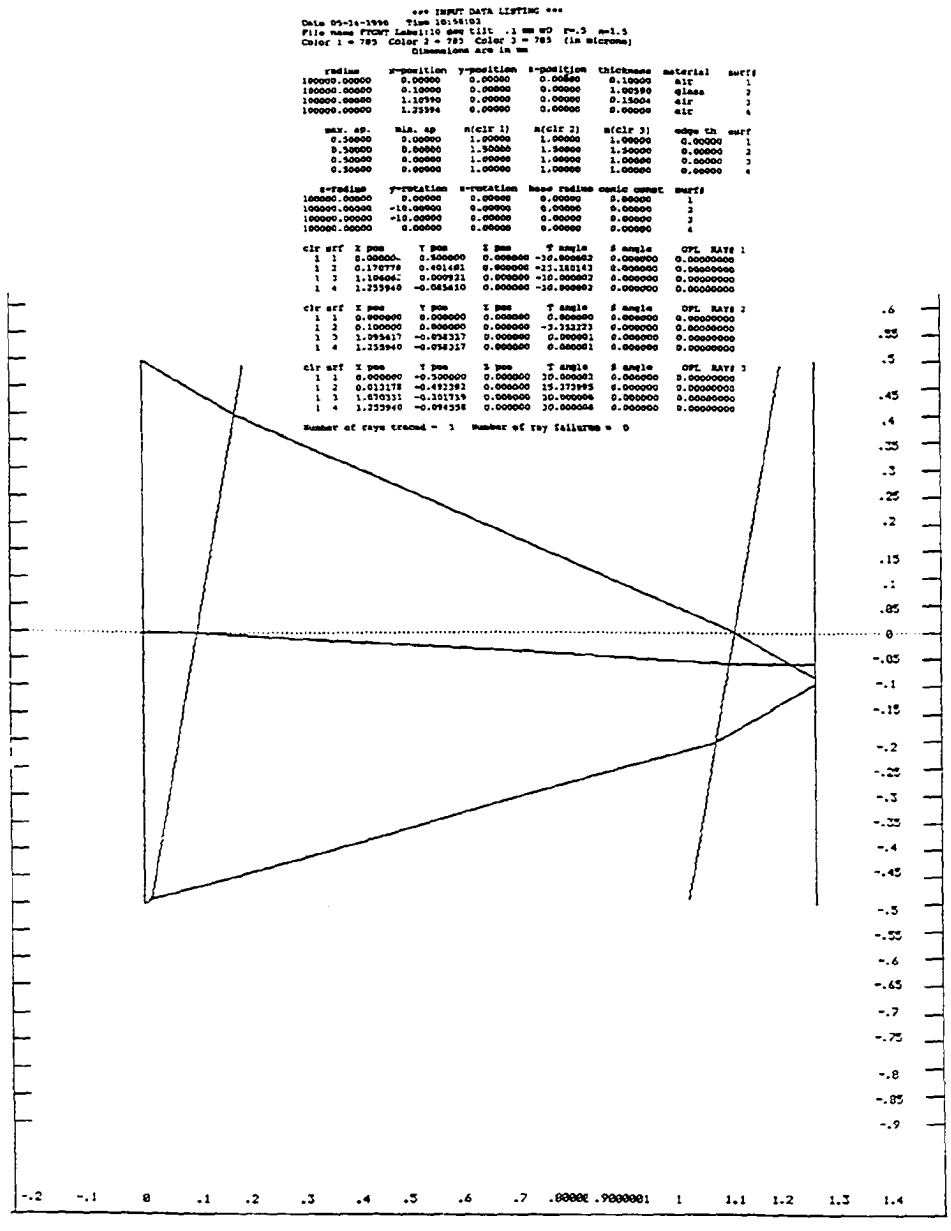

Figure 2.9 An OPTEC 11/87 ray trace was used to verify the spreadsheet model results for the case of focusing through a tilted flat plate. The system prescription and ray coordinates are shown in tabular form with the graphical output.

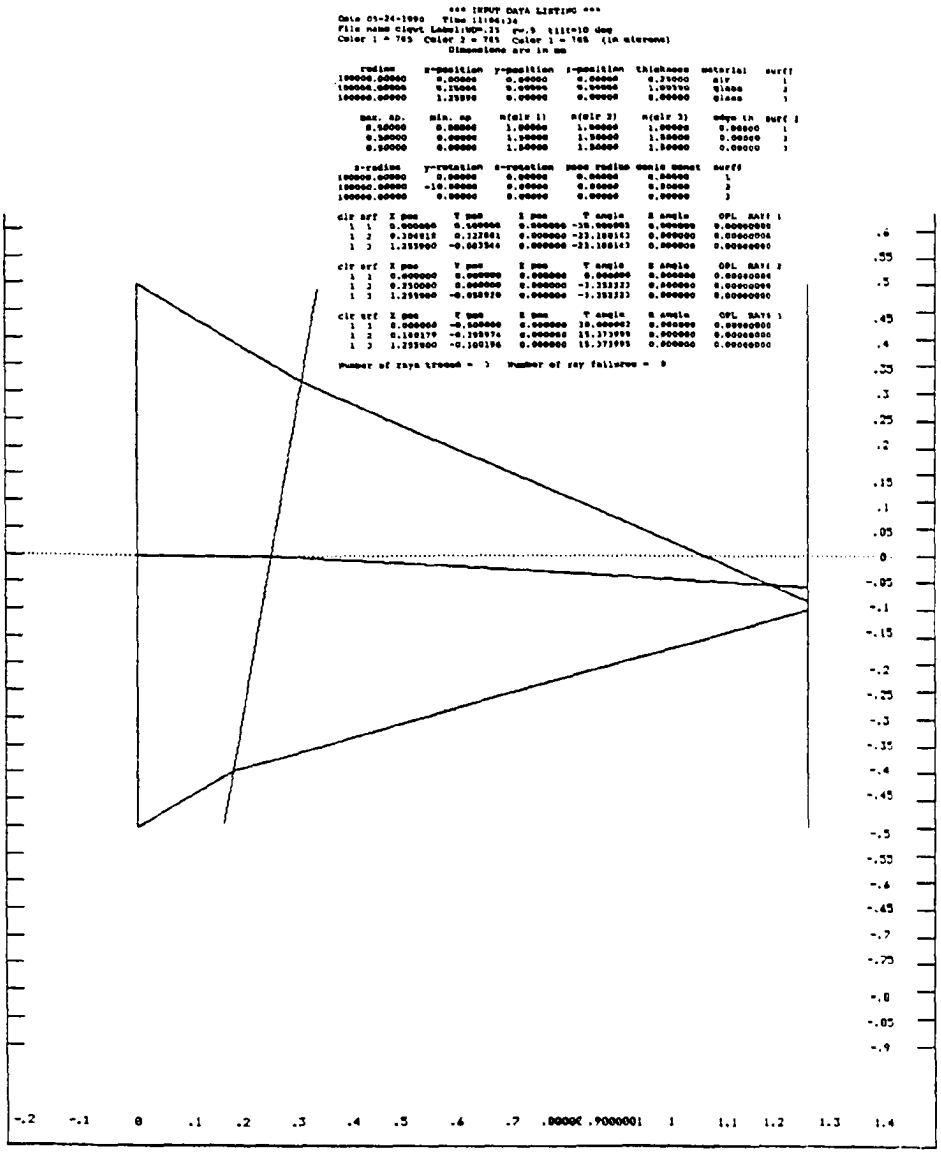

Figure 2.10 An OPTEC 11/87 ray trace was used to verify the spreadsheet model results for the case of focusing inside of a tilted flat plate. The system prescription and ray coordinates are shown in tabular form with the graphical output.

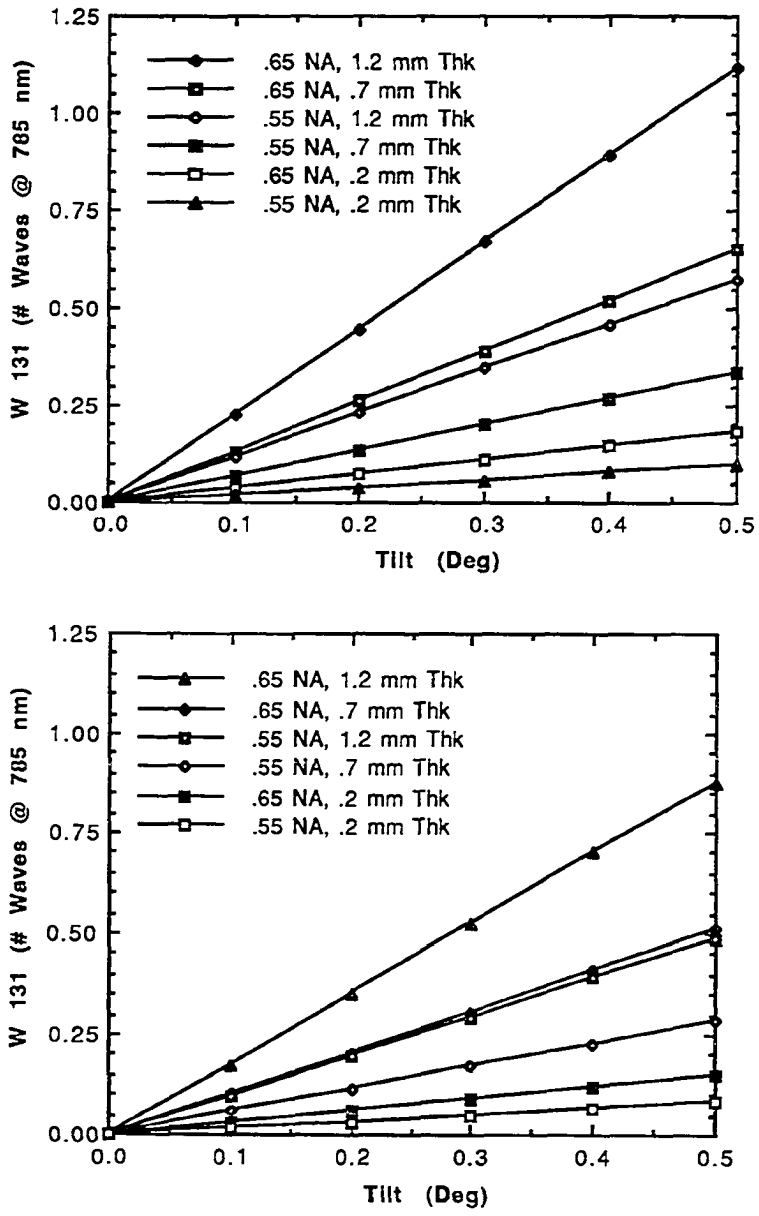

Figure 2.11 The exact solution (top) and the small angle approximation (bottom) of coma (W131) are plotted as a function of tilt angle for various lens NA's and plate thicknesses. The results of the small angle approximation proved to underestimate the amount of aberration by 30% compared to the exact model.

be accurate to better than 30%.

The exact model shows that for an ideal 0.65 NA lens, the wave aberration coefficient, W_{131}, will be limited to 0.25 waves when the tilt is less than 0.1 degrees. This relaxes to 0.2 degrees for a 0.55 NA lens, and to 1.4 degrees for 0.2 mm thick plate and 0.55 NA lens. The last case is similar to the thin cover with an air gap design discussed earlier in this chapter.

The exact model was also used to calculate the aberration of an ideally focused beam for the case where the focus spot was located inside of the cover plate. These results were compared to the earlier exact results for the focus spot located outside of the plate. The optical path length (OPL) in the plate was the same for both calculations. Figure 2.12 is a plot of the wave aberration coefficient as a function of increasing plate tilt for two ideal lenses (0.65 and 0.55 NA) and various thicknesses. Figure 2.12 can be compared to Figure 2.11 (top) to show that the aberration due to the tilted plate is very similar for both cases.

Finally, the model was used to characterize the aberrations due to a tilted plate located in the converging beam of an ideal 0.5 mm radius objective lens for various different numerical apertures, plate tilts and working distances. Figure 2.13 shows the results of these calculations.

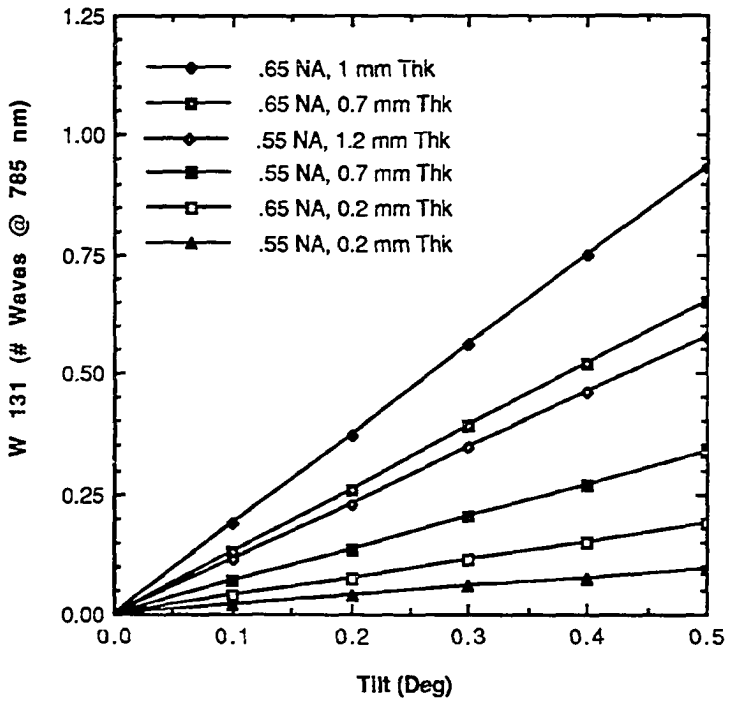

Figure 2.12 Coma (W131) is plotted versus tilt for the focus in glass case for various lens NA's and optical path lengths in the glass. The model showed that the wave aberration introduced by a tilted plate was the same for both the focus in the plate case and the focus through the plate case for similar optical path lengths in the plate. Note that in the case when the focus is inside of the plate, a 0.65 NA lens focuses light at a length of 1.04 mm in a medium of index 1.5. Therefore, a direct comparison with the 1.2 mm, 0.65 NA curve in the upper plot in Figure 2.11 is not possible.

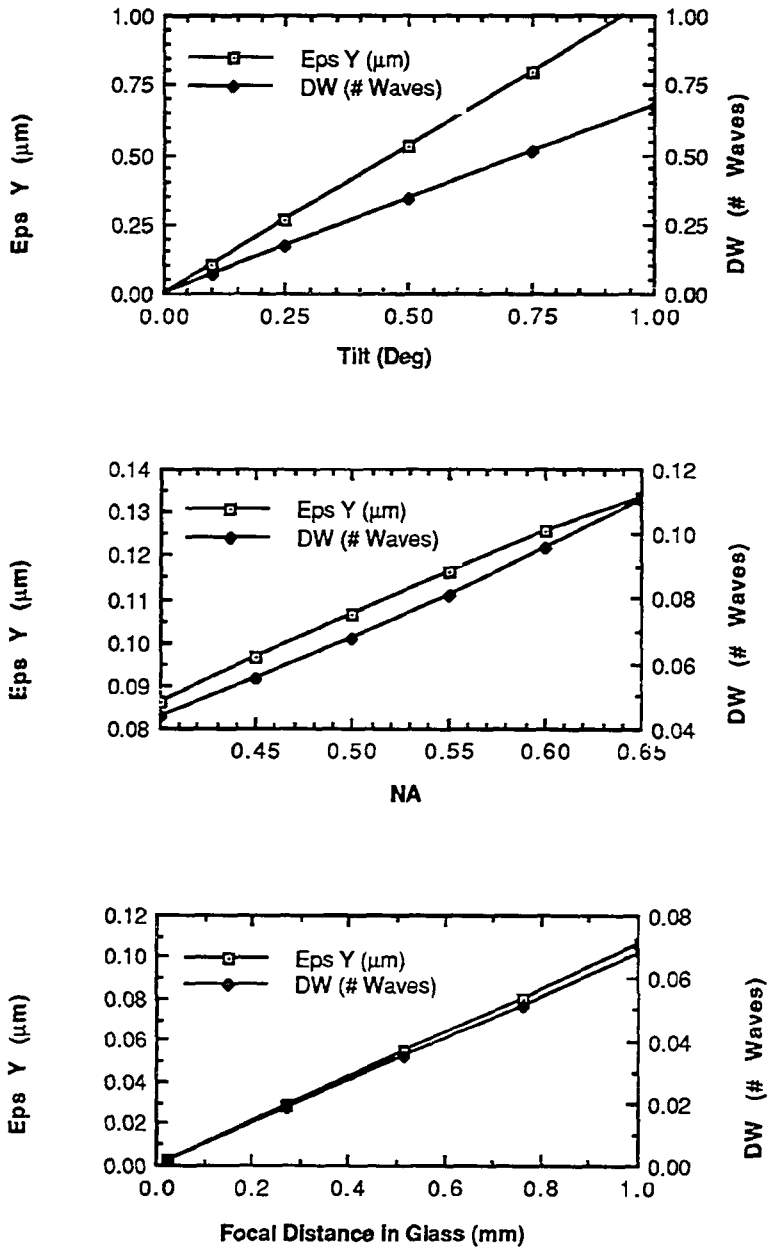

Figure 2.13 The ray and wave aberrations are plotted against tilt (top), NA (middle) and optical path length (bottom) to explore the design space for optical disk and head systems.

Summary

This chapter has described how the minimum size of an objective lens for ODS systems is limited by several factors. The need to keep surface defects and dust out of focus of the objective lens forces the lens to be a minimum distance away from the optical medium on the disk. A lens diameter of 0.43 mm was found to be the minimum size for the BER performance to remain limited by manufacturing defects in the presence of moderate amounts of dust. Non-removable, sealed systems could further reduce the minimum lens size by reducing the dust and scratch protection requirements.

It was shown that the small-angle approximations used for calculating coma due to a tilted flat plate in a focusing beam were not accurate enough for high NA beams. A model was developed with improved accuracy. This model showed that, for similar path lengths inside of the plate, the coma introduced when focusing in the plate was very close to the same as when focusing through the plate. This model also explored the design space to determine the amount of coma introduced as a function of tilt, lens NA and working distance. These results may be used to help determine the allowable field angle and minimum working distance for an optical head in order to remain diffraction limited. These design parameters will effectively determine the lower size limit of the objective lens for given amounts of coma.

CHAPTER III

MICROOPTICS; A LITERATURE REVIEW

There are several different types of lenses described in the literature that are significantly smaller and lighter than a conventional objective lens used in optical data storage systems. In this chapter, several microlens (small aperture lens) types are examined and compared to the conventional objective in terms of size, weight, focusing quality and fabrication complexity. Several different standard objective lenses used in today's ODS technology are described. A technology that is a hybrid of a conventional glass lens and a molded asphere is discussed. A molded refractive microlens and a miniature Luneburg lens are discussed, and a SMILE lens is introduced. A lens formed through surface tension in melted photo resist is also introduced. Refractive and diffractive Fresnel lenses and some different techniques used to fabricate them are described. The type of microoptic which is demonstrated in this thesis is presented.

Standard Objective Lens for Optical Data Storage

The purpose of the objective lens is to focus a collimated beam of laser light through the cover plate on the optical disk onto the optical medium in a diffraction-limited spot. The lens is mounted on actuators as described in Chapter II. Moving mass mounted on the actuator limits access time of the

system, so the mass of the objective should be minimized for quick response time. Objectives used in ODS typically have an NA of 0.5 (or higher), in order to minimize the size of the focused spot. The disk cover plate introduces spherical aberration that the lens must correct. To correct for spherical aberration with only spherical and flat elements, a multi-element lens module is required. This approach produces objectives of relatively high mass and long access time. This mass may be decreased by using plastic elements, but they are less stable than glass with respect to temperature, humidity and mounting hardware stress. The birefringence and dispersion properties of plastic are worse than glass as well [9].

One method of correcting for spherical aberration while minimizing the mass is to use a single aspheric element. This element may be specially ground and polished, or it could be molded in glass or plastic. A typical lens clear aperture is 4.5 mm. Grinding and polishing is not conducive to mass production techniques, while molding is. Plastic lenslets are easy to mold, but can suffer the instability and optical property problems mentioned above. The molding of a high performance glass aspheric singlet objective for ODS has been demonstrated [10]. For molded glass objectives, reducing the diameter of a lens from 6.325 mm to 4.00 mm, reduces the mass from 248 to 58 mg [9]. A similar proportional reduction in the moving mass of the mounting hardware and actuators could be expected.

The optical design parameters of several typical objectives has been summarized [5]. Figure 3.1 lists lenses of several different designs: multi-element glass, molded plastic and molded glass. Lens mass varies from 110 to 530 mg. Typical access times are restricted to about 50 msec for even the lowest mass lens elements [5]. The clear aperture is between 3.0 and 4.6 mm. The NA is between 0.50 and 0.60. The wavefront aberration varies from 0.02 to 0.05 waves.

To summarize, the "typical" objective lens mass is around 100 mg, and the diameter is 4.5 mm. The following sections describe several different types of optics that show improvement in both mass and diameter.

Hybrid Aspherical Lenses

The molded glass asphere produced by Corning Glass described earlier in this chapter is difficult to manufacture. Molten glass is difficult to handle and is a material that limits the mold life. One method to improve manufacturability while also decreasing size and mass of the lens is to make what is known as a hybrid asphere. A hybrid asphere is described that was fabricated using an aspherical mold to form a thin lacquer asphere on the surface of a spherical glass plano-convex lens [11]. Figure 3.2 shows the fabrication technique schematically.

Manufacturer	Kodak	Corning	Fujinon	Olympus	Pentax
Designation	A-365-D	350080	LSR-F5045A	AV4453	PLD-210
Lens type	aspheric singlet	bi-asphere	bi-asphere	na	multi-element
Lens material	molded glass	molded glass	molded plastic	molded glass	glass
Numerical aperture	0.55	0.55	0.50	0.53	0.60
Wavelength (nm)	800	805	780	780	780
Focal length (mm)	4.6	3.9	4.5	4.4	3.0
Aperture (mm)	4.6	4.3	4.5	4.65	3.6
Working dist. (mm)	2.1	1.5	2.0	1.75	1.25
Wavefront (RMS)	0.05λ	0.04λ	na	0.02λ	na
Weight (mg)	400	250	110	340	530
Cover glass (mm,n)	1.2, 1.57	1.2, 1.57	1.25, 1.48	1.25, 1.49	1.2, 1.58

Figure 3.1 Optical design parameters for some typical objective lenses (After [5]).

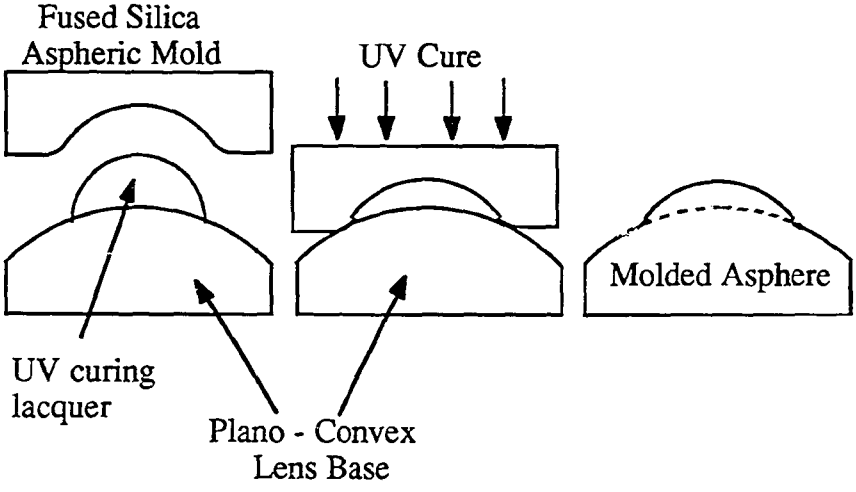

Figure 3.2 A hybrid asphere is formed by pressing a fused silica mold over a drop of UV curing lacquer placed on a plano-convex glass lens.

The resulting lens has an NA of 0.45, and a clear aperture of 3.6 mm and is corrected for a 1.2 mm thick polycarbonate cover plate. The RMS optical path difference was reported to be less than 0.045 waves at 780 nm. The mass was not reported, but if results are similar to the asphere discussed earlier, a lens with a 3.6 mm diameter would weigh 50 mg. From Equation 1.1, a reduction in stack height for the same number of disks in the stack due to the lens diameter reduction could improve the volumetric storage density by a factor of 1.25 compared to a "typical" system with an objective diameter of 4.5 mm.

Molded Refractive Microlenses

Fabrication and testing of refractive monolithic lenslet module (MLM) arrays has been reported [12]. MLM's are arrays of square, linear or heptagonal shaped aperture lenslets molded in epoxy on glass substrates. Lenslet sizes from 80 μm to 1 mm and numerical apertures up to 0.18 are reported. The metal master for the mold is fabricated by coining the pattern into high purity, polished material. Epoxy is then sandwiched between the mold and a glass substrate and cured. The mold surface may be either spherical or aspherical. Figure 3.3 illustrates this technique. Analysis predicts diffraction-limited spot sizes for on-axis illumination for up to 0.1 NA at 0.5 μm wavelength. The technique could be extended to fabricate aspheres by making the coining master in an aspheric configuration.

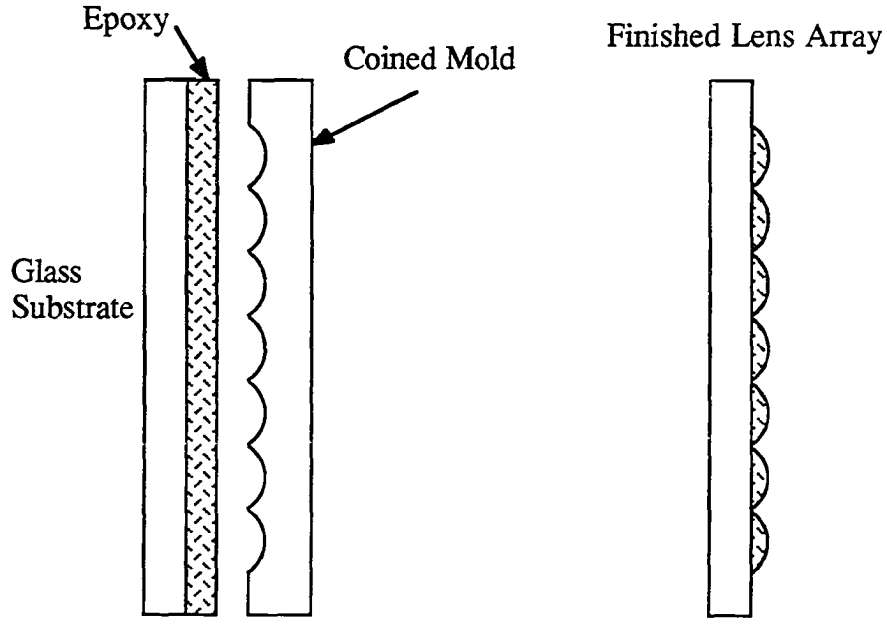

Figure 3.3 A monolithic lens module (MLM) was fabricated using a coined mold to impress a refractive lenslet array pattern into epoxy on a glass substrate. Lens sizes from 80 μm to 1 mm are reported [12].

For use in ODS, a single lens of this type could be made onto a thin substrate. A 1 mm diameter lens on a 100 μm thick glass substrate would weigh about 1.6 mg. The diameter reduction could provide a factor of 4.5 reduction in optical head height, and, therefore, a factor of 4.5 increase in volumetric data storage.

Luneburg Microlenses

A Luneburg, or distributed-index planar microlens, is a lens with an index of refraction that is radially symmetric. The index begins at a high value at the center and decreases to the index value of the substrate at the edge of the lens. The function that describes radial variation of the index is given by Equation 3.1, where n is the index of refraction at ρ, n_0 is the index of the substrate and ρ is the fractional radius. The numerical aperture of such a lens is proportional to the difference in index from the center to the edge of the lens.

$$n = n_0 \sqrt{2 - \rho^2} \qquad \text{Equation 3.1}$$

These lenses are typically fabricated in flat substrates, yielding hemispherical lenses. Two of these placed flat sides together will produce a spherical lens. Descriptions of fabrication and testing of these arrays has been reported in the literature [20,21].

An ion-exchange technique has been used to introduce the index gradient [13]. This technique is shown in Figure 3.4. A molten salt bath is prepared in adjacent cells separated by the substrate. The substrate is masked such that a pattern of circular holes allows contact between the substrate and the molten salt. A voltage is applied across the two cells, that introduces an ion exchange into the substrate. The result is a radially symmetric index variation closely approximating the ideal Luneburg distribution. Arrays with lens diameters from 0.25 to 2.0 mm and numerical apertures from 0.13 to 0.30 are reported for the hemispherical configuration, and between 0.20 and 0.54 NA for the stacked spherical array. A 0.9 mm diameter lens of 0.22 NA was tested to have a wave aberration of $< 0.25\ \lambda$ (p-v). A focus spot diameter of 3.8 μm at 633 nm was reported [13].

An ion exchange fabrication of microlens arrays with diameters of 10 - 1000 μm and 0.25 NA has been reported. This lens is described as producing 4.0 μm spot diameters at 633 nm [14]. Diffraction-limited performance was claimed, but, using Equation 1.4, diffraction-limited performance would exhibit a FWHM of less than 2 μm.

A distributed index microlens array using a plasma chemical vapor deposition (CVD) method has been reported [15]. Hemispherical holes are etched into a planar glass substrate. The holes are filled with thin layers of a combination of SiO_2 and Si_3N_4. These materials have different indices

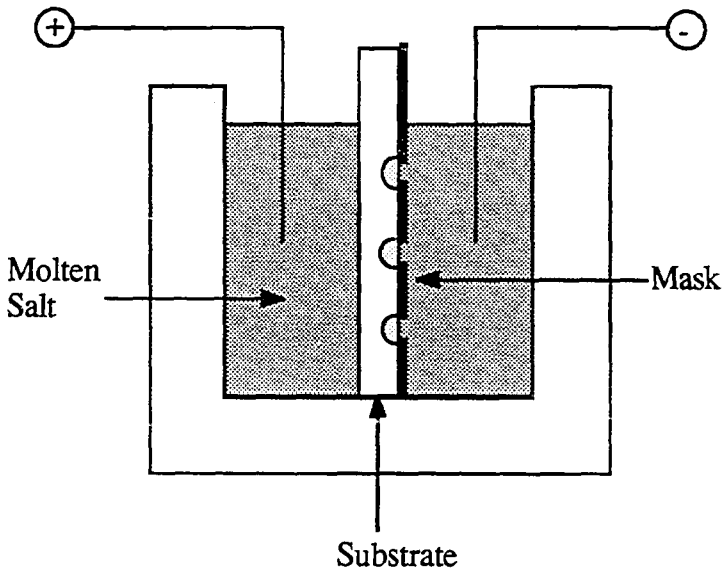

Figure 3.4 A Luneburg lens was produced by applying a voltage across a glass substrate immersed in a molten salt solution. This drives an ion exchange from the solution into the glass that produces a radial index variation in the substrate [13].

of refraction and the composition is varied from the outside shell to the center to produce a Luneburg index distribution.

For an ODS optical head, a lens should have at least a 0.5 NA. The Luneburg lenses only approach that NA for a spherical construction. Ray tracing has shown that the wave aberration remains below 0.25 λ (p-v) only for 0.15 NA or less [13]. While these lenses are attractive in terms of size and weight, the technology must mature further before it can be applied to ODS.

SMILE Lenses

A spherical micro integrated lens (SMILE) array has been described in the literature [16]. Each lens is a refractive microlens formed in plates of photosensitive glass (photosensitive glass is glass that undergoes a change in color after exposure to ultra-violet (UV) radiation and thermally cycled). A new class of these glasses has been developed that contains noble metal micro-particles [16]. They undergo a phase change as well as a color change. The phase change includes a change in density of the material. It was shown that if a plate of this new glass is masked with opaque dots, exposed to UV, and thermally cycled, the exposed glass shrinks. This shrinkage causes the unexposed cylindrical regions to be extruded such that surface tension forms a spherical surface relief of the ends of the unexposed cylindrical regions. A by product of the process is that the exposed region becomes optically dense, and can serve as an aperture. The process is summarized in Figure 3.5. The geometry is given by Equation

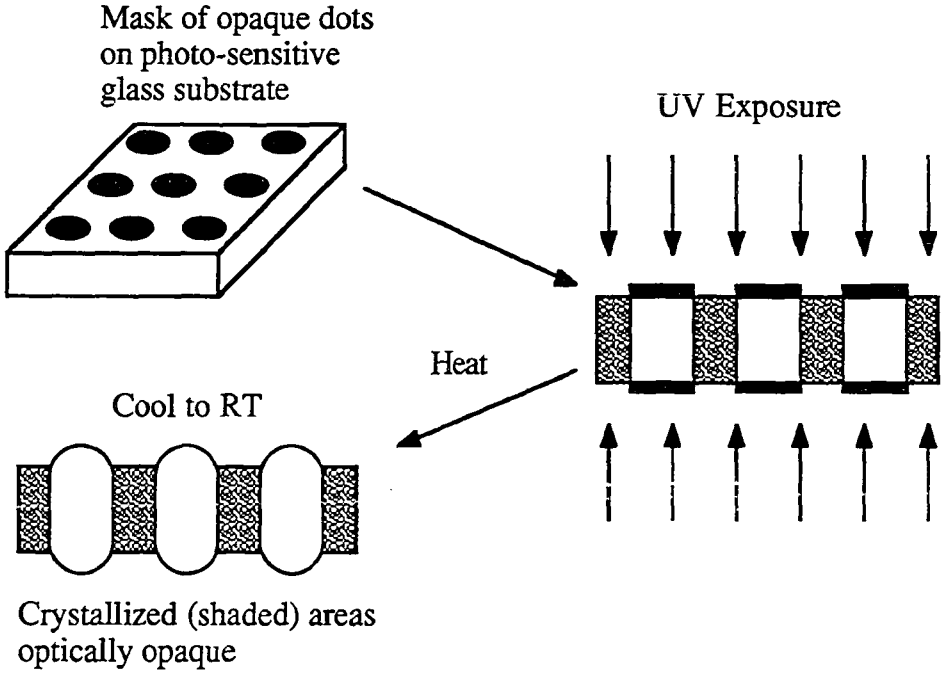

Figure 3.5 A SMILE lens was fabricated by masking a photosensitive glass plate with opaque chrome dots, then exposing to collimated UV, and heating to promote a density change in the unmasked region. As the glass cools, the unexposed region is squeezed to produce a spherical surface [16].

3.2, where δ is the height of the extruded region, T is the glass thickness, ρ is the unexposed glass density, and ρ_0 is the crystallized region density. The surface height is the sag of a spherical surface, and knowing the lens diameter will yield the radius of curvature and the power of the lens. Figure 3.6 shows the resulting lens in an electron micrograph and its measured profile.

$$\frac{\delta}{T} = \frac{2}{3}\left(1 - \frac{\rho}{\rho_0}\right)$$

Equation 3.2

Lenses from 150 to 500 μm in diameter were produced in arrays with center-to-center spacing of 1.2 diameters. With precision photolithographic techniques, a second mask was placed on the back side of the glass, and a symmetrical spherical surface was formed on the plate bottom. The sag was measured to be 26.6 μm for a lens diameter, 2r, of 400 μm. The radius of curvature, R, for this lens was calculated to be 765 μm using Equation 3.3. A plano convex lens would have an NA of 0.37 assuming an index of 1.5. Deviations from perfectly spherical geometry were shown interferometrically to be within 0.4 waves.

$$R = \frac{r^2 + \delta^2}{2\delta}$$

Equation 3.3

The size and mass of this lens is attractive for ODS, but an ODS objective must be able to offset the spherical aberration introduced by the disk cover plate, and the SMILE lens fabrication relies on surface tension for the lens

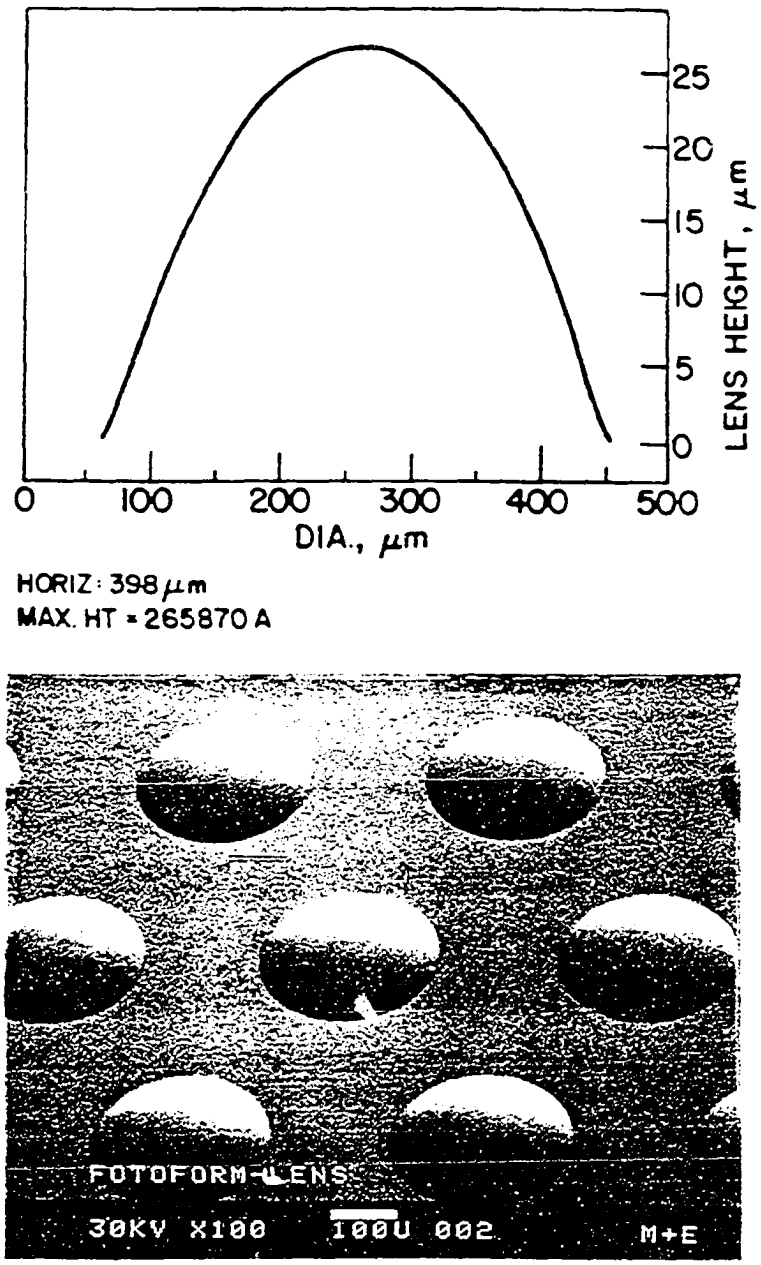

Figure 3.6 This scanning electron micrograph shows the extruded spherical surface profile of the SMILE lens. The results of a profilometer measurement of the surface profile are shown. An interferometer confirmed sphericity to within 0.4 waves. (After [16])

form. Currently, this cannot be adjusted to yield a desired aspherical surface.

Surface Melt Microlens

A process has been described that utilizes IC processing techniques to create spherical microlenses in photo resist [17]. Figure 3.7 depicts the process schematically. A quartz wafer is first coated with an aluminum film (2500 Å). An array of 15 μm diameter holes is etched through the aluminum. A 1 μm thick layer of photo resist is spun onto the wafer, and exposed and developed to leave 30 μm diameter, 1 μm thick pedestals sitting above the aluminum. A second and third layer of a different photo resist is spun on to a depth of 15 μm. The photo resist in these last layers has a melting temperature that is lower than the pedestal photo resist. The wafer is exposed and developed to leave 25 μm diameter pedestals on top of the 30 μm pedestals. The wafer is then heated to a temperature that melts the photo resist in the 25 μm pedestals, but does not affect the 30 μm pedestals. As the photo resist melts, it fills out to the edge of the larger pedestal and stops moving outward. Surface tension dictates that the melted surface is spherical as it cools.

The focus spot intensity profile was measured and the FWHM was 1.2 μm at 730 nm in quartz. The focal length was determined to be 36 μm in quartz (n=1.455), and the aperture was 15.8 μm diameter. Equation 3.4 was used to determine the diffraction-limited FWHM spot size, where $d_{1/2}$ is the diffraction-limited focal spot FWHM, R=radius of the clear aperture

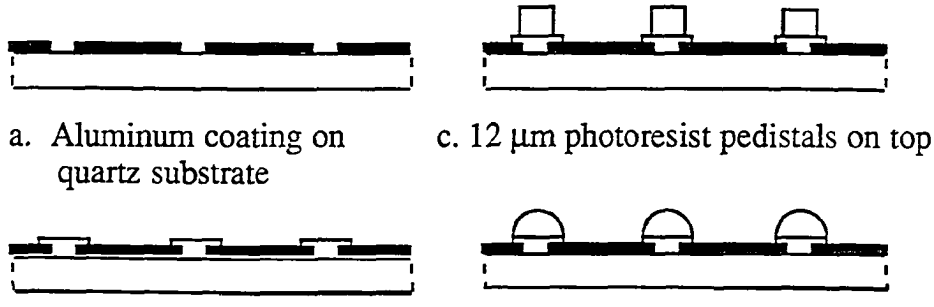

a. Aluminum coating on quartz substrate

c. 12 µm photoresist pedistals on top

b. 1 µm photoresist pedistals

d. Heating melts thick pedistals and forms spherical surfaces

Figure 3.7 A microlens was fabricated using IC manufacturing techniques. Photo resist was melted to form perfectly spherical lenslet arrays (a,b,c,d). An SEM micrograph shows the lens array. (After [17])

of the lens. For this experiment, a diffraction-limited FWHM of 1.2 μm was calculated, agreeing with experiment. Focal length uniformity for the 6 x 7 arrays was ± 0.5 μm. An SEM micrograph of the lens array is shown in Figure 3.7. The NA of these lenses could be increased for ODS applications, but, as with the SMILE lens, the technique cannot produce aspherical surfaces of a prescribed figure at this time.

$$d_{1/2} = 0.514 \frac{\lambda f}{n(R)}$$

Equation 3.4

Fresnel Lenses

A Fresnel lens is a flat version of a conventional spherical or aspherical lens. An ideal Fresnel lens performs exactly the same as a conventional lens but has reduced mass. This is accomplished by reproducing the phase function of a lens in a series of stepped and setback annular zones, as shown in Figure 3.8 . Optical properties of the original spherical or aspherical lens are reproduced by the planar lens. When used as an objective lens, the Fresnel lens focuses light to a diffraction-limited spot at the focal point of the lens, as shown in Figure 3.9.

Let the lens have a focal length, f, a radius, r_{max}, a thickness, T(r) and let the radius of the m^{th} zone be r_m. Each consecutive zone is defined as the radial location where the phase difference between the converging spherical wave and the planar surface is 2π, as shown in Figure 3.10.

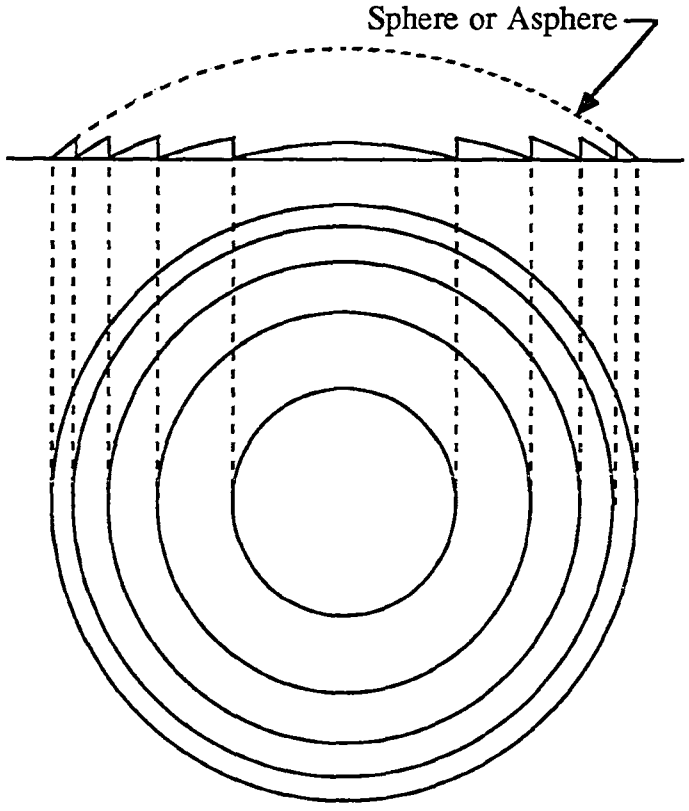

Figure 3.8 A conventional spherical or aspherical lens can be planarized into a Fresnel lens.

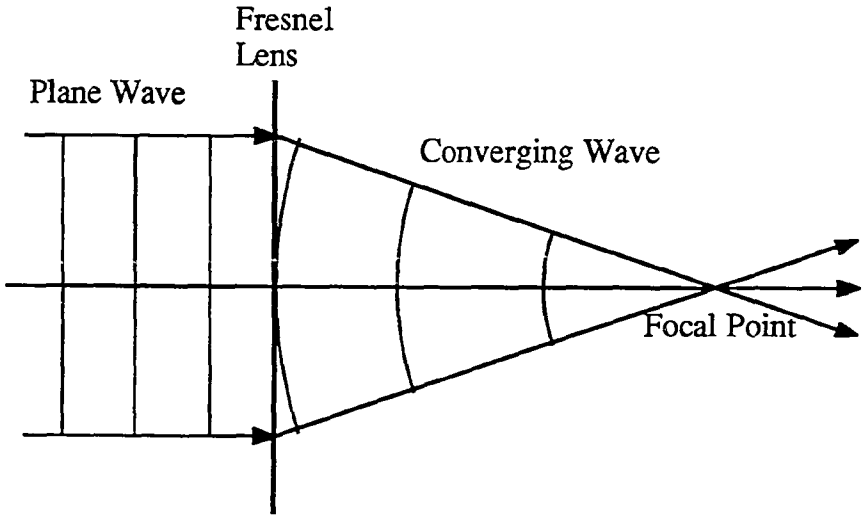

Figure 3.9 A Fresnel lens focuses a plane wave at the focal point.

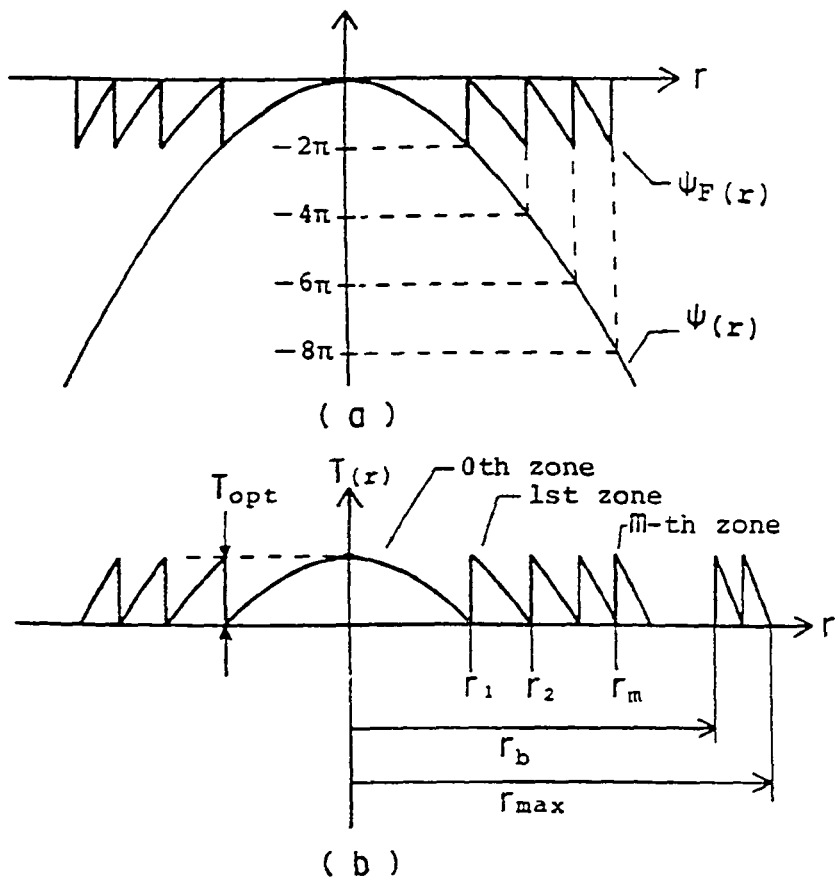

Figure 3.10 The phase shift function of the Fresnel lens (a) and the thickness distribution (b) (after [23])

The phase is given as

$$\Psi = \left[f - \sqrt{f^2 + r^2} \right] \frac{2\pi}{\lambda},$$

where Ψ is the phase and λ is the wavelength. For a phase lens made from a material of index n, the thickness as a function of radius is given by Equation 3.5, when $r^2 << f^2$.

$$T(r) \approx \frac{\lambda}{(n-1)} \left\{ 1 - \frac{r^2}{2\lambda f} \right\} \qquad \text{Equation 3.5}$$

The m$^{\underline{th}}$ Fresnel zone radius is given by Equation 3.6.

$$r_m \approx \sqrt{2\, m\, \lambda\, f} \qquad \text{Equation 3.6}$$

For a lens of maximum radius, R, the total number of zones in the lens, M, is given as

$$M = \frac{R^2}{2\,\lambda\, f},$$

and, for f>>R, the numerical aperture can be approximated as R/f and is given as

$$NA = \frac{2M\lambda}{R}$$

The smallest zone of a Fresnel lens is at the edge of the lens and is given as $r_M - r_{M-1}$. Since $\lambda f << R^2$, the smallest zone width, ε, of the lens is given by Equation 3.7.

$$\varepsilon \approx \frac{\lambda}{NA} \qquad \text{Equation 3.7}$$

A Fresnel lens is ideally constructed by a process with the capability to produce smoothly curved structure across the entire lens. From Equation 3.7, the minimum Fresnel zone width at 0.8 μm wavelength is 1.6 μm for a 0.5 NA lenslet (1.2 μm from an exact calculation). To make the lens surface continuous and smooth, the fabrication process resolution must be significantly smaller, perhaps 0.16 μm for a true Fresnel lens. This fine resolution is a challenge for any method of fabrication.

Two different types of lenses based on Fresnel zones are possible. The first, called the Fresnel lens, was described earlier and shown in Figure 3.8. It is a refractive element that focuses light by refracting rays according to Snell's law. The second type of lens is the Fresnel zone plate (FZP). This lens focuses light according to diffraction theory. Both lenses share the same zone locations. In the FZP, each zone is sectioned into two halves. Half is opaque, the other half is clear. The FZP diffracts the light to focus like a linear grating that has been circularized.

The diffraction efficiency of such a lens is defined as the ratio of the power diffracted into the $+1^{st}$ order (the power focused at f) to the total collimated power incident on the lens. Ideally, the diffraction efficiency of a Fresnel lens can be 100%, i.e. no loss. However, a perfect FZP has a diffraction efficiency of only 40% [18].

Another lens type has been developed that is a cross between the Fresnel lens and the FZP. Through the use of planar etching techniques used in IC technology, smooth Fresnel lenses have been approximated by a series of discontinuous planar steps. Such a lens is shown schematically in Figure 3.11. An equation was developed that gives the diffraction efficiency, η, of a stepped Fresnel lens as a function of the number of sub-levels, N, in each zone and is given here as Equation 3.8 [18]. This equation shows that for a binary (2 level) phase plate, the best efficiency obtainable is 40.5%. A 4 level lenslet can be 81% efficient and an 8 level lenslet can be 95% efficient. Thus, almost any desired efficiency can be obtained if the methods producing the lens are good enough. Equations 3.6 and 3.7 are now modified to include the number of discrete levels and are given as Equations 3.9 and 3.10. Thus, to fabricate a 0.5 NA lens for use at 0.8 μm with 95% diffraction efficiency, the smallest feature size would be 0.24 μm.

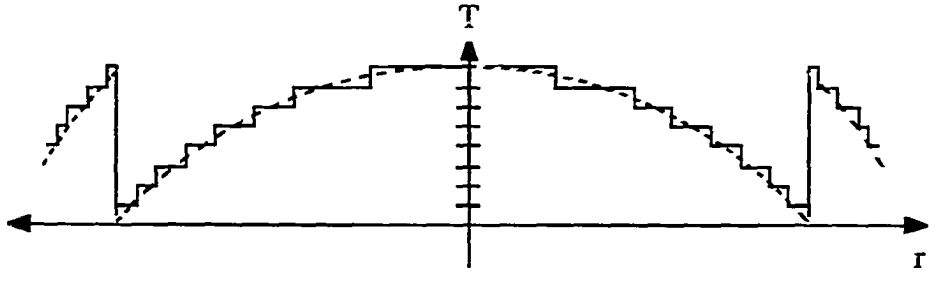

Figure 3.11 An 8 level discrete stepped approximation to a smooth curved surface can produce a diffractive lens that is 95 % efficient.

$$\eta = \left\{ \frac{\sin\left[\frac{\pi}{N}\right]}{\frac{\pi}{N}} \right\}^2$$

Equation 3.8

$$r_m \approx \sqrt{\frac{2\,m\,\lambda\,f}{N}}$$

Equation 3.9

$$\varepsilon \approx \frac{\lambda}{N\ NA}$$

Equation 3.10

The discrete sub-zone approach has been given the generic names, "binary optics" and "etched planar microoptics" in the literature [19]. This type of lens can be fabricated using modern techniques such as photolithography and electron beam writing. These techniques are discussed separately below.

Photolithographic Fabrication of Micro-Fresnel Lenses

Fresnel microlenses fabricated using photolithographic techniques have been reported in the literature [19,20,21]. A linear array of 8-level rectangular aperture microlenses used to collimate laser diodes was described [19]. The microlens apertures are 100 x 200 μm with circular Fresnel zones. Their technique employed a computer-controlled electron-beam (E-beam) writer to generate a series of three masks used in photo-pattern and etch processing. Figure 3.12 shows the mask and etch steps. To collimate a typical diode laser, the lenses must have an NA of about 0.3. For a radius of 200 μm, and an NA of 0.3 and 8 levels, Equation 3.10

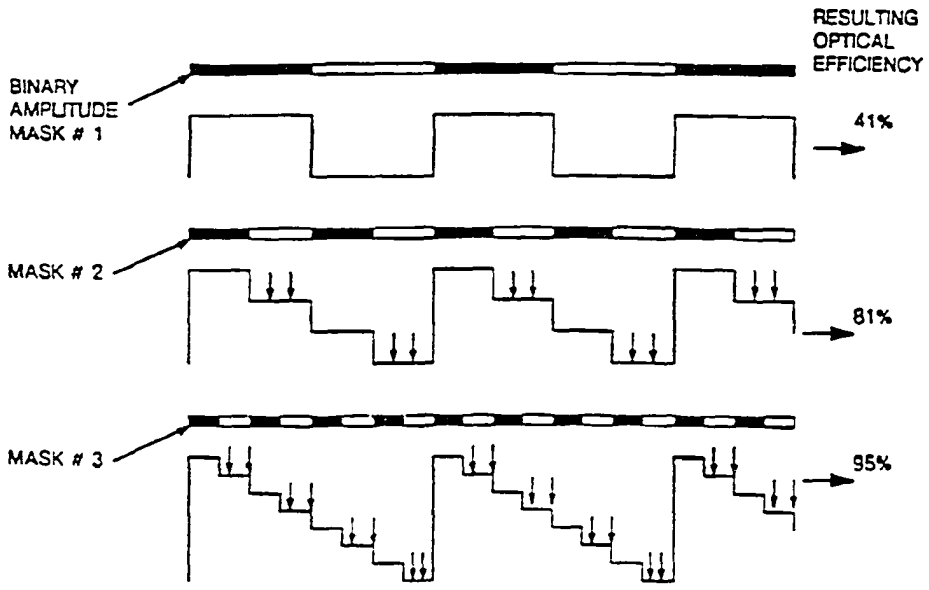

Figure 3.12 An 8 level etched planar microlens is fabricated using 3 photo-mask and etch steps. (After [19])

yields a minimum feature size of 0.33 μm. The minimum feature size reproducible using this technique is 0.4 μm [20]. This value is a result of summing a mask error of 0.1 μm, an exposure and development inconsistency error of 0.2 μm and an alignment inaccuracy of 0.1 μm. Based on this error analysis, the photolithographic fabrication technique would not be able to produce a 95% efficient, 0.5 NA, 1 mm diameter lens.

Because the lens masks are computer generated, the lenses can take on almost any form required to correct a known aberration. Many different aberrations can be corrected, including spherical aberration. This is a very powerful capability and is potentially important for ODS applications.

A 4 level, one dimensional array of etched planer microlenses for collimating an array of laser diodes was fabricated and tested [20]. The lenslets were 50 μm diameter and were also designed to remove 1.23 waves of astigmatism present in the laser diodes. This was accomplished by designing the lens to provide different focal lengths in the sagital and tangential planes. Equation 3.11 describes the quantized version of the transmission function necessary to remove the astigmatism [20]. In this equation, f_1 is the focal length in the tangential plane, f_2 is the focal length in the sagital plane, k is $2\pi/\lambda$, r and θ are the radial coordinates of the zone edge. The locus of points (r,θ) that satisfy Equation 3.11 describe the boundaries between the zones of the lens. The result of the design was that lenslets were elliptical in shape instead of circular.

$$k\sqrt{f_1^2 + r^2} + \frac{k}{2f_2} r^2 \sin^2\theta = n\pi + kf_1 \qquad \text{Equation 3.11}$$

The lenses were fabricated using E-beam mask generation and photolithographic mask and etch techniques. The diffraction efficiency was measured to be 80% in the central f/4.4 region and 52% in the f/1 aperture. The reduction in performance was explained as a result of the mask production, alignment and exposure and etch errors manifesting themselves in the region where the zone size approaches the fabrication error tolerance. Equation 3.10 estimates that the minimum feature size for their 4 level, 0.5 NA, 50 μm diameter lens would be 0.4 μm. The finished lenses were reported to collimate the lasers with only a 0.016 wave RMS error.

Mass-Transport Microlenses

A mass transport process for fabricating microlenses that improves diffraction efficiency has been demonstrated [22]. Etched planar microlens structures are produced using a photolithographic technique, and then the discrete structure is smoothed into a into a refractive element using a mass transport process, as shown in Figure 3.13. The step radii and depths are not designed as they would be for ideal etched planar lenses. Instead, they are designed to provide the desired refractive surface profile after the mass transport process takes place.

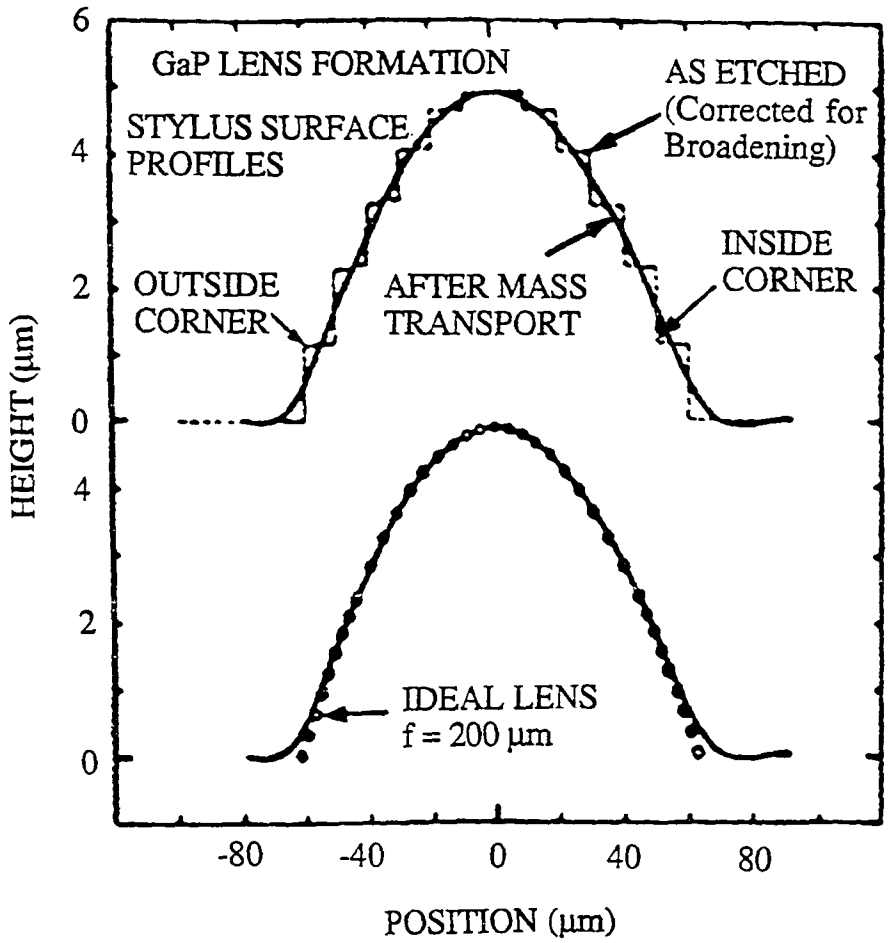

Figure 3.13 A mass-transport process is used to convert a stepped, diffractive microlens into a smooth refractive microlens. The process induces free atoms that are located in regions of high surface energy (high positive curvature) to move to areas of low surface energy (high negative curvature) (After [22]).

In this process, free atoms at the surface of the lens material are produced through surface decomposition at elevated temperature. The concentration of free atoms is highest in areas of high positive surface curvature, because the surface energy associated with high surface curvature translates into lower binding energy. The atoms of low binding energy tend to become unbound, or "free" atoms during the decomposition process. The mass transport occurs when the free atoms in areas of high surface energy re-locate to areas of low surface energy. The sharp corners of the etched, planar microlens are smoothed as atoms travel from outside corners (high surface energy) to inside corners (low surface energy) to obey the law of conservation of mass. As the process continues, the structure becomes smoother and smoother. Finally, the surface energy equalizes, and the process slows by orders of magnitude. Because the process is essentially self-limiting, it is highly repeatable.

The resulting lens is formed in GaP and InP substrates ($n \approx 3$) that are transparent for wavelengths larger than 0.55 μm and 0.93 μm respectively. The authors report diffraction-limited performance at 0.45 NA with diameters between 60 and 130 μm. This technique could be used to create a lens that has a controllable aspherical profile. Such a microlens would be a reasonable choice for ODS applications. The capability of producing such small diameters monolithically integrated with diode lasers make these lenses strong contenders for the optical slider head design discussed in Chapter I.

Direct Electron Beam Fabrication of Micro-Fresnel Lenses

An E-beam can be used to write lenses directly into E-beam resist, eliminating mask alignment and exposure errors associated with photolithographic techniques, as well as eliminating several steps in the process. An E-beam writer has the capability of controlling the dose level of the beam at any location during the writing process. This capability allows one to adjust the exposure depth, and thus the etch depth, in the resist. The E-beam focuses to a 0.2 μm diameter spot, which, potentially, is the minimum feature size of a lens. Since the E-beam head is computer controlled, radial steps of 0.2 μm or smaller can be taken across the entire lens aperture. By taking advantage of the fine stepping and dose control, it is possible to fabricate a refractive Fresnel lens in E-beam resist, with a diffraction efficiency of nearly 100%. This technique is shown schematically in Figure 3.14. This technique has been used to fabricate Fresnel lenses and gratings [23]. One lens was reported to have a 1 mm diameter, and a 5 mm focal length. The diffraction efficiency was 60% and the average wavefront aberration was 0.054 waves at 6328 nm. Because the fabrication process is completely computer controlled, it is possible to design and fabricate a lens that can correct almost any aberration present in a system.

An application of the E-beam technique, where the master is fabricated using direct E-beam writing, and many other lenses are made through molding from the master has been reported [24]. The master micro-

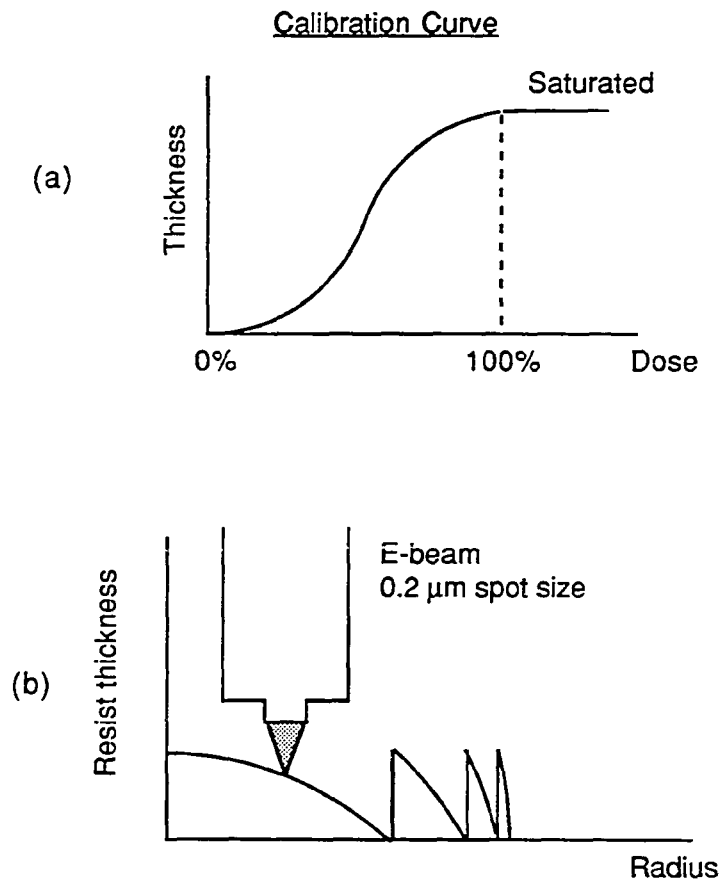

Figure 3.14 A calibration curve can be developed relating the etched resist thickness to the E-beam dose (a), that will yield high quality, high efficiency, refractive micro-Fresnel lenses (b).

Fresnel lens had an NA of 0.25, and a 0.5 mm lens diameter and was designed to work at 0.8 μm as a compact disk objective lens. As shown in Figure 3.15, a negative of the master was made using an electro-forming technique, and was inserted into a stamper. The stamper was pressed against a glass substrate with a layer of UV curing resin on it. The resin was cured and the nickel mold was removed. The resulting lenses were reported to have a 0.038λ rms wave aberration and 50% diffraction efficiency, the same as the master lens.

To summarize, Fresnel lens technology is very attractive for producing aberration-corrected, high efficiency, small, and lightweight objective lenses for ODS. Lens sizes from 50 μm diameter have been demonstrated and the mass is potentially insignificant. While the photolithographic techniques offer high efficiency and error correction, the process is not accurate enough to produce the minimum feature sizes needed for a 1 mm diameter, high NA objective lens. The E-beam technique solves this problem and can produce high efficiency lenses in a single step process. Both techniques would lend themselves to a molding process to reduce fabrication costs of the lens.

Summary

This chapter discussed several different types of microlenses and compared them to a conventional ODS objective lens in terms of performance, size, mass and manufacturability. Based on a criteria that desires to minimize

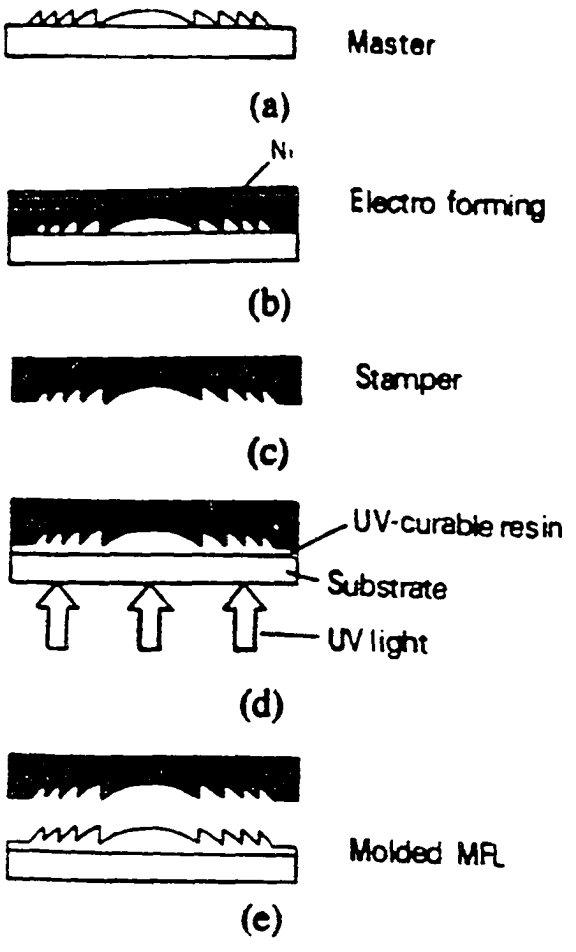

Figure 3.15 A molded micro-Fresnel lens was fabricated using a master created using direct E-beam writing. A nickel negative was made of the master and became a mold that formed UV resin on a glass substrate into inexpensive reproductions of the master.(After [24])

the access time of an ODS system by reducing the lens mass and maximize the volumetric storage density, many of the lenses discussed would show large potential improvements over the conventional objective. In terms of aberration correction and ease of fabrication, the Fresnel lenses have an advantage over all of the others. The most promising, highest accuracy and simplest fabrication technique for a micro-Fresnel lens is a direct E-beam writing technique. To minimize costs, the lens could be used to mold many plastic lenslets, rather than writing each lens individually.

CHAPTER IV

DESIGN OF A FRESNEL MICROLENS ON A SPHERICAL SHELL SUBSTRATE

Chapter II described why a microlens must perform over a larger range of viewing angles than a conventionally sized objective lens. Chapter III introduced several different types of microlenses that could be used as objective lenses in optical data storage. It was shown that it is possible to design and fabricate a Fresnel lens that corrects for spherical aberration introduced by the cover plate. This chapter analyzes off-axis aberrations of a flat Fresnel lens. It then introduces the concept of placing a diffractive Fresnel zone plate on a hemispherical shell substrate (spherical FZP) to reduce off-axis aberrations. The off-axis aberrations for this type of lens are derived. Finally, an analysis is performed to determine the acceptable range of spherical FZP fabrication tolerances.

Off-Axis Aberrations of Fresnel Zone Plates

A Fresnel zone plate images collimated light into several diffractive orders. The 0th order passes through the lens unchanged except in amplitude. The -1st order diverges from an imaginary object located at $-f$ along the Z axis, while the +1st order converges to $+f$ on the Z axis, as shown in Figure 4.1. Off-axis aberrations such as coma, astigmatism and field curvature are introduced when the collimated beam is incident from an off-axis angle.

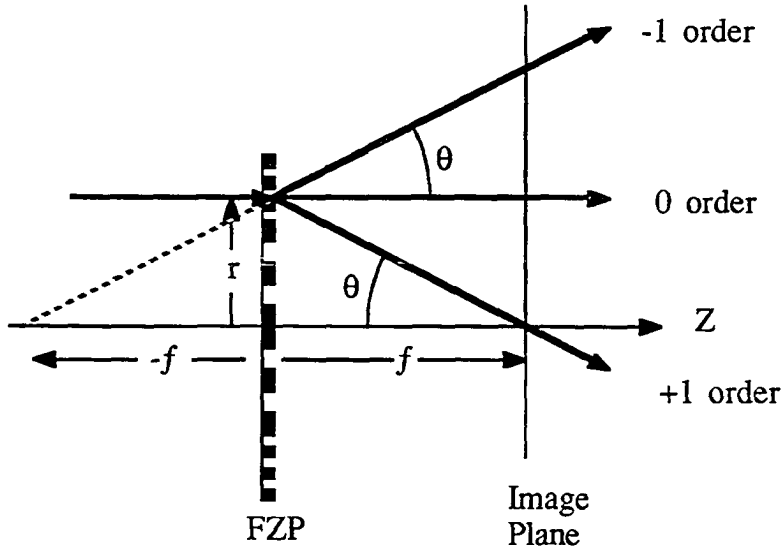

Figure 4.1 A Fresnel zone plate images collimated incident light into several diffractive orders. An ideal zone plate focuses collimated light to an aberration-free image in the focal plane located at f along the Z axis.

These aberrations reduce the spot quality by removing energy from the center of the diffraction spot and relocating it to the outer edges. The result is an increased focused spot size. Figure 4.2 illustrates the geometry of the FZP for an incident beam tilted an angle, α, relative to the lens axis. Only the +1st order is shown.

The off-axis aberrations of a FZP have been derived in the literature [25]. The setup and results of that derivation follows. From Figure 4.2, it can be seen that the line segments, S_1 and S_2, may be defined as follows:

$$S_1 = r_n \sin \alpha$$

$$S_2 = \sqrt{(r_n - f \tan \alpha)^2 + f^2} \quad ,$$

where r_n is the radius of the nth Fresnel zone.

Also, the optical path difference (OPD) between the chief ray and the edge ray is given as:

$$OPD = S_1 + S_2 - d \quad .$$

By making a small field angle approximation and truncating the series approximation of the square root to three terms,

$$\sqrt{1 + x} \approx 1 + \frac{x}{2} - \frac{x^2}{8} \quad ,$$

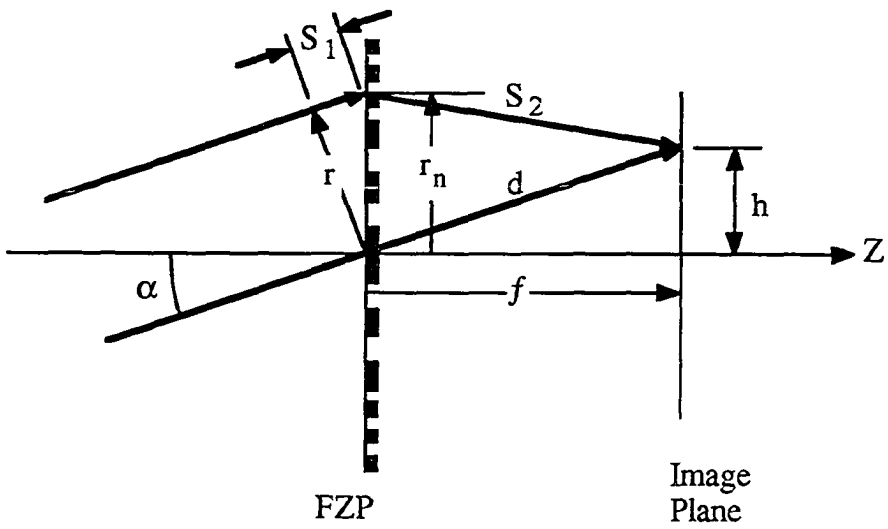

Figure 4.2 When the incident collimated beam is tilted, the +1st order is focused to an off-axis spot and is aberrated.

one may derive the following expression describing the optical path difference between the edge and axial rays:

$$OPD \approx -\frac{r_n^4}{8f^3} + \frac{r_n^2}{2f} + \frac{r_n^3\alpha}{2f^2} - \frac{3\, r_n^2\, \alpha^2}{4f}$$

Rearranging the terms yields:

$$OPD \approx \frac{r_n^2}{2f} - \frac{r_n^4}{8f^3} + \left[\frac{r_n^3\alpha}{2f^2} - \frac{r_n^2\, \alpha^2}{2f} - \frac{r_n^2\, \alpha^2}{4f} \right] \qquad \text{Equation 4.1}$$

When the radius of the nth zone of a Fresnel lens was defined in Equation 3.6, only the first two terms of the square root approximation were retained. If three terms are kept, the radius of the nth zone is given by Equation 4.2 for a two-level zone plate.

$$\frac{n\lambda}{2} \approx \frac{r_n^2}{2f} - \frac{r_n^4}{8f^3} \qquad \text{Equation 4.2}$$

Therefore, the first two terms in Equation 4.1 are equal to $n\lambda/2$. The form of the remaining terms in Equation 4.1 are similar to Seidel aberration coefficients and are defined as follows:

$$\text{coma} = \frac{r_n^3\alpha}{2f^2}$$

$$\text{astigmatism} = \frac{r_n^2 \alpha^2}{2f},$$

$$\text{field curvature} = \frac{r_n^2 \alpha^2}{4f}.$$

It can be shown that, if the image surface were a sphere with negative radius of curvature, $-f$, the field curvature would be identically zero for all field angles.

The wavefront aberrations from Equation 4.1 are plotted as a function of the field angle in Figure 4.3 for a lens of 1 mm diameter, and a 0.5 NA. The limiting aberration over the field of interest is coma. One criterion for determining the quality of a focal spot is the Rayleigh limit. This is the point where the aberration contributes more than 0.25λ departure from an ideal spherical wavefront. The Rayleigh limit is reached at a field angle of only 0.13º for coma, 2.1º for astigmatism, and 3.0º for field curvature. At a field of ±3.3º (the minimum tilt required for a 0.5 NA, 1 mm diameter lens to maintain a ± 30 track field), the coma is 6.11 waves, the astigmatism is 0.610 waves, and the field curvature is 0.305 waves. From these results, the FZP microlens is not acceptable for use as an objective in an ODS system. The useable field angle is too small.

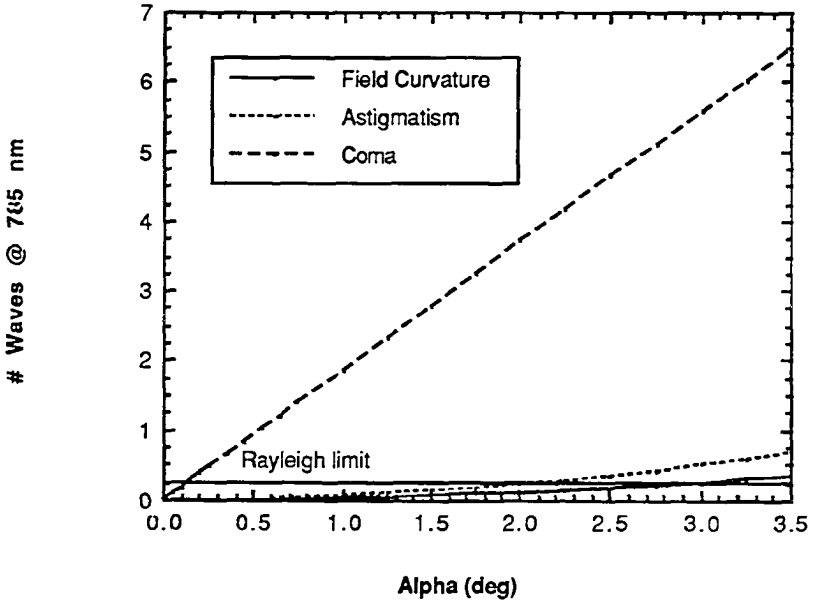

Figure 4.3 The wavefront aberrations of a 0.5 NA, 1 mm diameter Fresnel zone plate are plotted versus field angle, α. The limiting aberration is coma.

Off-Axis Aberrations of a Spherical Fresnel Zone Lens

A modification of the Fresnel zone plate was introduced in the literature [26]. By placing a hologram, or FZP, of focal length f on the surface of a zero power spherical shell with radius of curvature f, one can form coma-free images of collimated sources over all field angles. A derivation of the off-axis aberrations of the spherical FZP follows.

Figure 4.4 illustrates the geometry of a spherical Fresnel zone plate. The line segments, S_1, S_2, S_3, and d may be defined as:

$$S_1 = \left\{ r_n - \left[f - \sqrt{f^2 - r_n^2} \right] \tan\alpha \right\} \sin\alpha \quad ,$$

$$S_2 = \frac{f - \sqrt{f^2 - r_n^2}}{\cos\alpha} = \sqrt{1 + \tan^2\alpha} \left(f - \sqrt{f^2 - r_n^2} \right) \quad ,$$

$$S_3 = f \sqrt{1 - \frac{2\, r_n}{f} \tan\alpha + \tan^2\alpha} \quad ,$$

$$d = \frac{f}{\cos\alpha} \quad ,$$

and the OPD is

$$OPD = S_1 + S_2 + S_3 - d \quad .$$

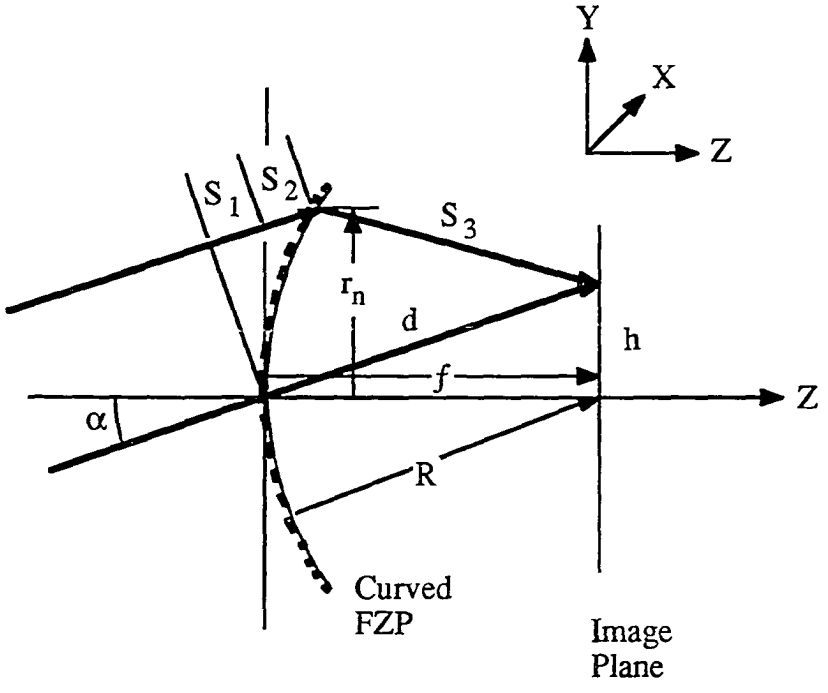

Figure 4.4 A Fresnel zone plate placed on a zero-power hemispherical surface whose radius of curvature is the same as the focal length of the zone plate, is coma-free for collimated light incident at any field angle.

After making approximations similar to those made in deriving Equation 4.1, these expressions may be simplified and combined to derive Equation 4.3, which describes the wave aberration of a spherical FZP.

$$OPD \approx \frac{r_n^2}{2f} - \frac{r_n^4}{8f^3} - \left[\frac{r_n^2 \alpha^2}{2f} + \frac{r_n^2 \alpha^2}{4f} \right] \qquad \text{Equation 4.3}$$

The result is identical to equation 4.1, except that the coma term is missing. Only field curvature and astigmatism are left. Similarly to the flat FZP, it can be shown that, for a spherical image surface, the field curvature is identically zero over all field angles for the spherical FZP. Therefore, the limiting off-axis aberration is astigmatism. With the absence of coma, the Rayleigh limit is not exceeded until a field angle of 2.1 º, an improvement in usable field of a factor of 16 over the planar FZP.

Tolerance Analysis of a Spherical Fresnel Zone Lens

A spherical Fresnel zone lens has been shown to be a good microlens choice for ODS based on size and aberration performance. However, the equations derived for describing off-axis aberration performance do not indicate how the performance would suffer if the focus of the zone lens was not located precisely at the center of curvature of the hemispherical substrate, which could happen during fabrication of a real lens. To determine the effects of a possible misalignment of this type, a tolerance analysis was performed [27]. Types of alignment errors include:

i) A radial misalignment, ΔX or ΔY, of the FZP focus relative to the sphere center

ii) A longitudinal misalignment, ΔZ, of the FZP focus relative to the sphere center .

The Code V optical modeling program was used to perform this tolerance analysis. The code has the capability of modeling a Fresnel zone plate by using a holographic optical element (HOE). This element is formed by Code V by interfering two ideal point sources on a specified surface. The resulting fringe pattern are Fresnel zones and can be inserted into an optical system, played back, and the resulting focal spot can be analyzed. For this analysis, the HOE was created by interfering a point source at Z = - infinity with a point source at the center of a hemispherical shell opening toward Z = + infinity. (Refer to Figure 4.4 for the coordinate system.) To model the effect of a FZP focus misalignment, the point source at the hemisphere center was moved by small amounts in the X direction, ΔX, Y direction, ΔY, and Z direction, ΔZ. HOEs were created with varying amounts of alignment error and played back at various different field angles. As each perturbation was analyzed, the focal plane was allowed to move along the Z axis to optimize focal spot quality. This is reasonable, since if used in ODS, the focus servo would act as a focus optimization.

The resulting focal spots were analyzed by Code V. The quality of the focal spots were described by the Strehl ratio and the wavefront aberration values. The Strehl ratio is defined as the ratio of the maximum irradiance

in the central diffraction spot to the theoretical maximum in the absence of aberrations. For ODS, the focal spot is considered to be diffraction limited when the Strehl ratio is above 0.9 [2]. A less restrictive definition states that the spot is diffraction limited when the rms wavefront aberration is less than 0.07 waves. The Rayleigh limit (0.25 waves) is an even less restrictive aberration level.

Because a proof-of-principle spherical FZP was to be made by interfering a plane and spherical wave at 442 nm in photo resist on a 1 mm diameter hemispherical shell, the modeling and tolerance analysis was also done for these parameters. Figure 4.5 is a plot of the Strehl ratio versus the ΔX alignment error for a 2.5º field angle. The spot remains diffraction limited ($SR \geq 0.9$) with a 2.5º field for ΔX errors between -21 and 0 μm. It is interesting to note that, for no misalignment, i.e. $\Delta X = 0$, the Strehl ratio is only 0.885. The analysis plane locates itself to maximize the Strehl ratio. Since the image is a diffraction spot and has no height, the field curvature aberration does not add to the Strehl ratio . Therefore, any remaining aberration is due to coma or astigmatism. Since it has been shown that this geometry is coma free for all field angles, the reduction of the Strehl ratio at a field of 2.5º for $\Delta X=\Delta Y=\Delta Z=0$ is due to the presence of astigmatism. It may also be noted from Figure 4.5 that the Strehl ratio is equal to 1 for a misalignment of -10.9 μm.

The Strehl ratio and wave aberration are plotted against field angle for -10.9 μm ΔX alignment error in Figure 4.6. This figure shows two field

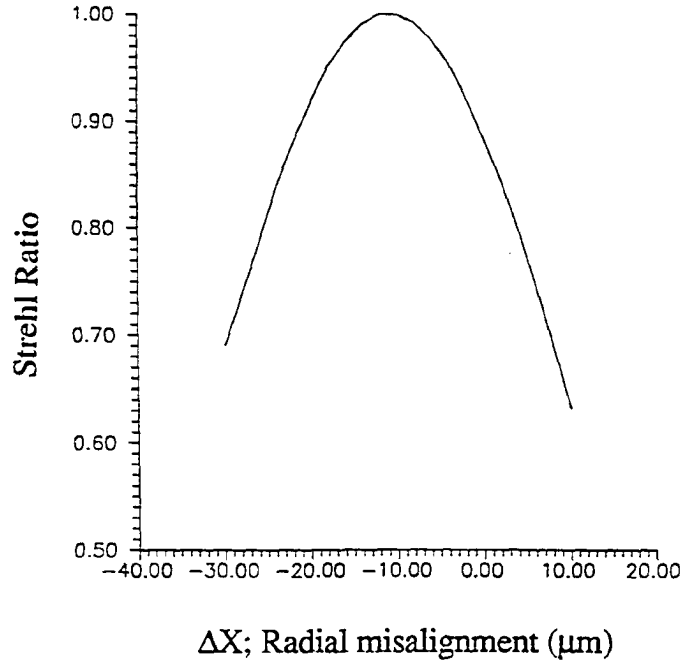

Figure 4.5 The Strehl ratio is plotted against the ΔX alignment error between the spherical FZP focus and the hemispherical substrate center of curvature for a 2.5º incident collimated field angle [27].

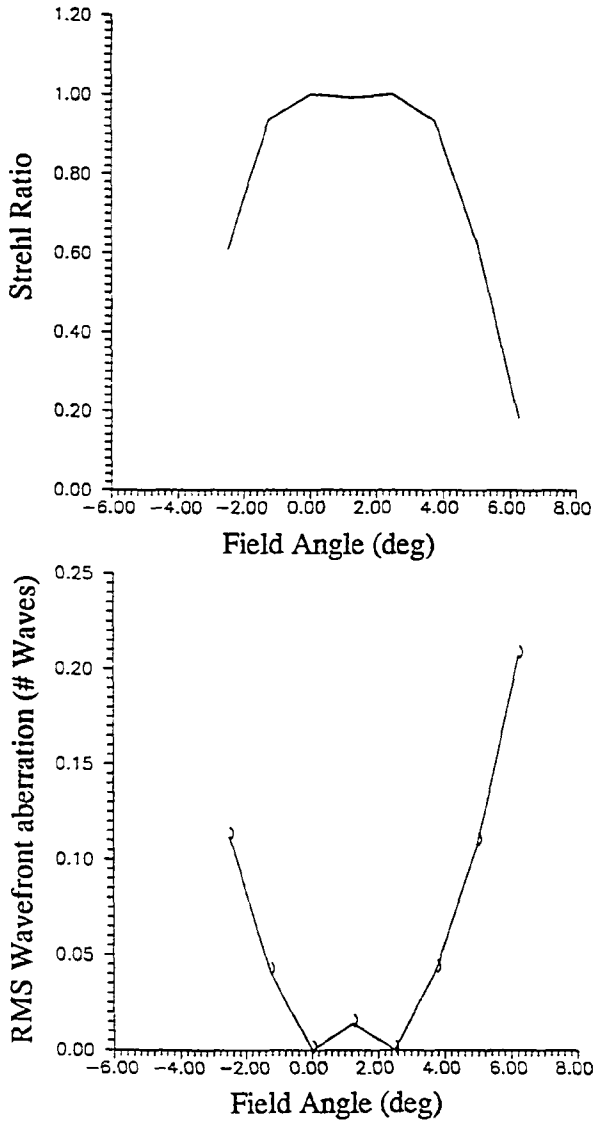

Figure 4.6 The Strehl ratio and the rms wavefront aberration are plotted versus field angle for a 10.9 μm. ΔX alignment error between the spherical FZP focus and the hemispherical substrate center of curvature. The two field angles where the rms wavefront aberration is zero indicate bi-nodal astigmatism [27].

angles that produce a focal spot with a unity Strehl ratio. This property of a decentered optical system where the Strehl ratio is unity for two different field angles is called bi-nodal astigmatism. Figure 4.7 shows the astigmatic line image plotted versus the field angle for a -10.9 μm ΔX alignment error. The astigmatism is minimum at two locations; 0º and 2.5º. For a given ΔX error of 10.9 μm, the spot remains diffraction limited over a range of field angles between -1.3º and +3.9º.

Figure 4.8 shows the Strehl ratio and the wavefront aberration plotted versus various ΔY alignment errors for a 2.5º field in the X-Z plane and no ΔX misalignment. Again, the Strehl ratio is 0.885, and the wavefront aberration, ΔW, is 0.056 waves for no misalignment. ΔW climbs above 0.07 waves after 8 μm of ΔY misalignment.

Figure 4.9 shows the Strehl ratio and the rms wavefront aberration plotted versus ΔZ misalignment, for a 2.5º field and no other misalignments. The Strehl ratio is 0.885 for ΔZ=0, which is worse than the diffraction limit defined for ODS. ΔW is at its minimum value of 0.056 for ΔZ=0, and becomes larger than 0.07 waves when the axial misalignment is worse than -42 μm or +75 μm.

Summary

Off-axis performance of the planar Fresnel zone plate was shown to be limited by coma. The Rayleigh limit was surpassed at only 0.13º field for

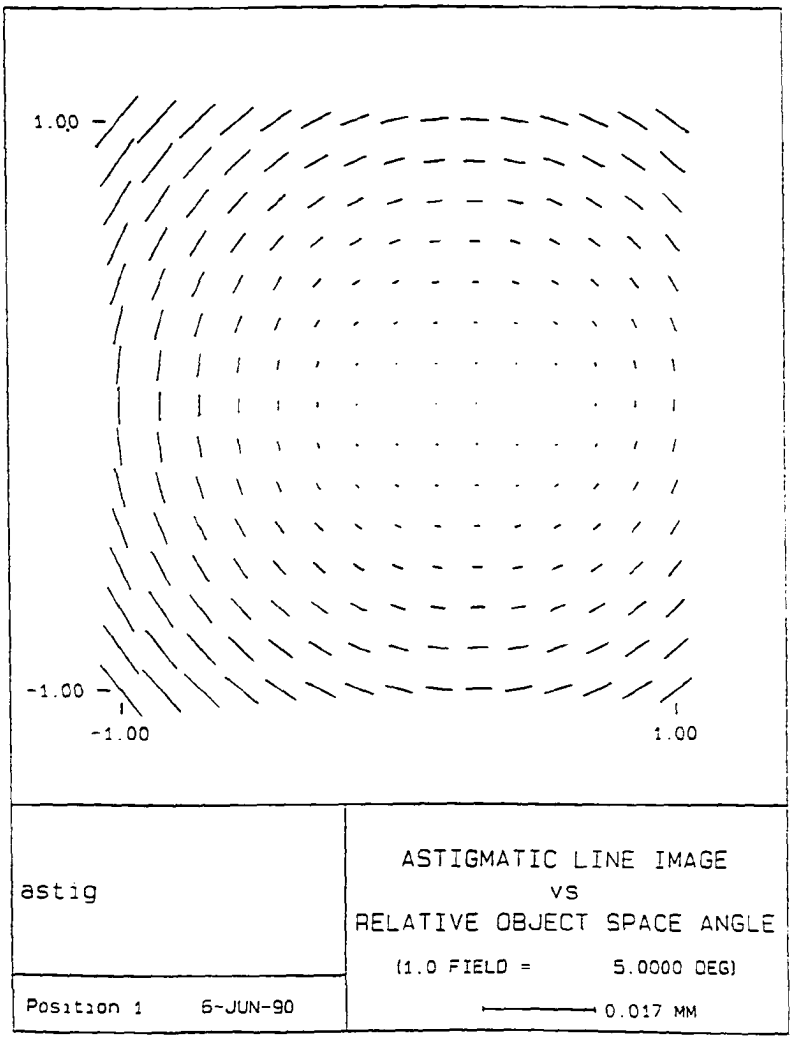

Figure 4.7 The astigmatic line images are shown as a function of field angle in two dimensions. Bi-nodal astigmatism is apparent because the image is a circular point at two different locations in this plot; when the field angle is 0 and 2.5º [27].

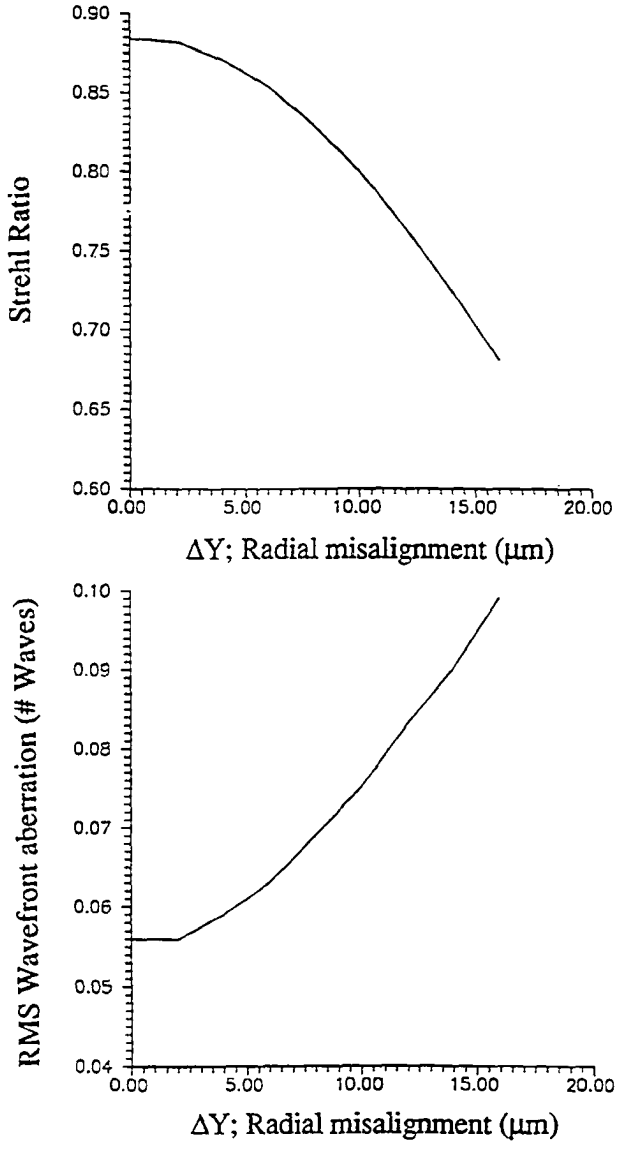

Figure 4.8 The Strehl ratio and the wavefront error are plotted versus ΔY misalignment error for a 2.5º field. With no misalignment introduced, the Strehl ratio is 0.885. This is due to the presence of astigmatism [27].

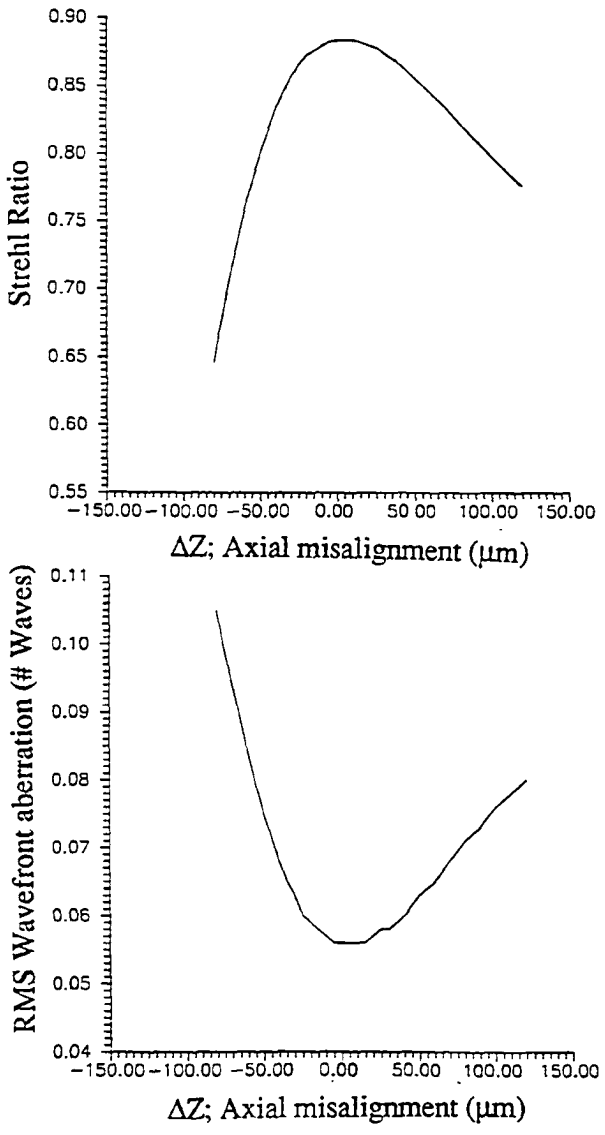

Figure 4.9 The Strehl ratio (top) and the rms wavefront aberration (bottom) are plotted versus ΔZ alignment error for a 2.5º field angle [27].

a 0.5 NA, 1 mm diameter lens. A spherical Fresnel zone plate was introduced and the aberrations were analyzed. It was shown that if the focal length of the FZP coincided with the center of curvature of a zero power spherical substrate, the coma is identically zero for all field angles. The useful field was increased from $\pm 0.13^{\circ}$ to $\pm 2.1^{\circ}$, where the astigmatism reached the Rayleigh limit of 0.25λ. Finally, a tolerance analysis was performed on a spherical FZP. The results showed that if 10.9 μm of radial ΔX alignment error were introduced during fabrication, the focal spot would remain diffraction limited over a $\pm 2.6^{\circ}$ field centered about 1.3°. The Rayleigh limit was not reached until the field exceeded $1^{\circ} \pm 5^{\circ}$. This type of misalignment introduced bi-nodal astigmatism, which means that the focal spot had a Strehl ratio of unity for two field angles; 0 and $+2.5^{\circ}$. For a ΔY radial misalignment, the wave aberration exceeded 0.07 waves for more than 8 μm of misalignment for a 2.5° field. The Rayleigh limit was not exceeded until the ΔY error was in excess of 35 μm. For a ΔZ misalignment between -50 and +75 μm, the rms wavefront aberration remained below 0.07 waves with a 2.5° field. Tolerance values for the X and Y directions are challenging with respect to fabricating a proof-of-principle lens, while the tolerance values for the Z direction should present no problem.

CHAPTER V

EXPERIMENTAL HARDWARE, TECHNIQUE AND PROCEDURES

It has been shown that access time and volumetric storage density of optical data storage systems can be improved by replacing the conventional objective lens and mounting hardware with a smaller lens. This will decrease the moving mass of the optical head and reduce platter spacing in multiple platter systems. When the incident beam is tilted for fine tracking control, a Fresnel lens on a hemispherical shell whose center of curvature corresponds with the lens focus will operate coma-free over all tilt angles. As shown in Chapter IV, a lens with 0.5 mm focal length must be located on the 0.5 mm radius hemispherical surface such that the focal point and the center of curvature coincide within about ±10 μm radially and ±50 μm axially, to remain acomatic. The limiting aberration for this type of lens is astigmatism.

This type of lens has never been demonstrated in the literature. To demonstrate the feasibility of substrate handling, photo resist application and lens exposure, this chapter describes how a 0.16 NA Fresnel zone-plate was fabricated in photo resist on a 0.4 mm radius of curvature microsphere. First a discussion of available techniques is presented, and one technique is chosen for a proof-of-principle experiment. The selection, handling, and mounting of the microsphere is discussed. The

photo resist application technique is described. Finally, the lens exposure system, alignment procedures and exposure techniques are described.

Fresnel Zone Lens Fabrication Techniques

There are several different techniques to choose from to demonstrate the fabrication of a spherical Fresnel zone lens. Flat Fresnel zone lenses have been made through photolithography, photoreduction, direct electron beam writing and, interferometric techniques. So far, no methods have demonstrated a Fresnel zone lens on a spherical surface.

Photolithography offers the advantage of computer generated mask design and fabrication and can make lenses with aberration correction for any wavelength. However, photolithographic techniques are usually used on flat surfaces. Extending them to curved surfaces would require extensive facility modification. State-of-the-art photolithography is limited to approximately 0.4 μm or larger feature size [5]. High NA, high efficiency (0.5 NA, 0.5 mm radius, and 8 level binary construction) Fresnel zone lenses require process resolution on the order of 0.24 μm for operation at 785 nm.

In the photoreduction technique, an enlarged image of the lens is drawn and reduced through photographic techniques. The reduced image is used to mask the substrate surface, which is then developed and etched. To use this technique on a curved substrate would require careful design to pre-

correct for the large image distortion associated with projecting a flat object onto a curved surface. Even if this were done, this technique does not demonstrate the small process resolution that is necessary for high NA microlenses.

The direct E-beam writing technique has demonstrated the capability for very small feature size on flat surfaces. In this technique, E-beam resist is applied to the substrate, and an electron beam is used to expose the lens pattern directly in the photo resist. This can be done either in an X-Y raster scan, or an R-theta ring writer, as shown in Figure 5.1. This technique could be used to write a smooth Fresnel lens through careful dose control, offering the possibility of 100% diffraction efficiency. Because the E-beam writer is computer controlled, lens zones can be written with arbitrary radii and widths. Therefore, a lens can be designed and fabricated to operate at any wavelength. An E-beam system can produce elliptical lenses for astigmatism correction. For very high NA lenses, the X-Y raster scan may not be smooth enough for circular zones. However, it has been reported in the literature that an E-beam system was developed that uses analog circular scanning and digital radius control to improve the smoothness of the zones [23]. If the radius of curvature of a spherical substrate is large enough, the depth of focus of an E-beam might be enough to accommodate a spherical substrate without significant error. However, some Z-axis control could be introduced, either into the writing head or on the substrate mount.

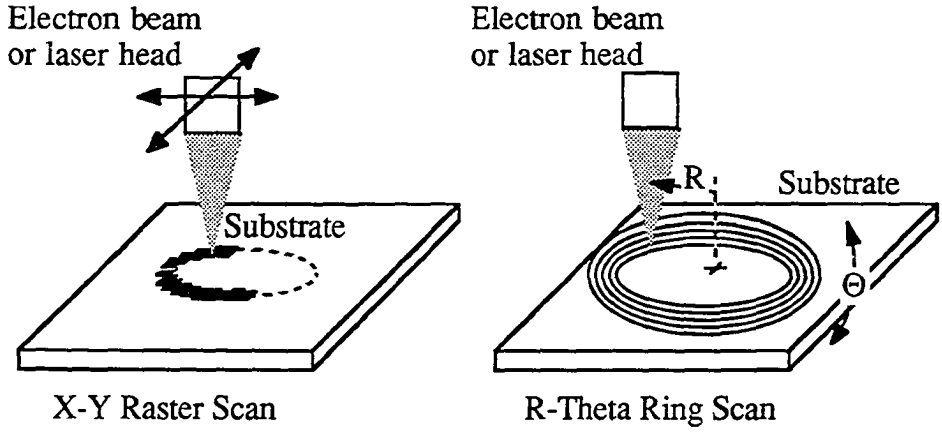

Figure 5.1 The electron beam writer system exposes the lens pattern directly in E-beam resist on a substrate using one of two scan methods, either an X-Y raster scan or an R-theta ring scan.

An E-beam system is a very flexible and attractive approach and is recommended when good quality, highly repeatable, aberration-corrected lenses are needed. E-beam writer systems are commercially available. An example is the Elphy system by Raith. These systems are very expensive and require much calibration and set-up. For a proof-of-principle experiment, something simpler is more attractive.

An interferometer can create Fresnel zones by interfering a plane and a spherical wave on a substrate coated with a recording medium. The wavelength of light must be within the sensitivity range of the recording medium. When the FZP is made this way, the lens can only be used at the wavelength at which it was fabricated. It is possible to create a zone-plate at one wavelength and use it at another if the plane beam is slightly defocused, but sphero-chromatism is introduced. One problem with creating a lens interferometrically for optical data storage is that there are no fringe recording media sensitive around 0.8 μm, the wavelength used by ODS systems. One wavelength at which photo resist is available is the blue HeCd line at 442 nm. This laser is available and has enough power and coherence length to be used to expose photo resist on a substrate. There are several different interferometric methods that could be used with the HeCd laser to form Fresnel fringes.

Point-Diffraction Interferometer

A point diffraction interferometer consists of a neutral density filter with a pinhole in it. A plane wave incident on the interferometer will split into two waves. One will pass through attenuated by the ND filter, but still planar. The second wave will be a spherically diverging wave created by diffraction through the pinhole. The sine of the diverging half angle is the NA of the lens being fabricated. The half-angle measuring divergence due to diffraction through a pinhole of diameter D is given by Equation 5.1. Visibility of the fringes is dictated by the ratio of the powers of the two waves in the area of the lens to be formed, and so is a function of the pinhole diameter and the amount of transmission in the filter. A pinhole size of 1 μm will diffract a 442 nm plane wave to form a lens of 0.5 NA. For a lens diameter of 1 mm, the ND required would be ND=6 (1 x 10^{-6} transmission). The amount of light getting through would be very small and would require long exposure times. In addition, controlled pinholes this small are hard to make on a coated surface. These and other problems combine to make this approach undesirable.

$$\Theta_{1/2} \approx 1.22 \frac{\lambda}{D}$$

Equation 5.1

Holographic Optical Elements

To create Fresnel fringes, a spherical wave must interfere coherently with a plane wave. This can be done by a holographic optical element (HOE)

formed by interfering a plane and spherical wave, on-axis, in a recording medium. When played back, this HOE would pass part of the incident plane wave unchanged (0th order) and focus part of the incident wave at the same NA as the lens used to create the HOE (+1st order). These two orders would interfere coherently, so a HOE could be used produce Fresnel fringes.

For high NA HOE's, it has proven to be difficult to fit a lens to the proper location in front of the HOE while passing a plane wave normal to the HOE surface due to spacing requirements [30]. This problem has been solved by making off-axis HOE's in a two step process.

To optimize the Fresnel fringe visibility, the power density of the two waves must be equivalent over the lens area to be exposed. The ratio of the power in the +1st and 0th orders of the HOE is related to the diffraction efficiency of the HOE. For maximum fringe visibility, a 0.4 mm focal length, 0.55 NA Fresnel zone lens on a 0.4 mm radius substrate requires a 6 mm diameter HOE to have a 0.53% diffraction efficiency in the +1st order. Smaller diameter HOE's could use higher diffraction efficiencies. Assuming equal distribution of power in the ±1st orders of the HOE, to maintain a visibility of better than 0.9 in the playback Fresnel fringes, the diffraction efficiency of the 6 mm HOE must be held to 0.53±0.06%. In fabricating HOE's, precise diffraction efficiencies are difficult to control, and this kind of tolerance is not realistic.

While it is possible to create Fresnel fringes using an HOE, high contrast fringes require an unrealistically tight fabrication tolerance on diffraction efficiency.

Mach-Zehnder Interferometer

A Mach-Zehnder interferometer can be used to form a FZP as shown in Figure 5.2. This type of interferometer was used with some modifications to fabricate a proof-of-principle spherical Fresnel zone-plate lens. The recording medium was photo resist, which is sensitive from 350 to 450 nm wavelength [28]. A HeCd laser operating a 442 nm was used to expose fringes in the photo resist.

The following sections describe some of the details of the experimental set up. First, the microsphere is described. The photo resist coating technique is then explained. Finally, the interferometer layout and alignment is described.

Spherical Substrate Description

The substrate on which the Fresnel zone lens is deposited should be spherical and add no power to the beam. Therefore, it should be a thin-walled shell. Code V modeling showed that substrate thicknesses up to 5 μm had no significant effect on aberrations of the lens [27]. The substrate must

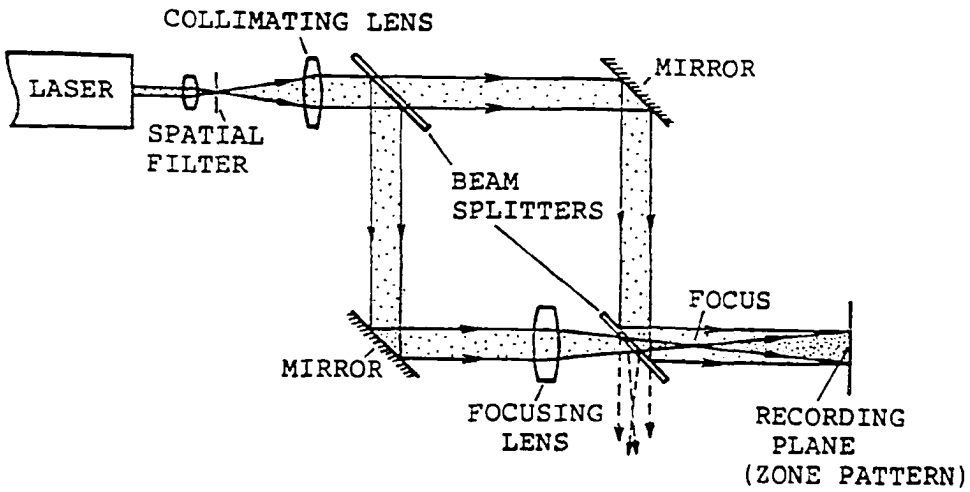

Figure 5.2 Optical arrangement tor making Fresnel zone lenses by the interference method. (After [23])

tolerate chemicals associated with cleaning, preparation for coating with photo resist, immersion in developer, and adhesives for mounting. It should be transparent at 442 nm, and the surface should be optically smooth. It must withstand the necessary handling during mounting and alignment procedures The substrate should have about a 0.5 mm radius of curvature.

One substrate that meets the requirements listed above is a glass microsphere. This is a hollow glass sphere that is typically used as a target for laser fusion experiments. The microspheres are made in a heated tower holding a mixture of molten glass. A standing pressure wave forces droplets of glass out of a small diameter tube, and they solidify into hollow spheres. The sphericity is controlled by surface tension of the cooling glass. After removal, the desired diameter can be selected through a sorting process.

For this experiment, the microspheres were between 0.7 and 1 mm diameter. A broken shard from a sphere was coated with gold, and an edge view in a scanning electron microscope (SEM) showed its wall thickness to be 1 μm. A microsphere was tested for sphericity in a ZYGO interferometer and analyzed with the WISP software. The sphere center of curvature was located at the focal point of a 0.7 NA reference lens in the ZYGO. The sphere was not coated, so the air-glass interface reflection (4%) was used to interfere with the reference wave. An interferogram

Figure 5.3 This interferogram is the result of placing a 0.8 mm. diameter microsphere at the focus of a 0.7 NA reference lens on the output of a ZYGO interferometer. The microsphere was imaged so that the outer most portion of the fringes are at the microsphere edge. The inner circle is an artifact of the reflection from the inner wall of the microsphere. The outer edges of the interferogram show significant departures from a perfect sphere, while the center section shows sphericity to better than $\lambda/10$.

showing the fringes from the ZYGO output is shown in Figure 5.3. The largest circular outline is the outline of the sphere. Tilt was introduced to add more straight line fringes for clarity. Deviations from straight lines indicate errors in sphericity. At the edge of the microsphere, significant ($\lambda/2$) deviations can be seen. The reflections off of the inner surface of the microsphere caused a stepped phase change in the center of the image that shows up as the smaller circle in the center. This confused the WISP software, so no numerical results are shown. Qualitatively, the sphericity appears to be within $\lambda/10$ over the central 0.5 NA section of the microsphere, which was good enough for this demonstration.

To use the microsphere in an experiment, a mounting fixture is required. Also, the sphere must be cut in half to create a clear aperture for the beam to exit. A hemisphere located over a hole in a flat plate is a geometry that provides a clear exit aperture and can be handled in an alignment fixture. Much effort was spent in trying to develop a technique to encapsulate the microsphere and then grind half of it away. First, epoxy was used for encapsulation, but it could not be easily removed after grinding. Next, plastic was dissolved in a solvent and used to mount the sphere to a tool for grinding. As the solvent evaporated, the plastic solidified and encapsulated the microsphere. Grinding the microsphere was done with 600 sandpaper on a jeweler's lathe. However, this proved to be a tedious task, and yielded less than 50% success. For the focal spot to be located clear of the sphere and mounting plate, the microsphere must be cut or ground well past half its diameter. The yield rate for grinding beyond the waistline of the

microsphere was minimal. A modification of this technique could be to encapsulate an entire layer of microspheres, and polish the whole batch at one time. This was not attempted.

Finally, a technique was developed where the complete microsphere was mounted into the aperture plate as shown in Figure 5.4. Epoxy was applied around the lip of the hole in the plate, and flowed through capillary action to seal the microsphere against the plate. After curing the epoxy, the sphere was carefully broken along the glue line to leave a small section of the microsphere inside of the aperture. The finished hemisphere does not extend above or below the aperture plate thickness (150 μm) and so is well-protected from handling. Also, using this technique allows for a sphere to be pre-coated with photo resist rather than trying to coat after mounting. Using this technique, the focal point of a lenslet could extend beyond the aperture plate providing a 0.2 mm working distance.

Photo Resist Properties and Handling

It is necessary to cover the microsphere with a smooth coating of photo resist of a reproducible, uniform thickness. It was decided to use Shipley model S1822 Microposit photo resist for recording the Fresnel fringes on the substrate. A primer (Shipley model P-20) was used to improve adhesion to the glass surface. The developer was Shipley model 352. Type P thinner was used to reduce the photo resist viscosity. This photo resist is sensitive to exposure from 350 to 450 nm wavelength. At 442 nm, it has

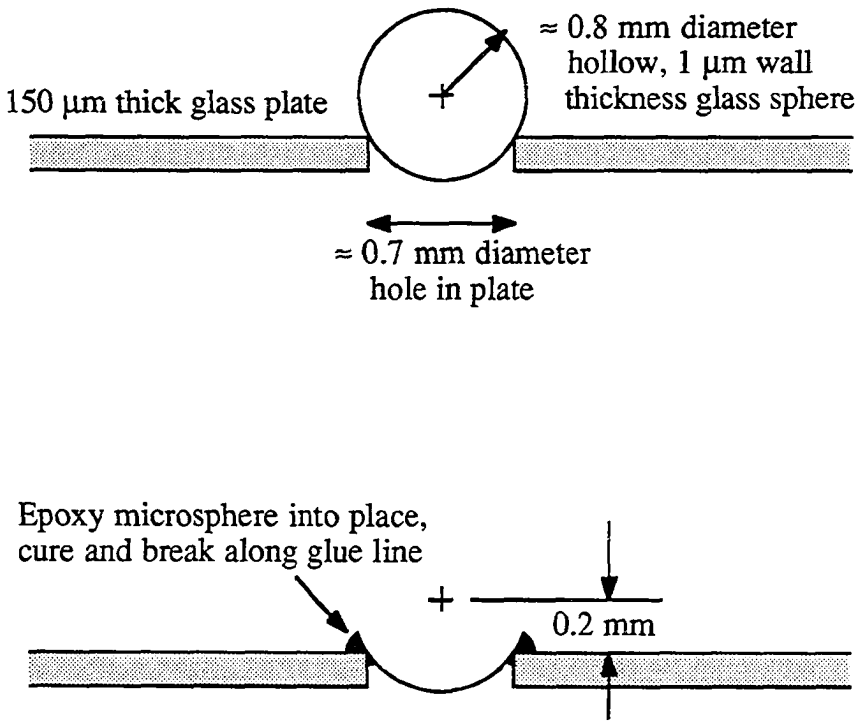

Figure 5.4 To mount a microsphere into a holding fixture, epoxy was placed around the edge of an aperture and a microsphere was placed in the aperture. After the epoxy cured, the sphere above the glue line was broken away, leaving a spherical surface whose center of curvature was 0.2 mm above the plate surface.

approximately 45% absorbance before exposure and after development. The index of refraction is about 1.67 at 442 nm.

Shipley provides photo resist layer thickness as a function of spin rate for flat surfaces, but since the microsphere is not flat, another application technique was developed. Each microsphere was placed on a 10-15 layer pad of absorptive lens tissues. The tissues were located in a petri dish, and a tent was formed over the dish to contain a dry air flow. The sphere was dried for 15 minutes. A drop of primer was applied through a small hole in the dry air tent to improve photo resist adhesion and further dry the surface. Fifteen minutes later a drop of acetone was applied and, after drying for 15 minutes, a drop of ethanol was applied to clean the surface. One hour later, a drop of photo resist/thinner combination was applied, and allowed to dry for 15 minutes. The petri dish containing the sphere was then placed in an oven for 1/2 hr. at 90º C.

After exposure and development, Fresnel zones exposed in the photo resist act as a combination of phase delay and amplitude reduction, forming a combination of a phase and an amplitude zone lens. The required photo resist thickness is given by Equation 5.2, where t=required photo resist thickness, n=refractive index of the photo resist, m=odd integer, and λ=wavelength.

$$t = \frac{m \lambda}{2 (n - 1)}$$

Equation 5.2

For 442 nm wavelength and n=1.67, m=1 yields a thickness of 0.33 μm, and m=3 yields 0.99 μm. These thickness are very reasonable to provide with photo resist.

To determine the thickness of the layer of photo resist after it was applied, a knife edge exposure was made. Half of the sphere was exposed, while half was not. The exposed half was over saturated with laser light, and the developing process removed all of the photo resist from this half, while leaving the photo resist on the unexposed half. The setup is shown in Figure 5.5. After the photo resist was exposed and developed, it was coated with a thin layer of gold and mounted in an SEM. The thickness was determined by looking at an edge view of the exposure step as shown in Figure 5.6. The resist to thinner ratio was varied, and for each ratio the exposure step height was measured. The end result was that the required thickness was obtained for a thinner:resist volume ratio of 2.25:1.

Humidity affects photo resist adhesion. During all of the testing, exposures, and experimentation, the most troublesome problem was with the photo resist adhering to the glass microspheres consistently. In general, the lower the humidity the better. The dry air tent used in the cleaning and resist deposition process improved the situation, but it was not perfect.

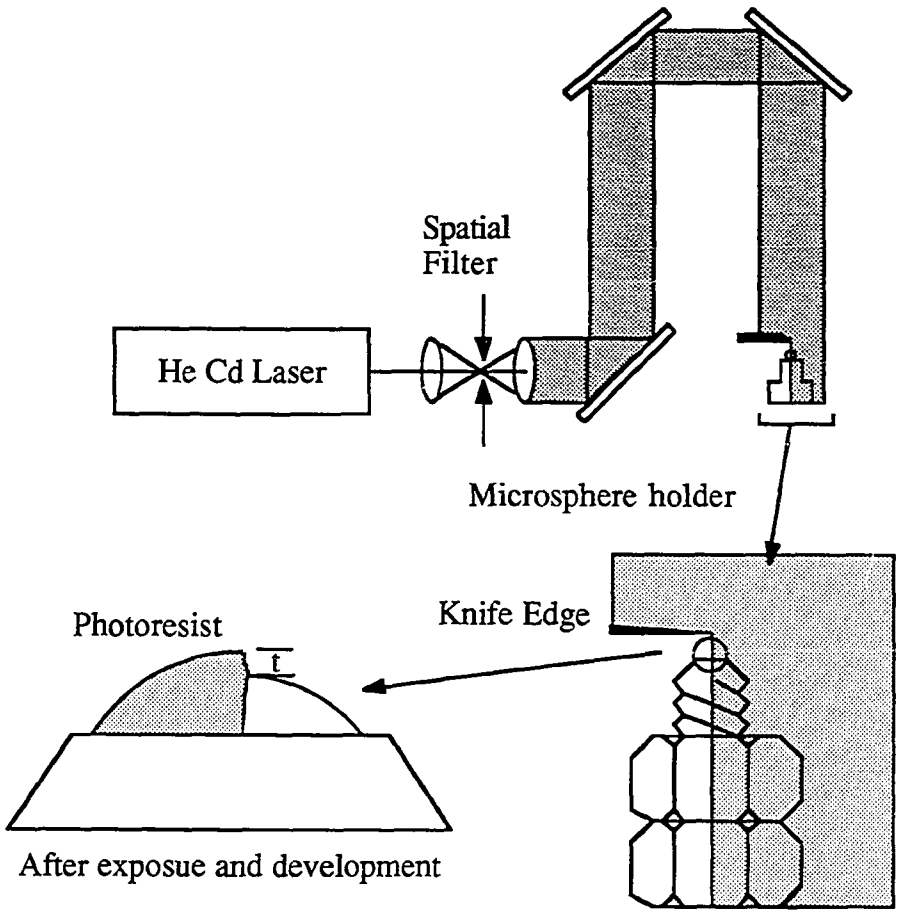

Figure 5.5 The setup used for performing the knife edge exposure of a microsphere for determining the resist thickness is shown. Once the resist was developed, it was flash coated with gold, and an SEM was used to view the exposed edge and determine the photo resist thickness.

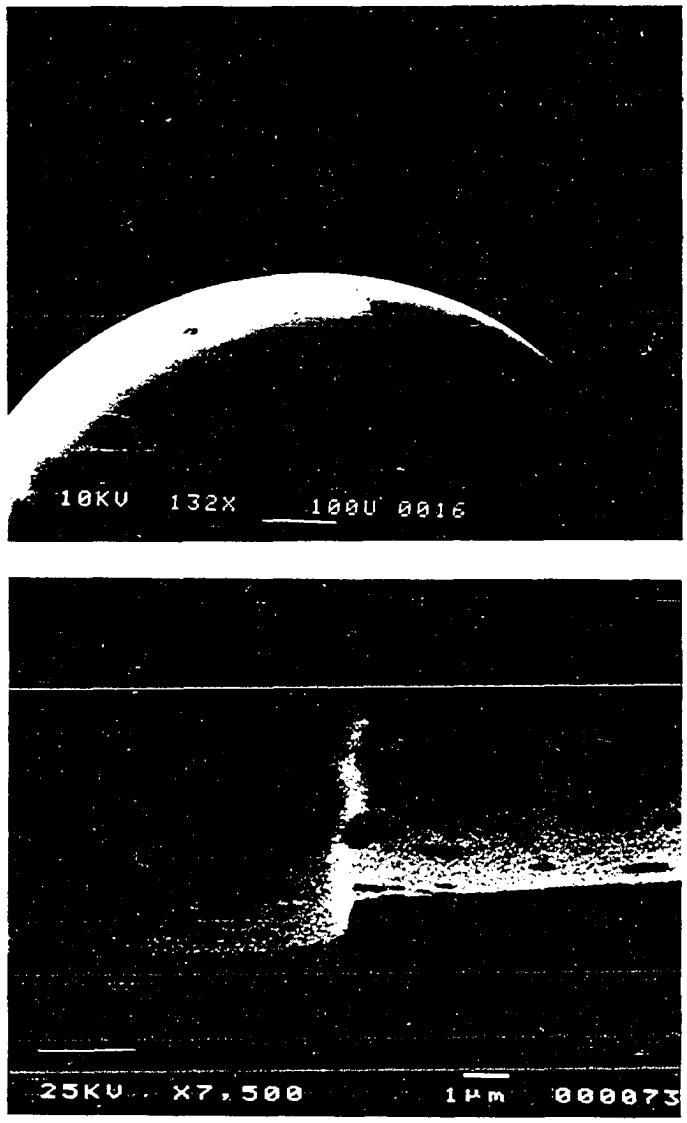

Figure 5.6 The SEM was used to measure the thickness of photo resist as applied to the microsphere by viewing along a knife edge exposure. A 1 µm. thickness was obtained when a thinner-to-resist ratio of 2.25:1 was used.

For alignment and exposure testing of the interferometer, it was desirable to expose some flat lenses on glass slides. Photo resist was applied to the slides in the conventional manner using spin coating, pre-baking, and resist to thinner ratios according to the Shipley procedure manual. This technique was already proven and presented no problems.

Interferometer Design and Alignment

The interferometer chosen for this experiment was a modified version of a Mach-Zehnder interferometer. A photograph and a system layout is shown in Figure 5.7. A schematic showing the beam paths is shown in Figure 5.8. The microsphere required precision alignment with respect to the focusing and planar waves prior to exposure. The alignment is accomplished using position information derived from reflecting off of the microsphere. However, if the sphere is in place and coated with photo resist, the HeCd beam will expose the photo resist during alignment. Therefore, it was desirable to have two different beams in the system, aligned coaxially. The first beam wavelength was 442 nm (HeCd blue line) for exposure of the Fresnel zone lens. The second beam wavelength was 633 nm (HeNe red line), a wavelength where the photo resist was insensitive. The HeNe and the HeCd lasers were aligned on an optical table and combined in a 50/50 beam splitter. The beams were aligned so that the two spots were coincident on the splitting surface of the beam splitter, and were coaxial in

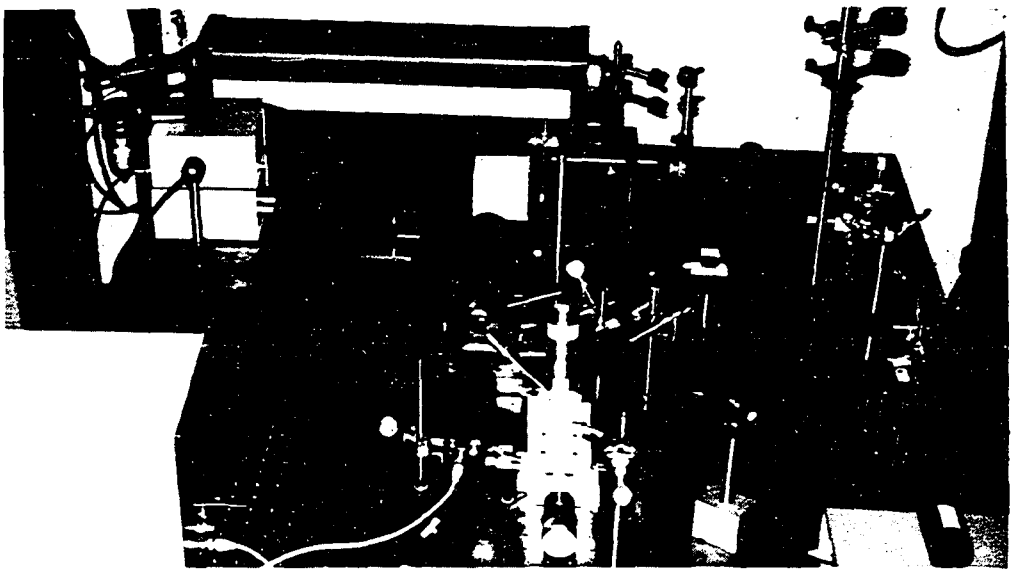

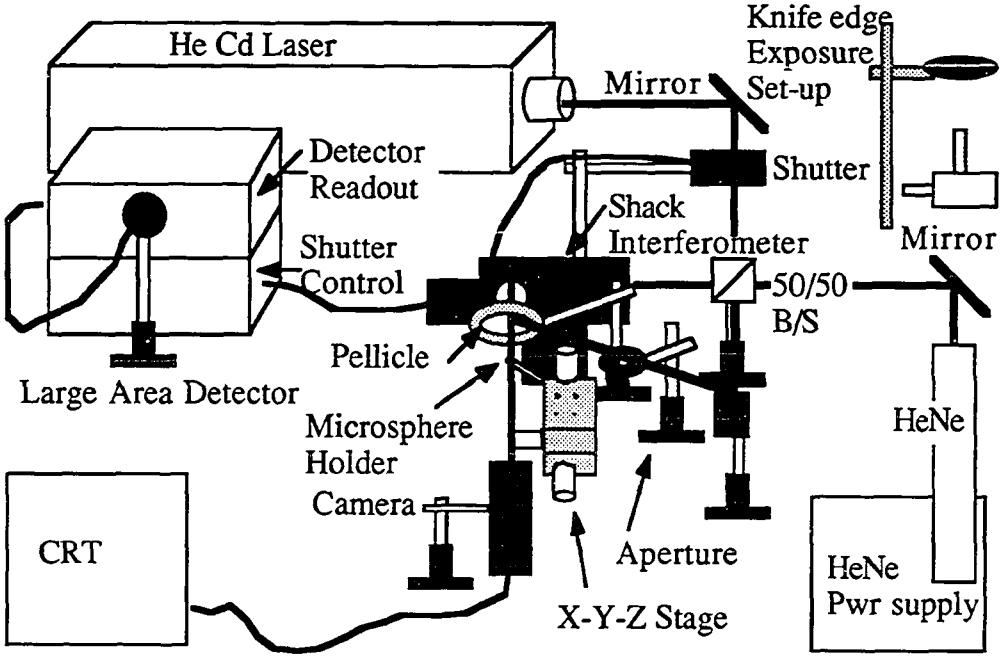

Figure 5.7 Interferometric system layout photograph and annotated sketch.

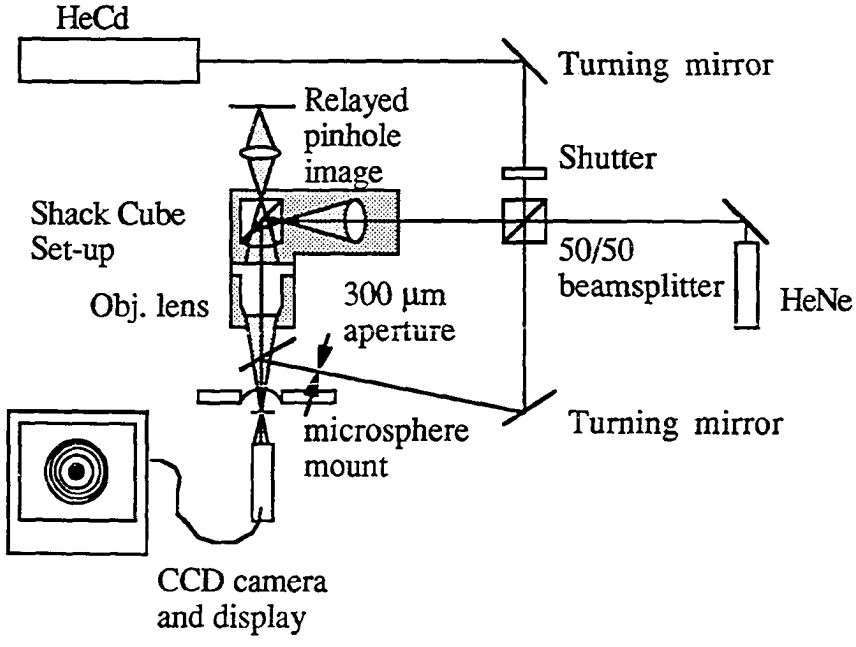

Figure 5.8 This idealized schematic shows beam paths of the Mach-Zehnder interferometer used for exposure of a spherical Fresnel zone lens.

both beam splitter outputs when viewed as a spot across the room (7 m). If the error in determining spot overlap was approximately 2 mm, this would yield an uncertainty of 0.001 radians, which was acceptable.

Shack Cube Interferometer

One set of beams left the beam splitter and entered a Shack cube interferometer [29]. This device is shown schematically in Figure 5.9. The Shack cube is a 50/50 beam splitter with a pinhole spatial filter located ≈2 mm off of one of the surfaces. A plano convex lens is applied to another surface such that its center of curvature coincides with the spatial filter. The spatial filter diffracts the incident beam according to Equation 5.1. For the HeNe, the half angle is 0.77 radians, and for the HeCd, the angle is 0.54 radians. Rays leave the Shack cube normal to the lens surface. Therefore, the lens adds no power or aberrations to the beams. The Shack cube was used to illuminate a 0.18 NA microscope objective that was aberration corrected for a 160 mm object length. It was located such that the optical path length from the Shack cube spatial filter was 160 mm. In addition to diffracting the incident beam, the pinhole filtered high frequency noise out of the incident beam, which provided a "clean" illumination of the microscope objective.

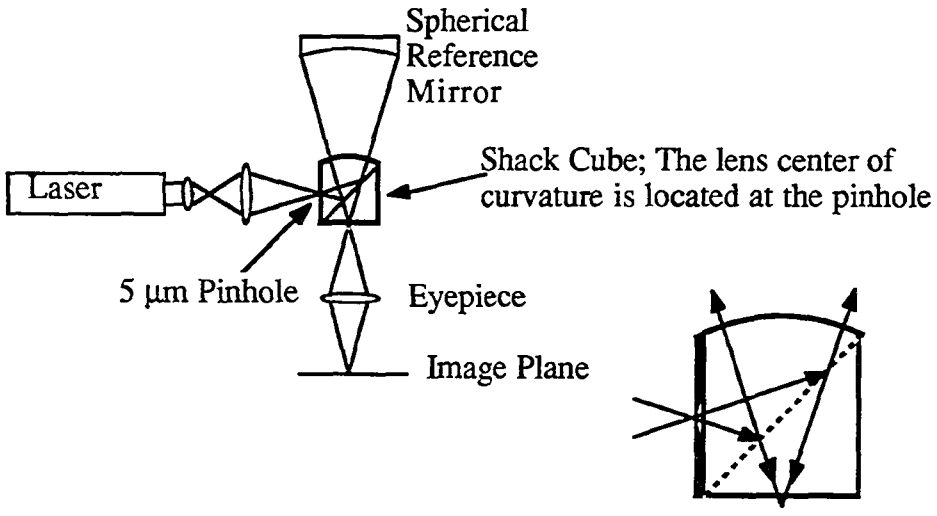

Figure 5.9 A Shack cube interferometer was used to provide "clean" illumination of a microscope objective, and to provide alignment feedback.

Microscope Objective

Several different microscope objectives were considered for use in this experiment. A long working distance was needed in the Mach-Zehnder set up for a pellicle to fit in the focusing beam. For the proof-of-principle experiment, it was decided that a 0.18 NA objective was sufficient to demonstrate all of the techniques and processes desired. A faster lens would have been nicer, but high NA lenses typically have short working distances. The 0.18 NA objective chosen had a working distance of approximately 20 mm, which was just adequate. It was aberration corrected for 160 mm object distance.

Because of the two wavelength alignment and exposure requirement, it was necessary to characterize the focus of the objective lens for both wavelengths. If a sphere were aligned in red, and the focal length of the lens were different for blue, the sphere would be out of alignment for exposure, unless a correction was applied. An in-situ measurement was performed to test the shift in focus for a change in wavelength. The objective was illuminated by the Shack cube as shown in Figure 5.10. A mirror was located normal to the optical axis near focus. The beam was reflected back through the objective, and when the objective focus coincided with the mirror surface, the spatial filter was re-imaged just outside of the Shack cube as shown in Figure 5.10. Location of the best spot was first identified at 633 nm. The system was then aligned at 442

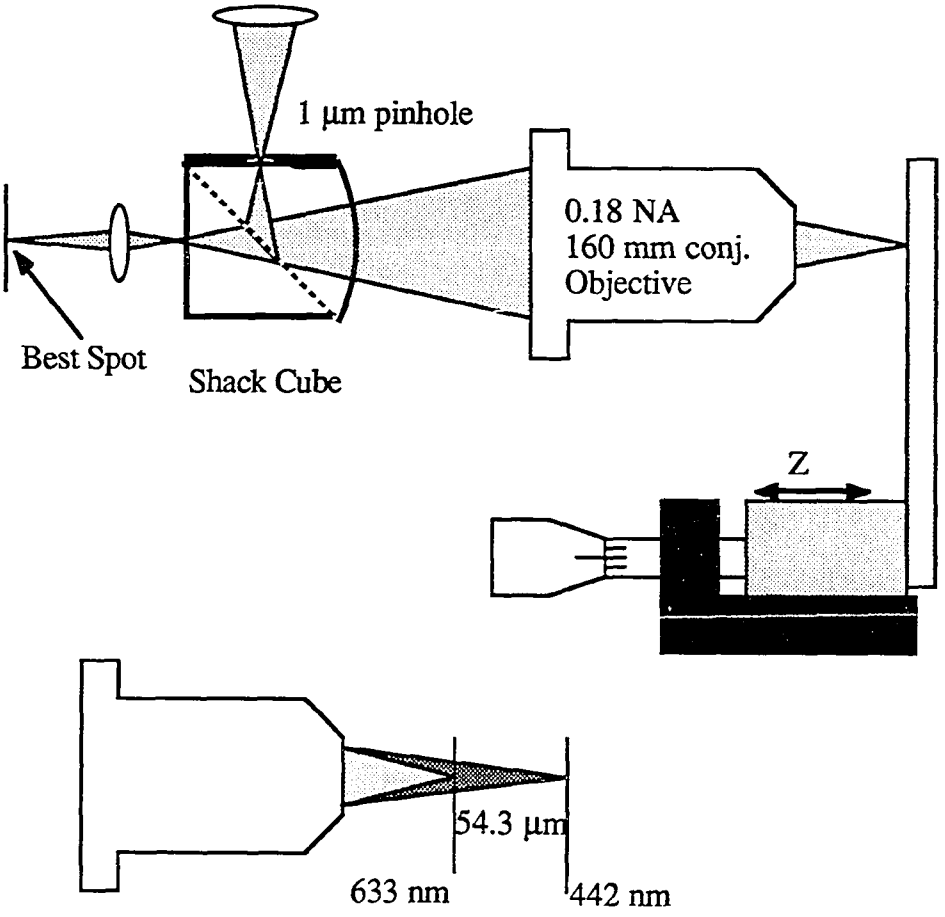

Figure 5.10 An experiment conducted *in situ* showed that the shift in focal length for a change in wavelength from 633 nm to 442 nm was 54 µm.

nm by moving the mirror with a precision X-Y-Z stage until the best spot was located in the same plane as for 633 nm. The shift in Z location of the mirror indicated the change in focal length.

Four repetitions of the measurement were performed on the 0.18 NA objective lens, and the average focal shift was 54.3 μm (1 σ = 4.1 μm). The focus was closer to the objective for 633 nm, and farther away for 442 nm. Based on this measurement, the alignment procedure includes the proper Z-axis correction of the sphere location for the HeCd/HeNe focal shift.

To determine the spot quality of the system, another in-situ measurement was performed. A Photon Inc. spot scanner was located at the objective lens focal plane. The spot profile was measured, and the FWHM was 2.50 and 2.38 μm at 633 nm in two orthogonal directions. The diffraction-limited FWHM given by Equation 1.4 was 2.11 μm. The FWHM measured corresponded to the diffraction limit for a 0.16 NA. It is possible that the objective was slightly under filled in this experiment. The detector in the spot scanner was not sensitive enough at 442 nm to measure the spot profile very well at that wavelength.

Planar Reference-Wave Considerations

The planar wave that interferes with the spherical wave is approximately 1 mm diameter as it exits the beamsplitter. For the 0.18 NA objective and

0.4 mm radius microsphere, the Fresnel lens diameter is 144 μm. Because of capillary action, the adhesive mounding the sphere to the 0.7 mm diameter aperture plate fills in the aperture edges and leave about 0.5 mm clear aperture. To avoid scatter caused by the adhesive, the planar beam should be smaller than 0.5 mm diameter. An aperture of approximately 0.25 mm was fabricated. It was located approximately 30 mm along the optical axis from the center of the microsphere. The diffraction through this large of an aperture over this distance was calculated. The beam size at the sample should have diverged to be 380 μm diameter. To verify the beam size at the microsphere location, a flat glass slide with photo resist was exposed to the planar beam. The measured beam size was approximately 300 μm.

A pellicle was used to align the planar beam with the focused beam. A beam splitter could not be used because aberrations would be introduced into the spherical beam due to focusing through a glass plate, as discussed in Chapter II. The pellicle could introduce some microphonics if the exposure time was too long. The fringes were visualized using a camera to verify stability.

Microsphere Alignment Procedure

The collimated beam height and angle were adjusted so that it was unchanged from the height at the laser to the end of the table after reflecting off of the pellicle. The same was done for the beam exiting the

microscope objective, although, because of divergence, this was less accurate. The two legs of the interferometer were axially aligned relative to one another at the pellicle. The focusing beam was larger than the collimated beam, which was adjusted horizontally such that it was precisely centered on the focused beam as shown in Figure 5.11. This was repeated on the other side of focus for angular alignment.

Once the microsphere was coated with photo resist, cut, and mounted in the aperture plate, the aperture plate was mounted to an X-Y-Z stage. The plate was clipped onto a rod that was bolted onto the stage. The plate was tipped and tilted until it reflected the collimated wave back onto itself, and passed through the 300 μm aperture. Since the aperture was about 30 mm away, and the detectable misalignment was about 1/4 of the beam diameter, this brought the plate alignment uncertainty to about ±0.3º. Since the geometry for the FZP is spherical, tip and tilt misalignment would not affect the quality of the lens as fabricated. However, if the lens were played back at an angle different than when fabricated, some astigmatism could be introduced. By aligning the aperture plate, it could be used as a reference surface for playback.

The microsphere reflects the focusing beam back through the microscope objective and re-images the Shack cube pinhole when it is located at either of two precise positions. The first is when the front surface of the sphere is at exact focus. Compared to the focal spot size (1.5 μm FWHM at the

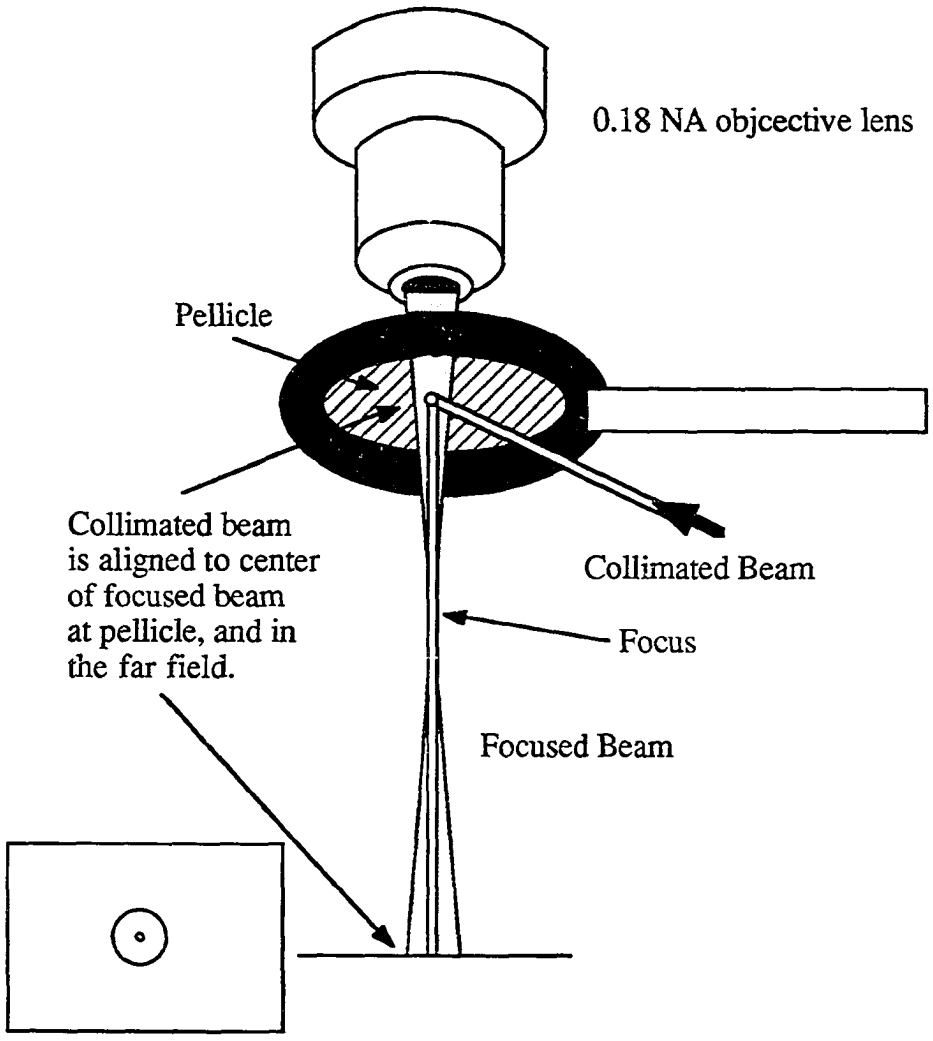

Figure 5.11 The collimated beam was aligned coaxially with the focused beam at the pellicle and in the far field.

diffraction limit at 442 nm) the spherical surface is flat, and it provides a reflection with the image inverted. The second position is when the center of the sphere is located at the focus of the microscope objective. In this case, the converging rays are exactly normal to the spherical surface and are reflected to form a non-inverted image. The pinhole image was used for fine alignment of the microsphere. An image of the pinhole is also formed by the air-glass Fresnel reflection of the beam exiting the Shack cube. A lens located at the back side of the Shack cube was used to relay the image of the the pinhole onto a card in the far field.

Once the microsphere mounting plate was aligned normal to the optical axis, and the two beams were coaxial, the microsphere was brought to front surface alignment, with the HeCd beam blocked. At this location, movement of the microsphere in X and Y did not affect the pinhole image position. The X and Y were adjusted so that the best focus was achieved , and the reading of the Z micrometer was noted. The sphere was then moved toward the pellicle until the second retro-reflected pinhole image was formed. In this position, movement of the microsphere in X and Y also moved the pinhole image in X and Y. The microsphere was adjusted in X and Y so that the image location was the same as for the front surface reflection. Multiple alignments for the same sphere were repeated to within ΔX, ΔY and ΔZ of about ± 5 μm, which, according to the tolerance analysis in Chapter IV, is good enough. Once the sphere is aligned in red, the focal shift for blue is accounted for by moving the Z-axis position 54 μm away from the pellicle.

Exposure Technique

Before exposing the sphere, the fringes were visualized using a CCD camera and video monitor. The camera was used without its lens, and was placed behind the microsphere by about 10 cm. At this distance, the fringes are of low visibility because the focused beam has diverged and, the power density is very low compared to the power density in the collimated beam. However, fringes were visible, and they were used to verify fringe stability. Once the fringes were stationary, the shutter was released. An example of the video output is shown in Figure 5.12. This photograph was also used to verify that the fringes were located properly for Fresnel zones. The radius of each dark ring center was measured using calipers on the photograph. The ring number (m=1/2, 1, 3/2, 2, 5/2, 3, 4, ... 11) was noted for each radius. Equation 5.3 was used to calculate the location of the focus for each ring, f_m. If the zones were Fresnel zones, f_m should be constant for all m and r_m. The values for f_m were calculated and averaged 194 with a standard deviation of 4.6. The units are meaningless, but small standard deviation indicates that the zones are correct Fresnel zones.

$$f_m = \frac{r_m^2}{2\,m\,\lambda}$$

Equation 5.3

To achieve maximum visibility of the fringes in the photo resist, the power in each of the two beams in the Fresnel lens area must be the same. A

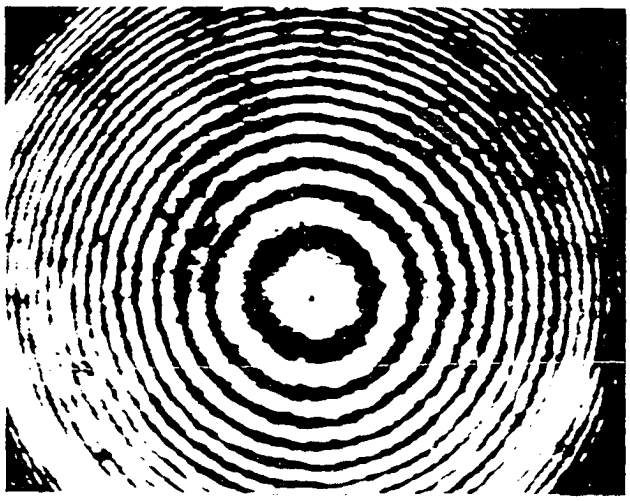

Figure 5.12 This photograph was taken of the video monitor output when the camera was located behind the sample with HeNe illumination. Fringe spacing verified that the fringes were located correctly for a Fresnel zone-plate exposure.

large area detector was used to measure the relative power ratio. The collimated beam is assumed to be uniform over the 300 μm diameter at the microsphere location. The diameter of the focused beam at the microsphere is somewhat different for each sphere radius. From the alignment procedure described previously, the difference between the Z axis location of the microsphere for the front surface reflection and the sphere center reflection is a measure of the sphere radius. Equation 5.4 calculates the diameter of the Fresnel lens on the microsphere, given the sphere radius, R , and the objective NA. For a 0.4 mm sphere radius and an NA of 0.18, the Fresnel lens diameter is 144 μm.

$$D_{FL} = 2\,R\,NA \qquad \text{Equation 5.4}$$

The total power in each beam is measured near focus. Care is taken not to overfill the detector. All of the power in the focused beam is incident on the Fresnel lens area. However, only a part of the collimated beam is used to expose the lens. If P_{col} is the total power in the collimated beam, and D_{col} is the diameter of the collimated beam, then the total useful power in the collimated beam is

$$P_{D_{FZP}} = P_{col}\left(\frac{D_{FL}}{D_{col}}\right)^2,$$

and the ratio of this power to the power in the focused beam should be unity. In the experimental setup, the focused beam had more power than

the collimated beam, so neutral density (ND) filters were added until the power ratio was as close to unity as possible, being careful not to misalign the beam while doing so.

Once the powers were equalized, the exposure time was calculated. It was experimentally determined that the proper exposure time for a lens exposed with a total incident power density of 6.34 $\mu W/cm^2$ was 0.15 seconds. This combination was used to expose a flat Fresnel zone-plate lens on a glass plate. After development, the zones were viewed under a microscope and were of good quality. While this power measurement is not a reliable absolute value, each measurement was done with the same equipment, so the ratios are accurate. Once the total power is measured with the large area detector near focus and the appropriate ND added, the power density can be calculated as

$$P'' = \frac{P_{foc} + P_{col,\,FZP}}{\pi R_{sphere}^2},$$

and the exposure time may be calculated as follows,

$$t_{exp} = \frac{633.8}{P''} * 0.15 \text{ sec}.$$

The shutter can be set with 10 ms. sensitivity. The required exposure time was calculated to be 0.15 ± 0.1 seconds for all of the spheres exposed in this experiment. The sphere radius varied from about 0.35 mm to 0.5 mm.

Summary

This chapter has described the different types of fabrication techniques for Fresnel zone plates. The interferometric technique that was employed for fabrication of a proof-of-principle lens was described. The microsphere mounting and handling techniques were explained. The photo resist application was described. The alignment and exposure procedures were outlined. The lenses that were fabricated with the interferometric technique will be described in Chapter VI.

CHAPTER VI

RESULTS AND CONCLUSIONS

The interferometric set-up described in Chapter V was used to expose several lenses. The first section of this chapter describes several lenses that were fabricated on flat plates and on spherical surfaces. The second section of this chapter describes conclusions drawn from the work described in this thesis.

Lens Fabrication Results

To bracket the proper exposure time and power levels, and to test the stability of the interferometer, several large diameter lenses were exposed and developed on flat plates. These exposures are described in this section, and some flat Fresnel lenses are shown. After the proper exposure levels were found for the large diameter lenses, some flat microlenses were exposed and developed and are also described in this section. After the best exposure parameters were identified using the flat plates, several exposures were made on microspheres. One such spherical Fresnel lens is described and shown. The NA was measured, and an attempt at measuring the wavefront quality was made.

Large Diameter Flat Fresnel Lens

An exposure test was made where a 5.36 mm diameter collimated beam (13.5 μW) was used to expose a flat plate with photo resist coated on it. Several exposures were made to find what power density and exposure time are needed to saturate the resist. The power density was 0.60 $\mu W/mm^2$. An exposure of 6 minutes left small amounts of photo resist in the center of the exposed area, while a 10 minute exposure completely cleaned the area off. All exposures were developed for 60 seconds. An extrapolation predicted that an 8 minute exposure of 0.60 $\mu W/mm^2$ just saturates the resist. This corresponds to an exposure of 2.88 $\mu J/mm^2$.

The interferometer described in Chapter V was then used to expose some large Fresnel lenses. The interferometer was modified with a spatial filter/up-collimator in the collimated leg. All but the most uniform central portion of the beam was removed with a 4.36 mm diameter aperture.

A large area silicon detector was used to measure the power in each leg of the interferometer near the focus of the objective. The collimated leg power was 60.6 μW, and the focused beam power was 20.9 μW. Since the lens diameter was to be the same as the collimated beam diameter, the resist-coated plate was adjusted axially to make the spherical beam the same diameter. Therefore, neutral density (ND) filters were added to the collimated leg until the power was 19.5 μW. With approximately equal power in each leg, the visibility of the fringes was maximized. Based on

the measured beam powers, a bright fringe was calculated to have a peak power density of 2.7 $\mu W/mm^2$, while a dark fringe had a calculated power density of 0.1 $\mu W/mm^2$.

The alignment was also somewhat different than for a spherical Fresnel lens. The flat plate was aligned to be normal to the optical axis similarly to the microsphere aperture plate. The Shack cube pinhole image was used to locate the resist-coated plate at the focal point of the objective at 633 nm wavelength. The microscope objective used to provide the spherical wave for the exposure was 0.18 NA. To provide complete overlap between the collimated and spherical beam, the resist-coated plate was moved away from the pellicle by 11.9 mm as measured by the X-Y-Z stage.

From the earlier photo resist saturation test, an extrapolation predicted that, an exposure time of 107 seconds was needed for proper exposure. A series of exposures was made from 30 seconds to 180 seconds. The best fringes were obtained for exposure times between 85 and 110 seconds, corresponding to an exposure of 2.30 $\mu J/mm^2$. The plate was developed for 60 seconds. A scanning electron microscope (SEM) micrograph showing a lens from 85 second exposure is shown in Figure 6.1. The ellipticity in the photo is an artifact of the viewing angle. This lens is probably slightly over-exposed, as there is not much resist left in the rings. For a Fresnel lens 4.36 mm diameter, there should be over 450 rings, and the last zone is 2.5 μm diameter. Figure 6.2 is an SEM micrograph of a cleaved edge of this lens. The zone spacing is about 5 μm. It appears that

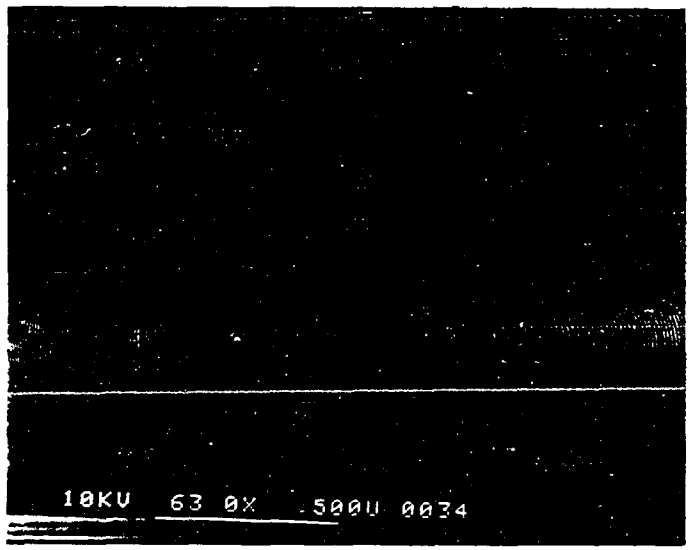

Figure 6.1 The SEM photomicrograph shows the Fresnel zones in photo resist for a 0.18 NA, 4.36 mm. diameter lens, whose diffraction efficiency was 31%. The ellipticity is an artifact of the photograph viewing angle.

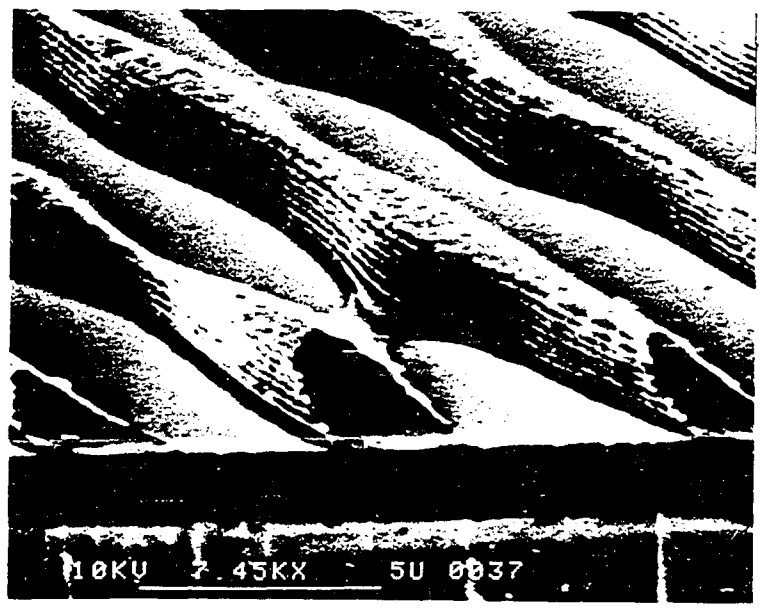

Figure 6.2 The SEM photomicrograph shows an edge view of several Fresnel zones of a 0.18 NA, 4.36 diameter Fresnel lens. The minimum distinguishable feature size approaches 0.25 μm.

feature sizes on the order of 0.25 to 0.5 μm are possible with this exposure technique and photo resist system. This figure also shows a series of steps in the side walls of the zones. These are due to the standing waves created in the resist layer by small reflections at the resist-glass interface interfering with return reflections from the resist-air interface. There appears to be 8 steps, which corresponds to a thickness of 4 waves, or 1.05 μm in a material with a refractive index of 1.67. The scale on the micrograph indicates the thickness to be approximately 1.4 μm, but the viewing angle can be misleading.

The diffraction efficiency of this lenslet was measured. The 4.36 mm diameter beam that was used to expose the lens was used to play the lens back. The power in the beam incident on the lens was 15.3 μW. The power measured in the zero order beam 600 mm behind the lens was 5.9 μW, and the total power getting through the glass plate was 12.8 μW. The diffraction efficiency is defined as the ratio of the power in the $+1^{st}$ order to the power incident on the lens. Because the power in the $+1^{st}$ order is not directly measurable, it is assumed that the non-zero-order power getting through the plate is evenly distributed into the $\pm 1^{st}$ order. The diffraction efficiency is

$$\eta_{dif} = \frac{P_{+1\,Order}}{P_{incident}} \approx \frac{1}{2}\,\frac{P_{incident} - P_{0\,order}}{P_{incident}} = \frac{1}{2}\,\frac{15.3 - 5.9}{15.3} = 30.7\%$$

Small-Diameter Flat Fresnel Lens

Using a technique similar to the lens of the previous section, a second lenslet was exposed and developed that was 300 μm in diameter. The up collimator was replaced in the planar beam interferometer arm with a 0.25 mm diameter aperture plate. The power in each interferometer arm was equalized. This lens was exposed for 0.15 seconds with a peak power density at a bright fringe of 6.28 $\mu W/mm^2$. This corresponds to 0.94 $\mu J/mm^2$ as compared to 2.88 $\mu J/mm^2$ for the test exposure described earlier in this chapter. Figure 6.3 is an SEM photomicrograph showing this lenslet. The lens exposure appears to be good, with approximately a 50% photo resist coverage of the substrate. However, the photo resist has a mottled appearance in a pair of "wings" radiating horizontally. This may be due to a dirty beam in one of the interferometer arms. This lens was about twice the diameter that the lens on the spherical substrate was to be.

Spherical Fresnel Lens

A spherical Fresnel zone lens was made following the alignment and exposure procedures outlined in Chapter V. A coating of photo resist approximately 1 μm thick was applied to a 0.85 mm diameter microsphere. The spherical wave had an NA of 0.18. The Fresnel lens diameter was calculated to be 156 μm. The planar beam was 300 μm diameter, but only the central 156 μm interfered with the spherical wave. The power in the plane wave was 25.7 μW, and the power in the focused

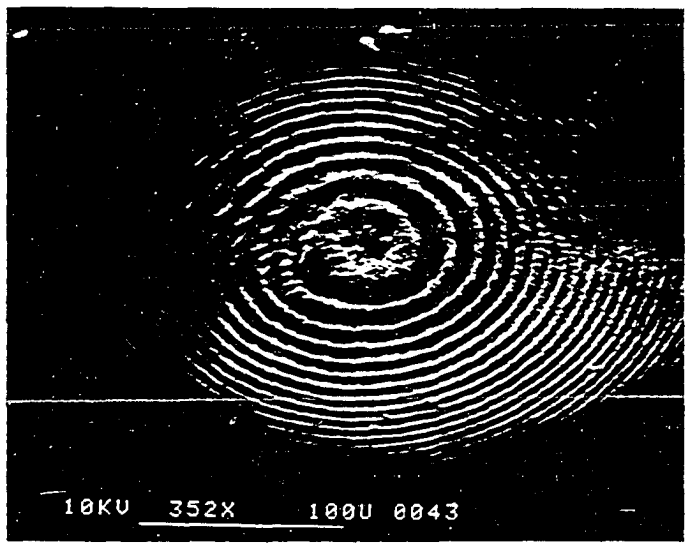

Figure 6.3 The SEM photomicrograph shows a Fresnel zone lens exposed in photo resist for a 0.18 NA, 300 μm. diameter lens. The ellipticity is an artifact of the photograph viewing angle.

beam was 26.3 μW. Assuming uniform power distribution, the power in the central 156 μm of the plane wave was 4.83 μW. Therefore, ND was applied to the focused beam arm of the interferometer until the power was reduced to 5.0 μW. The power density for a bright fringe was 7.27 $\mu W/mm^2$. The exposure time was 0.12 seconds, corresponding to an exposure of 0.87 $\mu J/mm^2$.

Figure 6.4 is a photomicrograph of the lens under white light. The reticule scale is 10 μm per minor division. The lens diameter was measured to be approximately 160 μm. An SEM photomicrograph is shown in Figure 6.5. This figure shows the spherical substrate recessed into the hole in the aperture plate. The smooth surface joining the aperture edge to the sphere is adhesive that has flowed part of the way onto the sphere surface.

A 0.18 NA Fresnel lens diameter of 160 μm should have 16 rings, and the last ring should be 2.5 μm wide. Figure 6.6 shows the lens under higher magnification, and 15 fringes are evident out to the edge of the photograph. This magnification also shows the same mottled appearance as was evident in the last planar lens. Also, this lens may be under-exposed or the photo resist was too thick, as the substrate is not visible between the rings of photo resist. Figure 6.7 is a higher magnification of a portion of the same lens that shows the mottled appearance, and also shows at least 16 rings. This roughness in the photo resist will cause scatter of the light as it passes through the lens, and will greatly reduce the diffraction efficiency.

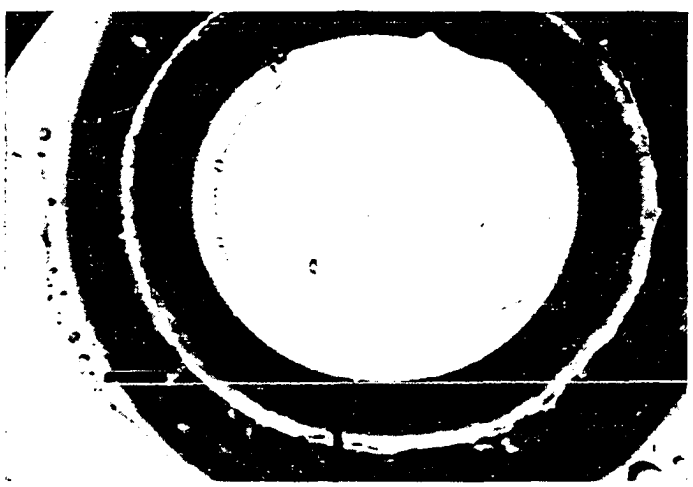

Figure 6.4 The photomicrograph shows an axial view of a 0.18 NA spherical Fresnel lens under white light. The scale shown is 10 μm. per minor division.

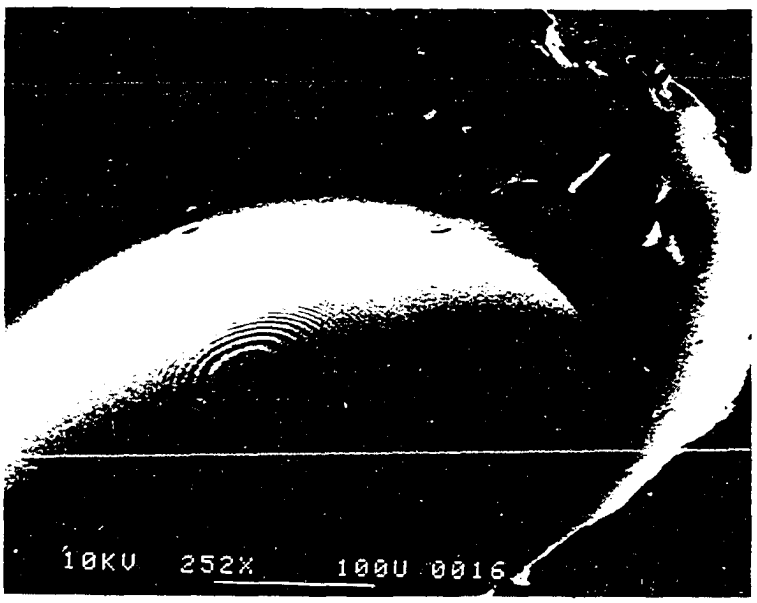

Figure 6.5 The SEM photomicrograph shows a 252 x magnification of a 0.18 NA, spherical Fresnel microlens recessed into the hole in an aperture plate used as a mounting fixture. The smooth material connecting the substrate to the aperture in the mounting plate is epoxy that has flowed onto the substrate surface.

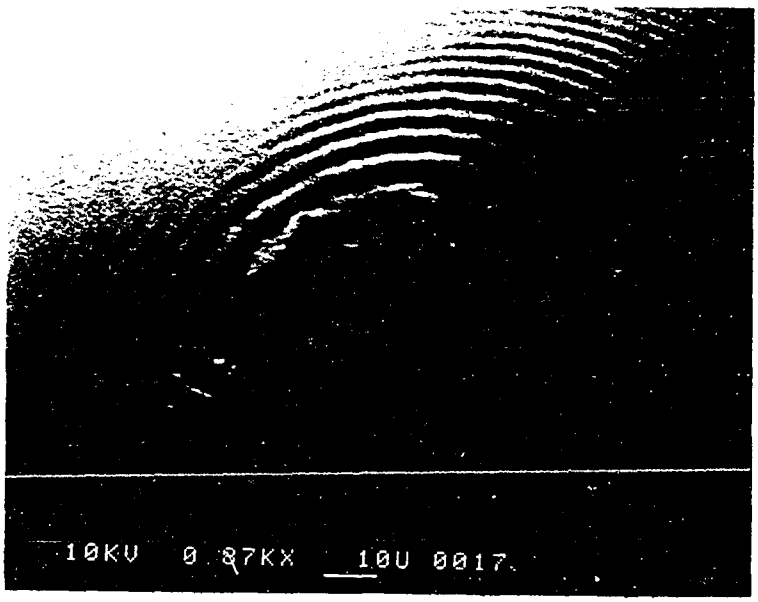

Figure 6.6 The SEM photomicrograph shows a 870 x magnification of a 0.18 NA, spherical Fresnel microlens. The rough surface is probably due to a "dirty" beam in the interferometer. At least 15 rings are visible in this photograph.

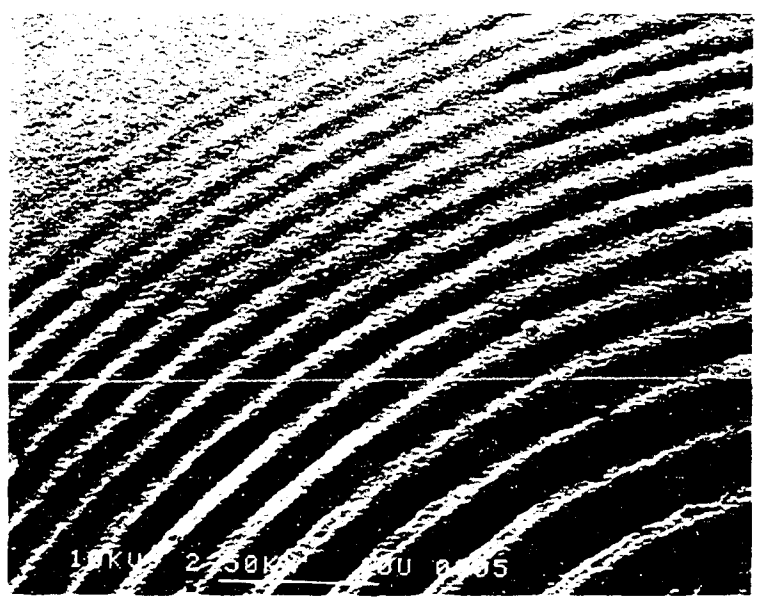

Figure 6.7 The SEM photomicrograph shows a 2500 x magnification of a part of a 0.18 NA, spherical Fresnel microlens. At least 16 rings are visible in this photograph. The lens may be under-exposed, or the resist layer may be too thick because the substrate is not visible between the Fresnel rings.

The set up shown in Figure 6.8 was used to measure the diffraction efficiency of this lens. The scatter caused by the surface roughness was shielded from the detector by an aperture. The zero-order beam power was measured by the detector approximately 600 mm from the lens, allowing the focal orders to diverge. The total power through the lens was measured with the detector close enough to capture all of the light, less the scatter. The power incident on the lens was 42 μW. The beam diameter incident on the lens was 300 μm, and the lens diameter was 160 μm. The power incident on the lens within the area of the lens was calculated to be 11.9 μW. The power measured in the zero order, after accounting for the oversized beam diameter, was 5.0 μW. After blocking the zero order beam, the total power through the lens, less the scatter was 1.55 μW. If this was evenly distributed between the + 1st and - 1st order, the diffraction efficiency is calculated to be

$$\eta_{dif} = \frac{P_{+1\ order}}{P_{\pm 1\ order} + P_{0\ order}} \approx \frac{1}{2}\,\frac{1.55}{1.55 + 5.0} = 11.8\%$$

The NA of the lens was measured with the same set-up. The diverging beam diameter was plotted as a function of the distance from the lens, and an NA of 0.16 was calculated. This was slightly less than the 0.18 NA expected. However, in Chapter V, the microscope objective FWHM spot size was measured in-situ to be the proper size for a 0.16 NA diffraction-limited lens. This may indicate that the 0.18 NA objective was underfilled.

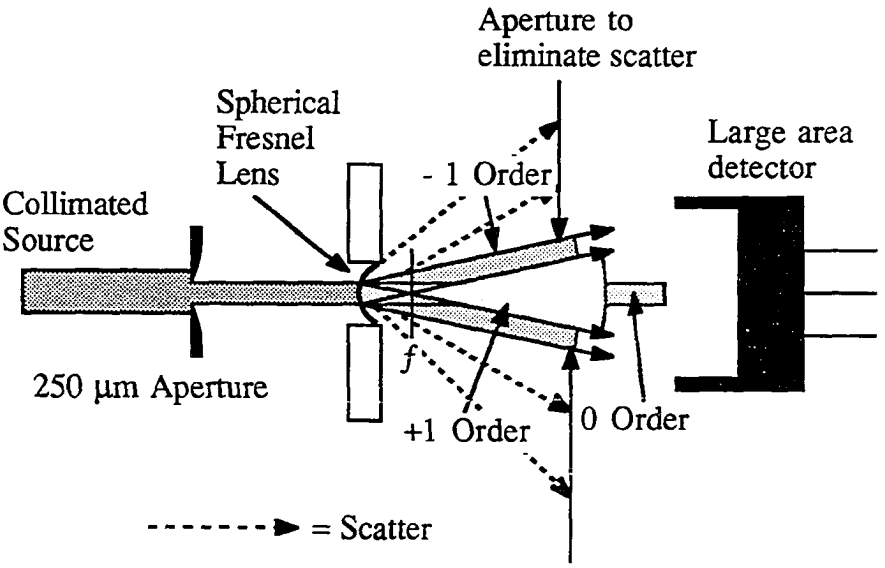

Figure 6.8 This sketch shows the set-up used to measure the diffraction efficiency and numerical aperture of the spherical Fresnel lens. An aperture was used to shield the scatter caused by the lens surface roughness.

The lens was set-up in a Twyman-Green interferometer. The wavefront from the Fresnel lens was focused onto a mirror, re-collimated, retro-reflected, and re-combined in a beamsplitter with a reference wave. The fringes were imaged onto a CCD array. However, there was too much scatter to form stable fringes, and no results were obtained.

Conclusions

There are several conclusions to be drawn from this work. It was shown that optical data storage systems would benefit from replacing the 4.5 mm diameter, 500 mg objective lenses with smaller, lighter lenses. A reduction in lens mass would allow the servo system to respond faster, providing a shorter data access time. It was shown that several different types of microlenses could be fabricated that would weigh around 2 mg, a mass reduction of a factor of 250. If the lens diameter were smaller, a storage system that uses stacked platters could reduce the spacing between successive platters, thus increasing the volumetric storage density. It was shown that a lens diameter on the order of 1 mm is very reasonable to fabricate. This would represent a factor of 4.5 improvement in volumetric storage density over the present system.

An analysis showed that a storage disk in a typical, non clean room environment, requires a minimum cover-plate thickness to keep dust and scratches out of focus of the objective lens and maintain a bit error rate equivalent to that associated with disk manufacturing defects. For a lens

NA of 0.5 and a 75 μm WD, the minimum cover thickness requires the lens diameter to be 0.43 mm or greater.

It was demonstrated that, if a microlens was to maintain the same field of view as a conventional objective, it must be aberration free through a much larger field angle. A 0.5 NA, 0.43 mm diameter lens requires a field angle of ± 7.7º to maintain a ±30 track field of view. The off-axis illumination of the cover plate due to this tilt introduces off-axis aberrations in the focused beam. It was shown that a disk design using a thin cover plate with an air gap decreased these aberrations, while keeping scratches and dust out of focus. A 0.2 mm thick cover plate introduces λ/4 of coma for a field angle of 1.5º. This shows that the 0.43 mm diameter lens is too small unless the field-of-view constraint can be relaxed. A field angle of ±3.3º is required for a 0.5 NA, 1 mm diameter lens.

It was shown that there are many different types of microlenses that can be fabricated. The most promising is a Fresnel microlens. This type of lens can be designed and fabricated under computer control to correct for the spherical aberration introduced by the disk cover plate. It can also be designed to remove on-axis astigmatism. An E-beam fabrication technique could fabricate a lens for any design wavelength. The minimum process resolution is on the order of 0.2 μm, which would allow the system to fabricate a 1 mm diameter, 0.5 NA lens with 95% diffraction efficiency. Several techniques were shown that could inexpensively duplicate a master Fresnel lens through mass-production molding technology.

Fresnel zone lenses were shown to be limited in off-axis performance by coma. A 1 mm diameter, 0.5 NA lens would exceed the Rayleigh limit ($\lambda/4$ wavefront aberration) for a field angle of only 0.13º. It was shown that, if the Fresnel lens were placed on a hollow spherical substrate whose center of curvature coincides with the Fresnel lens focus, coma is identically zero for all tilts. The lens is then limited by astigmatism and does not exceed the Rayleigh limit until the field angle exceeds 2.1º. A tolerance analysis showed that, to remain diffraction limited, a lens such as this must be fabricated so that the focus of the zone plate is coincident with the substrate center of curvature to within ±10 μm radially and ±50 μm axially. It was also shown that the wall thickness of the spherical substrate should remain below 5 μm.

An interferometer was set up to expose a spherical Fresnel zone plate at 442 nm. A hollow spherical substrate with a diameter of around 1 mm and wall thickness of 1 μm was used as the spherical substrate for the Fresnel lens. A technique was demonstrated for mounting the microsphere onto an alignment fixture and cutting the sphere to provide a clear exit aperture. A technique was demonstrated for coating the sphere with the proper thickness of photo resist needed to record the interferometric Fresnel fringes. The interferometer was used to fabricate several flat Fresnel zone lenses and a spherical Fresnel zone lens. The diffraction efficiency of the spherical lens was low, and the surface was rough, causing significant scatter.

The biggest problem with the preparation of the substrate was the application of the photo resist. The resist adhesion to the substrate was inconsistent and was dependant on humidity. Even when the humidity was controlled, the resist would sometimes flake off. Improvement is needed in this area.

Substrate handling and preparation was demonstrated. It is clear that the interferometer is not the ideal lens fabrication technique, but it was the simplest. Future work in this area should concentrate on solving photo resist problems, and should also focus on computer controlled E-beam or laser beam fabrication systems. A high quality spherical micro-Fresnel lens should be fabricated. The focal spot quality should be measured as a function of illumination angle to verify the lens quality and show closure with theory.

REFERENCES

1 Donald Kenneth Cohen, "Analysis of methods for detecting focus error in optical data storage systems", Ph.D. Dissertation, University of Arizona, Optical Sciences Center, 1987.

2 Alan B. Marchant, Optical Recording, a Technical Overview, Addison-Wesley Publishing Co., 1990

3 J. Braat, A. Huijser, J. Pasman, G Van Rosmalen, K. Schouhamer Immink, Principles of Optical Disk Systems, G. Bouwhuis, Adam Hilger Ltd., Ch. 6, 1985

4 M. Chen and K.A. Rubin, "Progress of erasable phase-change materials", Optical Data Storage Topical Meeting, 150-156, SPIE Vol 1078 (1989)

5 Glenn T. Sincerbox, "Miniature optics for optical recording", SPIE, V935, p.63-76, 1988

6 H. Ukita, Y. Katagire, and Y. Uenishi, Jap. J. Appl. Phys., Vol 26, 111-116 (1987)

7 Marchant, A., "Cover sheets for dust protection", OSA Topical Meeting on Optical Data Storage Technical Digest, FC-A4, (1984)

8 Warren J. Smith, Modern Optical Engineering, McGraw-Hill Book Company, 1966

9 Mark A. Fitch, Y. K. Konishi, "Technical directions in glass precision molded optics", SPIE, Vol. 1139, p.187-190, 1989

10 Paul I. Kingsbury, "Molded glass collimator/objective lens pair for optical pickup applications", SPIE, V. 740, p. 24, 1987

11 Joop Andrea, "Mass-production of diffraction-limited replicated objective lenses for compact-disk players", SPIE, V. 803, p. 3, 1987

REFERENCES (Continued)

12 D. D'Amato, S. Barletta, P. Cone, J. Hizny, R. Martinsen, L. Schmutz, "Fabrication and testing of monolithic lenslet module (MLM) arrays, Paper presented at the Monterey Optical Fabrication and Testing Topical Meeting, OSA, 1990 Technical Digest Series, Vol 11, p. 74-77, 1990

13 K. Iga and S. Misawa, "Distributed-index planar microlens and stacked planar optics: a review of progress", Appl. Opt., V. 25, no. 19, p. 3388, 1986

14 M. Oikawa, E. Okuda, K. Hamanaka and H. Nemoto, "Integrated planar microlens and its applications", SPIE, V. 898, p 3, 1988

15 G.D. Khoe, H.G. Kock, J. A. Luijendijk, C.H.J. van den Brekel, and D Küppers, "Plasma CVD Prepared SiO2/Si3N4 Graded Index Lenses Integrated in Windows of Laser Diode Packages", Technical Digest, Seventh European Conference on Optical Communication, Copenhagen, p. 7.6, 1981

16 Nicholas F. Borrelli, David L. Morse, Robert H. Bellman, and Walter L. Morgan, "Photolytic technique for producing microlenses in photosensitive glass", Appl. Opt. Vol. 24, No. 16, 1985

17 Zoran D. Popovic, Robert A. Sprague and G. A. N. Connell, "A process for monolithic fabrication of microlenses on integrated circuits", SPIE, V. 898, p. 23, 1988

18 R. Magnusson, T. K. Gaylord, "Diffraction efficiencies of thin phase gratings with arbitrary grating shape", J. Opt. Soc. Am., Vol. 68, No. 6, pg. 806-809, 1978

19 James Logue and Thomas McHugh, "Current trends in binary optics at Perkin Elmer", SPIE, V 1168, p. 74-82, 1989

20 James R. Leger, Miles L. Scott, Philip Bundman, and Maraden P. Griswold, "Astigmatic wavefront correction of a gain-guided laser diode array using anamorphic diffractive microlenses", SPIE, V 884, p. 82, 1988

REFERENCES (Continued)

21 W.B. Veldkamp, G.J. Swanson, and D.C. Shaver, "High efficiency binary lenses", Opt. Comm., Vol. 53, No. 6, p. 353-358, 1985

22 V. Diadiuk, Z.L. Liau and J. N. Walpole, "Fabrication and characterization of semiconductor microlens arrays", International lens design conference, Monterey, 1990

23 N. Nishihara and T. Suhara, "Micro Fresnel lenses", Progress In Optics V XXIV, E. Wolf, editor, North-Holland Physics Publishing, pg 3-35, 1987

24 M. Tanigami, S. Ogata, S. Aoyama, T. Yamashita, and K. Imanaka, "Low-wavefront aberration and high-temperature stability molded micro Fresnel lens", IEEE Phot. Tech, Let., Vol. 1, No. 11, p. 384-385, 1989

25 M. Young, "Zone plates and their aberrations", J. Opt. Soc. Am., V. 62, no. 8, p. 972, 1972

26 W.T. Welford, "Aplanatic hologram lenses on spherical surfaces", Opt. Com., Vol. 9, No.3, p. 268-269, 1973

27 Private communication with Mark Shi-Wang, Optical Sciences Center June, 1990

28 Shipley Microposit S1800 series photo resist technical literature

29 Roland V. Shack and George W. Hopkins, "The Shack Interferometer", Opt Eng. Vol. 18, No. 2, p. 226-228, 1979

30 Private communication with Chien-Wei Han, University of Arizona, Optical Sciences Center, June, 1990